Nanoscale

Accepted Manuscript

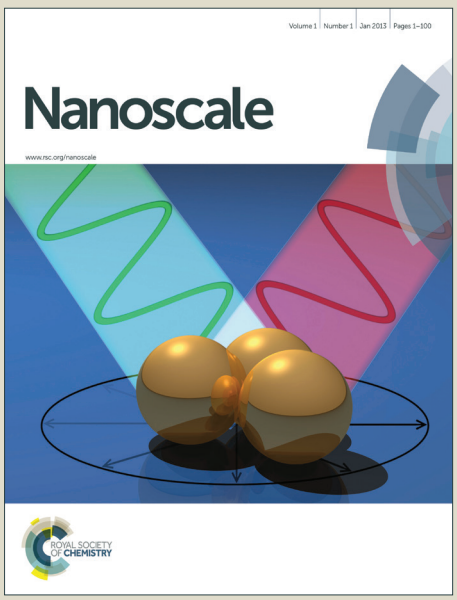

ROYAL SOCIETY OF CHEMISTRY

www.rsc.org/nanoscale

Solution Synthesis of Metal Oxides for Electrochemical Energy Storage Applications

Xinhui Xia,[a,b,‡] Yongqi Zhang,[a,‡] Dongliang Chao,[a] Cao Guan,[a] Yijun Zhang,[b] Lu Li,[b] Xiang Ge,[b] Ignacio Mínguez Bacho,[a] Jiangping Tu,[b,*] and Hong Jin Fan[a,*]

[a] Division of Physics and Applied Physics, School of Physical and Mathematical Sciences, Nanyang Technological University, Singapore 637371, Singapore
[b] State Key Laboratory of Silicon Materials, Key Laboratory of Advanced Materials and Applications for Batteries of Zhejiang Province, and Department of Materials Science and Engineering, Zhejiang University, Hangzhou 310027, China

* Address correspondence to fanhj@ntu.edu.sg (H.J. Fan), tujp@zju.edu.cn (J.P. Tu)
‡ These authors contributed equally to this work.

Abstract

This article provides an overview of solution-based methods for the controllable synthesis of metal oxides and their applications for electrochemical energy storage. Typical solution synthesis strategies are summarized and the detailed chemical reactions are elaborated for several common nanostructured transition metal oxides and their composites. The merits and demerits of these synthesis methods and some important considerations are discussed in association with their electrochemical performance. We also propose the basic guideline for designing advanced nanostructure electrode materials, and the future research trend in the development of high power and energy density electrochemical energy storage devices.

Keywords: *solution growth methods, nanostructure electrodes, metal oxides, composite nanostructures, electrochemical energy storage*

1. Introduction

Energy is the eternal pursuit of human kind and plays an important role in the development of human civilization and advancement of modern technology. Energy storage, an important intermediate step towards the subsequent versatile and efficient energy applications, has received great attention both in academy and industry. Among various energy storage systems, electrochemical energy storage (EES) devices (such as batteries and supercapacitors) have been extensively studied and considered to be one of the most promising green energy storage systems for the sustainable energy supply in near future, due to their high efficiency, versatility, and flexibility.

In the past decades, a dramatic expansion of EES research has been driven to meet the increasing demand of modern electronics, transportation and smart grid. Batteries and supercapacitors are two dominating types of EES devices, which consist of four parts: a positive electrode, a negative electrode, a separator, and an electrolyte. Noticeably, lithium ion batteries (LIBs) are the most important and widely used rechargeable batteries with advantages of high working voltage, high capacity and long cycling life. Meanwhile, supercapacitors have matured significantly over the last decade and emerged with the potential to facilitate major advances in energy storage due to their unique characteristics of high power density, long cycling life and fast recharge capability. Supercapacitors have an important role in complementing batteries in the energy storage field. EES is realized by electrochemical processes associated with electron and ion transports. During a discharge process, electrochemical reactions take place at the electrodes and the generated electrons flow through an external circuit to drive external loads. During the charge process, an external voltage is applied to store electrons at the electrodes by reversible electrochemical reactions. The performance of EES systems, both batteries and supercapacitors, is mainly determined by the electrode materials, which are the core parts and the key to high

performance. Advanced electrode materials play a decisive role in the efficient and versatile use of energy. Therefore, the development of EES techniques is largely attributed to the innovation and advance of electrode materials with tailored structure and high reactivity.

To date, various active materials have been studied for EES systems as anode or cathode materials including metal (Sn),[1] metal sulfides (NiS, CoS, etc.),[2] metal oxides (NiO, Co_3O_4, MnO_2, CuO, etc.),[3-7] metal hydroxides ($Ni(OH)_2$, $Co(OH)_2$, etc.),[1, 3, 5] carbon materials (carbon nanotube, graphene, etc.),[8, 9] metal hydrides (AB_5 type),[10] metal carbides (TiC, TaC, etc.),[3, 11] metal nitrides (MoN, TiN, TaN, etc.),[1, 3, 5, 12] conducting polymers (polyaniline, polypyrrole, polythiophene, etc.),[2, 13, 14] sulphur,[15, 16] and silicon,[17-19] and so on. Among all these explored electrode materials, transition metal oxides are important classes of semiconductors with wide applications in EES systems due to their unique electrochemical reactivity. With the rapid development of materials design strategies and synthesis techniques, great progress has been achieved in fabrication of transition metal oxides with bespoke nanostructures and enhanced electrochemical performance. Nanostructured transition metal oxides have been proven to exhibit superior electrochemical performances to the bulk counterparts because of their novel properties associated with decreased size, unique shape, and defective nature. The nanoscale structure can effectively improve electrochemical reaction efficiency and utilization of active materials with improved energy and power densities. Up to now, lots of chemical and physical methodologies have been developed to prepare nanostructured transition metal oxides for EES applications. Compared to physical techniques, solution chemical synthesis method (or called “soft approach”) is a facile and alternative synthetic strategy for the preparation of advanced transition metal oxides with desirable morphology and improved performance. Solution-based synthesis methods are a big and rich family including hydrothermal (HT) synthesis method, solvothermal (ST) synthesis method, electro-deposition (ED) method, chemical bath deposition (CBD) method, electrophoretic deposition (EPD) method, sol-gel method, direct chemical precipitation (CP)

method, microwave synthesis (MS) method, and so on. The above solution-based synthetic methods do not need expensive equipment and high vacuum, and are usually easy to process and conducted under mild conditions with lower temperature. Different solution-based synthetic methods have their own advantages and disadvantages, and sometimes they can be complementary to each other or cooperate with each to fabricate advanced nanomaterials.

In this Featured Article, we spot the recent progress in solution-based synthetic methods for designing and fabricating nanostructured electrode materials of typical transition metal oxides (e.g., nickel oxide, cobalt oxide, iron oxide, copper oxide, manganese oxide, vanadium oxide, tungsten oxide, and their composites) for applications in LIBs and supercapacitors. We focus on the detailed solution synthesis details and their corresponding reaction mechanisms. Furthermore, we will address the structural and morphological advantages of solution-synthesized nanostructured transition metal oxides and their composites for EES applications. Finally, we summarize and compare the merits and demerits of different solution-based methods and propose general rules on how to design and fabricate high-performance electrode EES materials.

2. NiO and NiO-based composites

Nickel oxide is a classic example of transition metal materials with wide applications in electrochromics, catalysis, chemical sensor and EES. It can be used as an anode material for LIBs or a cathode material for supercapacitors. Pure NiO is an insulator with a bulk band gap of ~3.4 eV. It crystallizes in the rock-salt structure (cubic crystal structure, JCPDS 4-0835) with a lattice constant of 0.417 nm and a high-spin anti-ferromagnetic spin structure at low temperatures. Lots of NiO nanostructures (such as nanowires, nanoflakes, nanobowls and nanospheres) have been prepared by different solution-based synthesis methods and applied as active materials for EES with enhanced electrochemical performance.

2.1 Chemical bath deposition of NiO and NiO-based composites

The CBD method was first proposed by Nagayama et al., who used this technique to prepare SiO_2 films on silicon wafers about 25 years ago.[20]. The CBD method involves immersion of a substrate in an aqueous solution containing a precursor species. Then the desired oxide/hydroxide precipitates preferentially on the substrate surface and produces a conformal film. The CBD method is an advantageous technique due to its low cost, low temperature and also convenient for large-scale deposition, especially suitable for the preparation of uniform oxide film samples. This method usually needs strong chemical oxidant or reducing agent to drive reactions to take place. The flatness of the final sample is even related with the fluid mechanics of the reaction solution.

Our group pioneered a facile modified CBD method for the synthesis of polycrystalline NiO nanoflake arrays and investigated their electrochromics, LIBs and supercapacitor performances.[21-28] The obtained NiO nanoflakes have diameters of 10–20 nm and grow vertically to the substrates. The nanoflakes are interconnected with each other forming a highly porous network with pore diameter of 30–300 nm (Figure 1). In our case, the electrolyte consists of nickel sulfate, ammonia and potassium persulfate. The precursor reactions for the growth of NiO nanoflake arrays via CBD could be simply represented as follows:[21, 22]

$$Ni[(H_2O)_{6-x}(NH_3)_x]^{2+} + 2OH^- \leftrightarrow Ni(OH)_2 + (6-x)H_2O + xNH_3 \quad (2.1)$$

$$2Ni(OH)_2 + S_2O_8^{2-} + 2OH^- + H_2O \rightarrow 2NiOOH{\cdot}H_2O + 2SO_4^{2-} + 2H_2O \quad (2.2)$$

During the annealing process:

$$NiOOH{\cdot}H_2O - e^- \rightarrow Ni(OH)_2 + OH^- \quad (2.3)$$

$$Ni(OH)_2 \rightarrow NiO + H_2O \quad (2.4)$$

It is noteworthy that potassium persulfate here plays an important role in the formation of the NiO nanoflake arrays. Potassium persulfate acts as an oxidant to drive the whole reaction and facilitate the heterogeneous nucleation in the supersaturated solution. Without potassium persulfate, no NiO nanoflake arrays will be formed on the substrates. Other persulfates (such

as $Na_2S_2O_8$ and $(NH_4)_2S_2O8$) have similar functions. Impressively, the CBD-NiO nanoflakes can be formed on arbitrary substrates including ITO, FTO, Ti foil, graphite, carbon cloth, nickel foam, and so on. More importantly, this CBD process is very high efficiency, only needs several minutes to finish the whole deposition process.

Based on the above CBD method, we fabricated hierarchically porous NiO films by the combination of CBD method and polystyrene sphere template.[27] The obtained NiO films show a multilayer architecture with a substructure of NiO monolayer hollow-sphere array and a superstructure of porous net-like NiO nanoflakes. These hierarchically porous NiO films exhibit enhanced supercapacitor performances with higher capacitances (309 F g^{-1} at 1 A g^{-1} and 221 F g^{-1} at 40 A g^{-1}) than the dense counterparts (121 F g^{-1} at 1 A g^{-1} and 99 F g^{-1} at 40 A g^{-1}) and improved cycling stability. In addition, Yan et al.[29] prepared NiO hollow spheres powder samples by a similar CBD method and reported a capacitance of 346 F g^{-1} at 1 A g^{-1}. The reactions of NiO for supercapacitos are given as below:[27]

$$NiO + OH^- - e^- \leftrightarrow NiOOH \qquad (2.5)$$

It is accepted that NiO is a p-type semiconductor whose conductivity is not good and kinetically unfavourable for high-rate capability. In order to further improve the pseudocapacitive performances of CBD-NiO nanoflake arrays, we adopted graphene to modify the conductivity of NiO to fabricate Graphene/NiO composite film by the combination of CBD and electrophoretic method, and improved capacitive performance was demonstrated in this composite film due to the conductivity modification by graphene.[28] In addition, Wu et al. modified the CBD-NiO nanoflakes by Ag nanoparticles, and verified that the introduction of Ag nanoparticles could effectively accelerate the electron transfer of the CBD-NiO nanoflakes leading to enhanced performance.[30] Meanwhile, the CBD-NiO nanoflakes are used to decorate other active material to form high-performance composite cathode materials for supercapacitors. We assembled the CBD-NiO nanoflake on porous Co_3O_4 nanowire core to form Co_3O_4/NiO core/shell nanowire arrays, which exhibited

noticeable supercapacitor performance with high specific capacitance of 853 F g^{-1} at 2 A g^{-1} after 6000 cycles owing to the unique porous core/shell nanowire array architecture.[31] Similar pseudocapacitive enhancement is also observed in the TiO_2/CBD-NiO core/shell nanorod arrays reported by Wu et al..[32]

NiO is one of promising anodes of LIBs with a theoretic capacity of 718 mAh g^{-1}. It has been proved that the electrochemical reaction mechanism of Li with transition metal oxides differs from the classical mechanisms, which are based either on reversible insertion/deinsertion of lithium into host structures or on lithium alloying reactions. The electrochemical reaction mechanism of Li with NiO in LIBs can be described as follows:[4]

$$NiO + 2\ Li^+ + 2e^- \leftrightarrow Li_2O + Ni \quad (2.6)$$

$$2\ Li \leftrightarrow 2Li^+ + 2e^- \quad (2.7)$$

$$NiO + 2\ Li \leftrightarrow Li_2O + Ni\ (Overall) \quad (2.8)$$

Nevertheless, its practical application is restrained by the poor cycling stability resulting from the large specific volume change causing pulverization and deterioration of active materials during cycling. The above CBD-NiO nanoflake arrays are also applied as anode materials for LIBs, but their LIBs performance, especially the cycling performance, is not satisfactory.[24] In order to improve their LIBs performance, our group used nanoporous and composite design strategies to deposit highly conductive layers (such as polyaniline, PEDOT, Ag, Co doping, and sputtered-Ni)[23, 25, 26, 33] on the surface of CBD-NiO nanoflake to form conductive composite arrays and enhanced LIBs performances were demonstrated in these systems. Meanwhile, Xia et al. reported a bio-template (lotus pollen grains) to prepare CBD-NiO/C composite nanoflake powder with high LIBs performance. These conductive layers can not only provide fast electron transportation path, but also act as a buffer layer to accommodate the strain caused by the lithium ion intercalation/deintercalation and alleviate the structure degradation caused by volume expansion during the cycling process. Expect for the outer decoration of conductive layers for CBD-NiO nanoflake, some other efforts have been directed at the search for hybrid materials such as ZnO/CBD-NiO,[34] and Fe_2O_3/CBD-

NiO core/shell nanoarrays as anode for LIBs.[35] Some effective synergistic effects have been proven in these composite arrays such as enhanced mechanical stability and increased reaction surface area.

In addition to the above CBD method, there is another CBD method for the deposition of NiO, quite different from the former. Some researchers call it ammonia-evaporation method, but we believe that it still belongs to CBD.[36] In this CBD, the reaction solution is always very easy, just ammonia and nickel nitrate. This CBD reaction occurs at about 80–90 ^{o}C, and finally forming sandwich-like NiO triangular prism nanoarrays with side length of 500 nm after heat treatment (Figure 2).[37, 38] The involved reactions may be expressed as follows.[36]

$$NH_4^+ + OH^- \leftrightarrow NH_3 \cdot H_2O \quad (2.9)$$

$$Ni[(H_2O)_{6-x}(NH_3)_x]^{2+} + 2OH^- \leftrightarrow Ni(OH)_2 + (6-x)H_2O + xNH_3 \quad (2.10)$$

After slow evaporation of ammonia, single-crystalline $Ni(OH)_2$ triangular prism nanoarrays precursors are formed. During annealing process:

$$Ni(OH)_2 \rightarrow NiO + H_2O \quad (2.11)$$

The NiO triangular prisms prepared by this CBD method have much bigger or larger size than those of the previous CBD method. It should be noticed that the quality of this NiO product is highly related with the position of substrates in the solution. The substrate should be 1–2 mm away from the bottom of reaction vessel. Otherwise, the film will not be uniform and homogeneous. Interestingly, the obtained NiO triangular prism is quasi-crystalline nature (Figure 2), and presents a capacity of 400 $mAhg^{-1}$ after 50 cycles at 2 C for LIBs, and a specific capacitance of 348 F g^{-1} at 2A g^{-1} after 4000 cycles for supercapacitors. [40, 41]

2.2 Hydrothermal synthesis and solvothermal synthesis of NiO and NiO-based composites

Hydrothermal synthesis is one of the most popular solution-based synthesis method and has been widely used for the synthesis of various transition metal oxides with specific size and morphology since the pioneering works from 1960s to 1980s. HT method is conducted in a sealed reaction container with the water as the reaction medium and the reaction temperature is usually above 100 ^{o}C. A high pressure will self-develop and increase with the reaction temperature. The pressure in the autoclaves is also associated with other parameters such as the percentage fill of the vessel and any dissolved salts. It should be mentioned that the concept of HT has been extrapolated to non-aqueous systems, called slovothermal synthesis (ST), in which organic solvent is used as the reaction medium instead of water. HT/ST is easy to control and only needs simple reaction equipment such as oven and autoclaves.

To date, the HT+ST papers account for ~30 % in all the published papers of solution synthesis of NiO for EES applications. The HT/ST usually needs nickel sources and precipitants to work together to drive the whole reaction to take place. Nickel nitrate, nickel chloride and nickel acetate are the most used nickel sources. The most popular precipitants are urea [$CO(NH_2)_2$] and hexamethylenetetramine (HMT), respectively, because they have low hydrolysis temperature (<100 ^{o}C) and relatively controllable hydrolysis rate. The precipitants provide OH^- or $C_2O_4^{2-}$, $CO_3^{2-}$for the deposition of Ni-precursors [such as $Ni(OH)_2$, $Ni_2(OH)_2CO_3$ and NiC_2O_4], which convert into NiO after annealing.

First, we introduce a typical and facile HT method for the synthesis of NiO nanoflake arrays. Previously, several research groups reported a similar HT method by using $Ni(NO_3)_2$ or $NiCl_2$ as the nickel source, urea as the precipitant, NH_4F as the growth promoter.[39, 40] The HT reactions can be illustrated as follows:

$$Ni^{2+} + xF^- \rightarrow [NiF_x]^{(x-2)-} \quad (2.12)$$

$$H_2NCoNH_2 + H_2O \rightarrow 2NH_3 + CO_2 \quad (2.13)$$

$$CO_2 + H_2O \rightarrow CO_3^{2-} + 2H^+ \quad (2.14)$$

$$NH_3{\cdot}H_2O \rightarrow NH_4^+ + OH^- \quad (2.15)$$

$$[NiF_x]^{(x-2)-} + (1-0.5y)CO_3^{2-} + yOH^- + nH_2O \rightarrow Ni(OH)_y(CO_3)_{(1-0.5y)}\cdot nH_2O + xF^- \quad (2.16)$$

During annealing process:

$$2Ni(OH)_y(CO_3)_{(1-0.5y)}\cdot nH_2O + 0.5O_2 \rightarrow 2NiO + (2n+y)H_2O + (2-y)CO_2 \quad (2.17)$$

The final NiO samples are nanoflake arrays vertical to the substrates and flower-like nanoflake power in the solution. The as-prepared NiO nanoflakes are single-crystalline nature. NH_4F is acted as growth promoter to improve the growth density of nanoflakes and prompt the formation of basic nickel carbonate hydroxide precursor. Without NH_4F, the load weight of NiO nanoflakes on the substrates will be much less, and the involved specific reactions are different, given as follows:[41, 42]

$$H_2NCoNH_2 + H_2O \rightarrow 2NH_3 + CO_2 \quad (2.18)$$

$$NH_3\cdot H_2O \rightarrow NH_4 + OH^- \quad (2.19)$$

$$CO_2 + H_2O \rightarrow CO_3^{2-} + 2H^+ \quad (2.20)$$

$$2Ni^{2+} + 2CO_3^{2-} + 2OH^- \rightarrow Ni_2(OH)_2CO_3 \quad (2.21)$$

During the annealing process:

$$Ni_2(OH)_2CO_3 \rightarrow 2NiO + H_2O + CO_2 \quad (2.22)$$

When the precipitant changes from urea to HMT,[43] the hydrolysis reaction will be

$$(CH_2)_6N_4 + 10H_2O \rightarrow 6HCHO + 4OH^- + 4NH_4^+ \quad (2.23)$$

$$Ni^{2+} + 2OH^- \rightarrow Ni(OH)_2 \quad (2.24)$$

During the annealing process:

$$Ni(OH)_2 \rightarrow NiO + H_2O \quad (2.25)$$

All the obtained NiO products by this HT method are nanoflakes or powders made up of nanoflakes. These nanoflake arrays show good LIBs performance with capacities of above 400 mAh g^{-1} after 50 cycles at 0.3 A g^{-1} and can deliver a capacitance of 300–500 F g^{-1} at 2 A g^{-1} after 3000 cycles as cathode materials of supercapacitors.[39-41, 44] In addition, several graphene/NiO, C/NiO, Ni/NiO composites have been reported via the above HT method to achieve enhanced electrochemical performance.[42, 43, 45-47]

Except for the above common precipitants, some other precipitants such as ammonia, NaOH, glycine, n-butylamine, N-methyl pyrrolidone, L-lysine, L-arginine, ethanolamine and butanol are also used to prepare NiO sampls composed of nanoflakes.[42, 46-55] As for the organic precipitants, they have specific or even more complex reaction mechanisms, which are not studied in detail in these papers. Among these NiO products, the powder samples are prone to exhibit sphere structures (Figure 3) due to the self-assembly of NiO nanoflakes. The electrochemical results reveal that the powder samples have inferior performance to film samples, both for supercapacitor and LIBs applications, due to the fact the powder active materials need to be mixed with carbon and polymer binders and compressed into pellets. This process risks negating the benefits associated with the reduced particle size and introduces supplementary, undesirable interfaces.

It is noticed that the morphology of NiO is highly related with that of precursors. If the precursors are hydroxides or oxyhydroxides, the final morphology of NiO will be nanoflakes. If the precursors are materials like oxalate which is prone to form nanowires, the final NiO products will keep the structure of nanowires. It is observed that the as-prepared NiO samples always show nanoflake structures or spheres composed of nanoflakes when the precursor is nickel hydroxide or oxyhydroxide. This phenomenon is mainly due to its typical crystal structure of hydroxide or oxyhydroxide precursor. It is well accepted that the brucite crystals ($M(OH)_2$ or MOOH, M=Mg, Ca, Ni, Co, and etc.) have a layered structure of the CdI_2 type, which shows weak interaction between layers and the strong binding within the layered planes.[56, 57] Neighboring layers are bound together by weak van der Waal forces. Therefore its (001) plane is stable, and the brucite crystal is prone to form two-dimensional nanoflakes. Then, these nanoflakes self-assemble with each other to form hollow spheres. The NiO preserves their morphology and show nanoflake structure. This phenomenon will change if the precursor is nickel oxalate. Su et al. used another precipitant ($K_2C_2O_4$) to prepare

mesoporous NiO nanowire by a modified HT method.[58] The specific reactions are shown as follows:[58]

$$NiCl_2 + K_2C_2O_4{\cdot}2H_2O \rightarrow NiC_2O_4{\cdot}2H_2O + 2KCl \quad (2.26)$$

$$NiC_2O_4{\cdot}2H_2O + O_2 \rightarrow 2NiO + 4CO_2 + 2H_2O \quad (2.27)$$

The mesoporous NiO nanowires exhibit a capacitance of 348 F g^{-1} as electrodes in supercapacitors and a capacity of 1280 mAh g^{-1} after 100 cycles for LIBs.[58] It is reasonable that the precipitant can affect the morphology of final NiO samples. The specific mechanism is still not clear and speculated that the $C_2O_4^{2-}$ plays an important role in the nanowire growth.

In view of the success of HT, scientific researchers extend the HT to the organic field, namely called solvothermal synthesis (ST). Nickel sources are dissolved in the organic solvent such as glycerol, ethylene glycol and ethanol to react and form NiO after annealing.[59-62] The organic solvent will decompose under high temperature and release precipitant ions to trigger reactions. To date, the detailed mechanisms of ST-NiO have not been studied well, and it is still hidden in the fog. Similarly, NiO nanoflake arrays and nanospheres composed of nanoflakes are obtained in the ST systems and show improved LIBs and supercapacitor performance.[59-62]

2.3 Electrochemical synthesis of NiO and NiO-based composites

Among the existing solution synthetic approaches to film materials, electrochemical techniques show unique principles and flexibility in the control of the structure and morphology of samples. Generally, two kinds of electrochemical synthesis methods are adopted to prepare nanostructured transition metal oxides, namely ED and electrophoretic deposition (EPD). ED is always involved with redox reactions related to electron transfer and phase change. ED is believed to be an ideal method for the fabrication of nanostructured films with various morphologies, because it occurs from the electrode surface and different morphologies of the materials can be obtained via the precise choice of deposition solution and conditions. ED provides the fabrication of films or coatings rather than powders, which is

required for a number of applications in batteries, and supercapacitors. Meanwhile, EPD technique, another electrochemical synthesis method, is an economical and versatile processing technique with many advantages in the preparation of films from suspensions, such as high deposition rate and throughput, good uniformity and controlled thickness of the obtained films, and simplicity of scaling up.

According to the reaction mechanism, the ED is classified into two types: anodic ED and cathodic ED. Several ED-NiO nanostructures have been reported and applied for EES. Here, we introduce pioneering works of Wu et al. about the anodic ED method for the synthesis of NiO nanoflake arrays and composites in the mixed solution of $NiSO_4$, Na_2SO_4, and CH_3COONa. The involved reactions can be simply illustrated as follows:[63]

$$CH_3COO^- + H_2O \leftrightarrow OH^- + CH_3COOH \quad (2.28)$$

$$Ni^{2+} + 2OH^- \rightarrow Ni(OH)_2 \quad (2.29)$$

$$Ni(OH)_2 - e^- + OH^- \leftrightarrow NiOOH + H_2O \quad (2.30)$$

During the annealing process:

$$NiOOH \cdot H_2O - e^- \rightarrow Ni(OH)_2 + OH^- \quad (2.31)$$

$$Ni(OH)_2 \rightarrow NiO + H_2O \quad (2.32)$$

This anodic ED method can be applicable for lots of substrates such as nickel foam, stainless steel, FTO and ITO. The deposited NiO film has an interconnecting network is made up of flaky nickel oxides of 15–20 nm. Wu and his co-workers also used this anodic ED method to fabricate macroporous NiO bowl-like arrays, NiO/$Ni(OH)_2$ and NiO/C composites and investigated their LIBs and supercapacitor performances.[64-68] The obtained NiO nanoflakes exhibit a very high capacity of ~990 mAh g^{-1} at 15 C as anode of LIBs,[64] and a capacitance of ~170 F g^{-1} at 1 A g^{-1} as cathode of supercapacitors.[66] The low supercapacitor performance is because that the samples are grown on flat stainless steel substrates, which is not an ideal substrate as good as nickel foam. The NiO bowl-like arrays show better

supercapacitor performances than the unmodified ED counterparts.[68] Moreover, the modified composites NiO/$Ni(OH)_2$ and NiO/C show further improved supercapacitor performances with a capacitance over 500 F g^{-1}.[65, 67] Inspired by these works, Wu et al. prepared TiO_2/NiO core/shell nanorod arrays (Figure 4) on carbon cloth and delivered a capacitance of 611 F g^{-1} at 2 A g^{-1}.[32]

As for the cathodic ED of NiO, the nickel source is usually $Ni(NO_3)_2$ and the reactions are shown as follows:[69]

$$NO_3^- + H_2O + 2e^- \rightarrow NO_2^- + 2OH^- \quad (2.33)$$

$$Ni^{2+} + 2OH^- \rightarrow Ni(OH)_2 \quad (2.34)$$

During the annealing process:

$$Ni(OH)_2 \rightarrow NiO + H_2O \quad (2.35)$$

In this electrochemical reduction process, metallic Ni cannot form because the reaction potential of Ni^{2+}/Ni is much more negative than that of NO^{3-}/NO^{2-}.[57] Yuan et al. prepared hierarchically ordered porous nickel oxide array film by the cathodic ED through monolayer polystyrene spheres template and reported a capacity of 518 mAh g^{-1} at 1C for LIBs. It is noticed that the NiO directly prepared by cathodic ED usually shows a dense film structure, not a porous structure.[69] Some other NiO nanostructures and composites such as nanocorn, Ni/NiO core/shell and randomly porous NiO are fabricated by another cathodic ED, in which Ni nanostructures forms first and then are converted into NiO during annealing in air.[70-72] These NiO samples converted from Ni exhibit good high rate capability with a capacity of 436 mAh g^{-1} at 20 C for LIBs as well as high capacitance above 1000 F g^{-1} for supercapacitors.[70-72]

Meanwhile, Wu et al. developed a EDP method to prepare NiO films via $Ni(OH)_2$ sol in isopropyl alcohol solution.[73, 74] No redox reactions occur in the EDP process, just electrostatic

effect to absorb the active material on the surface of substrates. The EDP-NiO films are composed of nanoparticles and exhibit a peudocapacitive capacitance of ~180 F g^{-1}.

2.4 Chemical precipitation synthesis of NiO and NiO-based composites

Chemical precipitation (CP) is an old and simple method, easy to process and especially suitable for large-scale synthesis of powder samples. CP occurs if the concentration of one solid is above the solubility limit in the host solid, due to rapid quenching or ion implantation, and the temperature is high enough that diffusion can lead to segregation into precipitates. Precipitation in solids is routinely used to synthesize large-scale micro/nano-size materials. CP is widely used to prepare nanoscale transition metal oxides, also reflected in the synthesis of NiO for EES. Similar to HT method, the CP also needs nickel sources and precipitants, and the precipitation process usually occurs fast. The reaction rate is very fast, sometimes, the whole reaction only needs several minutes. The operation process of CP is conducted at room temperature and does not need high temperature. Nevertheless, it is difficult for CP to precisely control the morphology of metal oxides due to the fast precipitation. The CP papers account for ~20 % in all the published papers of solution synthesis of NiO for EES applications.

Compared to other solution synthesis methods, the reactions in the CP is much easier. The adopted precipitant is common reagent such ammonia, KOH and NaOH. The whole reactions can be shown as below:[75-78]

$$Ni^{2+} + 2OH^{-} \rightarrow Ni(OH)_2 \quad (2.36)$$

During the annealing process:

$$Ni(OH)_2 \rightarrow NiO + H_2O \quad (2.37)$$

Lots of NiO nanostructures such as nanoplates, nanoparticles, nanospheres, nanclusters have been prepared by the CP method and applied for EES. [71, 75-83] However, the pure nanosize CP-NiO samples do not show very good electrochemical performance, no matter in LIBs or supercapacitors. Hence, researchers combine other conductive scaffolds with CP-

NiO to construct new NiO composites with enhanced EES performance. A series of composites (such as graphene/NiO, C/NiO, Ni/NiO) have been prepared by the co-chemical precipitation method,[59, 71, 84-89] and high capacitance (300-800 F g^{-1}) and capacity (500-1000 mAh g^{-1}) are demonstrated in these composite systems.

2.5 Sol-gel and Microwave synthesis of NiO and NiO-based composites

The name sol-gel derives from the fact that micro particles or molecules in a solution (sols) agglomerate and under controlled conditions eventually link together to form a coherent network (gel). There are two generic variations of the sol-gel technique. One is called the colloidal method, and the other is called the polymeric (or alkoxide) route. The differences between the two stem from the types of starting materials (precursors) that are used. Both routes involve suspending or dissolving the precursor(s) in a suitable liquid, usually water for the colloidal route and alcohol for the polymeric route. The precursor is then activated by the addition of an acid (such as hydrochloric acid) or a base (such as potassium hydroxide). The activated precursors react together to form a network. The network grows and ages with time and temperature until it is the size of the container. At this point the viscosity of the liquid increases at an exponential rate until gelation occurs, that is, no more flow is observed. Many different industries could benefit from adopting sol-gel because of its versatility in fabricating a wide range of materials with different properties. Current examples are found in the construction, electronics, communications, automotive and EES.

To date, there are only a few reports about the sol-gel method for the synthesis of NiO and NiO-based composites for EES applications. Previously, our group used $NiCl_2$, HCl and formaldehyde to form $NiCl_2$/resorcinol-formaldehyde (RF) gel and finally obtained NiO hollow spheres after heat treatment (Figure 5).[90] This sol-gel process belongs to polymeric (or alkoxide) route. The as-prepared NiO hollow spheres present a high reversible LIBs capacity of 635 mAh g^{-1} at 200 mA g^{-1}. Kim et al. prepared NiO nanostructures with three distinct morphologies by a sol−gel method and their morphology-dependent supercapacitor properties

were exploited.[91] They used $Ni(NO_3)_2$, $Ni(CH_3COO)_2$, hexamethylene tetramine and ammonia as the starting materials and utilized different control reagent to fabricate three NiO nanostructures (flower-like, slice-like and particle-like NiO). Their sol-gel method is a typical colloidal route. These NiO samples can deliver a capacitance of 480 F g^{-1} at 0.5 A g^{-1} for supercapacitors. Meanwhile, Liu et al. reported a $NiO/NiCo_2O_4/Co_3O_4$ composite via a sol-gel method by using $Ni(NO_3)_2$, $CoCl_2$, and propylene oxide. The composite shows a high specific capacitance (1717 F g^{-1}) and enhanced rate capability.[92]

Microwave synthesis (MS) has become the method of choice for many chemists and biochemists for a multitude of reactions for one reason: it simply works better. Reactions that took hours, or even days, to complete can now be performed in minutes with better yields and cleaner chemistries. In many of the published examples, microwave heating has been shown to dramatically reduce reaction times, increase product yields and enhance product purities by reducing unwanted side reactions compared to conventional heating methods. The advantages of this enabling technology have, more recently, also been exploited in the context of multistep total synthesis of transition metal oxides. MS is suitable for large-scale synthesis of powder products.

According to the published papers about MS process of nanostructured NiO, notice the fact that the MS method can be regarded as a modified solution synthesis method built on the traditional CP method. First, a precipitation is formed by simply mixing precipitants (ammonia or sodium hydroxide) and nickel sources. Then transfer the precipitation into a microwave oven to go deep reaction to obtain NiO nanostructures such as nanospheres, nanoflakes, nanoplates, nanoparticles.[93-97] These MS-NiO nanostructures show a capacity of 884 mAh g^{-1} and a pseudocapacitane of (277–585 F g^{-1}).[93, 94, 96, 97]

3. Cobalt oxides and cobalt oxides-based composites

Cobalt oxides (Co_3O_4 and CoO) have attracted great attention for EES due to their excellent electrochemical reactivity and redox reversibility since the pioneering works of Tarason's group and Conway et al.[3, 4] Co_3O_4 is a black antiferromagnetic solid with a band gap of ~2.0 V. As a mixed valence compound, its formula is sometimes written as $Co^{II}Co^{III}{}_2O_4$, which adopts the normal spinel structure, with Co^{2+} ions in tetrahedral interstices and Co^{3+} ions in the octahedral interstices of the cubic close-packed lattice of oxide anions. The spinel Co_3O_4 is a magnetic semiconductor with a lattice constant a=0.808 nm (JCPDS 42-1467). The other interesting cobalt oxide is CoO (cobalt monoxide), which has rock salt structure (NaCl structure, JCPDS 09-0402) consists of two interpenetrating fcc sublattices of Co^{2+} and O^{2-} with a lattice constant of 0.426 nm and a band gap of ~2.6 V. The CoO is not stable in the air and will be oxidized into the thermodynamically favoured form–Co_3O_4. In view of their high capacity (LIBs: the theoretical capacity of Co_3O_4 and CoO is 890 mAh g^{-1} and 718 mAh g^{-1}, respectively) and capacitance (Supercapacitors: a theoretical capacitance of >2000 F g^{-1}), the cobalt oxides (Co_3O_4 and CoO) have been extensively studied as active materials for EES. Numerous nanostructured cobalt oxides (such as nanowires, nanoflakes, nanocage, nanorods, nanoparticles nanobowls and nanospheres) have been prepared by different solution-based synthesis methods and enhanced electrochemical performances have been demonstrated in these systems.

3.1 Hydrothermal synthesis and solvothermal synthesis of cobalt oxides and cobalt oxides-based composites

Among all the solution-based synthetic routes for the synthesis of cobalt oxides for EES, HT is the most popular solution synthesis method and the published HT papers account for ~40 % in all the published solution-based literature. Combined with our works, we introduce one of the most fascinating HT methods for the preparation of cobalt oxides (Co_3O_4 and CoO) nanowire arrays and their composite materials. In our case, we used $Co(NO_3)_2$ (can also be

$CoSO_4$ or $CoCl_2$), NH_4F and urea as the starting materials and the whole reactions were conducted at 110−120 °C. The involved HT reactions can be illustrated as follows:[31, 98-102]

$$Co^{2+} + xF^- \rightarrow [CoF_x]^{(x-2)-} \quad (3.1)$$

$$H_2NCoNH_2 + H_2O \rightarrow 2NH_3 + CO_2 \quad (3.2)$$

$$CO_2 + H_2O \rightarrow CO_3^{2-} + 2H^+ \quad (3.3)$$

$$NH_3 \cdot H_2O \rightarrow NH_4^+ + OH^- \quad (3.4)$$

$$2[CoF_x]^{(x-2)-} + CO_3^{2-} + 2OH^- + nH_2O \rightarrow Co_2(OH)_2CO_3 \cdot nH_2O + 2xF^- \quad (3.5)$$

The Co_3O_4 and CoO nanowires can be formed after heat treatment under different atmospheres: Co_3O_4 in air and CoO in pure argon or nitrogen. If the argon is just normal, not high-purity, the final product will also be Co_3O_4 nanowires. The different reactions in the annealing process are as follows:

During the annealing process for Co_3O_4 nanowires:[2, 31]

$$3Co_2(OH)_2CO_3 \cdot nH_2O + O_2 \rightarrow 2Co_3O_4 + (3n+3)H_2O + 3CO_2 \quad (3.6)$$

During annealing process for CoO nanowires:[100, 101]

$$Co_2(OH)_2CO_3 \cdot nH_2O \rightarrow 2CoO + CO_2 + (n+1)H_2O \quad (3.7)$$

The cobalt oxides (Co_3O_4 or CoO) nanowires show sharp tips and have an average diameter of ~80 nm, length up to around 5–25 μm (Figure 6). The length of nanowires could be easily controlled by the growth time. The as-prepared Co_3O_4 or CoO nanowires consist of numerous interconnected nanoparticles and presents a rough appearance with a large quantity of mesoporous structure, which is ascribed to the successive release and loss of CO_2 and H_2O during the thermal decomposition of $Co_2(OH)_2CO_3$ precursor,[102-105] which is single crystalline in nature.[103]

The above HT-cobalt oxides can be grown on almost all the substrates including ITO, FTO, glass slide, nickel foam, carbon cloth, Ti foil, nickel foil, copper foil and stainless steel and so on.[2, 31, 98-101, 103, 106] In the HT solution, the powder products can be collected and are some

interesting cobalt oxides (Co_3O_4 or CoO) nanostructures (such as balls, spheres and hexapods) assembled by nanowires.[107-110] The NH_4F in the above HT method is acted as the growth promoter to improve the growth density of nanowires and prompt the formation of basic cobalt carbonate hydroxide precursor. Another problem to be noticed is that the reaction time also has great influence on the morphology of samples. When the time is less than 3 h, the products may not be nanowires, but nanoflakes. This special change is still under investigation.

The as-prepared HT-Co_3O_4 and HT-CoO nanowire arrays are well characterized as electrode materials for LIBs and supercapcitors. For supercapacitors application, the cobalt oxides (Co_3O_4 and CoO) undergo reversible redox reactions in the alkaline electrolyte. The reactions for Co_3O_4 in supercapacitors are illustrated as follows:[98, 106, 111-113]

$$Co_3O_4 + OH^- + H_2O \leftrightarrow 3CoOOH + e^- \quad (3.8)$$

$$CoOOH + OH^- \leftrightarrow CoO_2 + H_2O + e^- \quad (3.9)$$

The electrochemical reactions for CoO are expressed d as follows:[31, 111, 114, 115]

$$CoO + OH^- \leftrightarrow CoOOH + e^- \quad (3.10)$$

$$CoOOH + OH^- \leftrightarrow CoO_2 + H_2O + e^- \quad (3.11)$$

These cobalt oxides (Co_3O_4 or CoO) nanowire arrays exhibit noticeable pseudocapacitive performances with high capacitance of 754 F g^{-1} at 2 A g^{-1} and 610 F g^{-1} at 40 A g^{-1} as well as excellent cycling stability.[100, 101, 103] Generally, two redox peaks will be found in the CV curves of cobalt oxides (Co_3O_4 or CoO) nanowire array, namely, CoOOH and CoO_2 will be formed at high oxidation potentials. CoOOH has been detected and confirmed, but CoO_2, sometimes, is considered as a virtual state, or not stable.

For LIBs application, the cobalt oxides (Co_3O_4 and CoO) can reversibly react with Li ion to store electrochemical energy and show promising applications as anode materials. The corresponding simplified reactions are expressed as follows:

Reactions for Co_3O_4 with Li ion:[116]

$$Co_3O_4 + 8\ Li^+ + 8e^- \leftrightarrow 4Li_2O + 3\ Co \quad (3.12)$$

$$8\ Li \leftrightarrow 8Li^+ + 8e^- \quad (3.13)$$

$$Co_3O_4 + 8\ Li \leftrightarrow 4Li_2O + 3\ Co\ (Overall) \quad (3.13)$$

Reactions for CoO with Li ion:[4, 117]

$$CoO + 2\ Li^+ + 2e^- \leftrightarrow Li_2O + Co \quad (3.14)$$

$$2\ Li \leftrightarrow 2Li^+ + 2e^- \quad (3.15)$$

$$CoO + 2\ Li \leftrightarrow Li_2O + Co\ (Overall) \quad (3.16)$$

The as-prepared HT-Co_3O_4 and HT-CoO nanowire arrays as anode of LIBs show high capacity more than 800 mAh g^{-1} (1167 mAh g^{-1} at 0.5C and 903 mAh g^{-1} at 1 C).[104, 105, 108, 110] The enhanced EES performance is due to the unique one-dimensional (1D) architecture, which provides fast diffusion paths for ions and facilitates the electron and ion transfer on the cobalt oxide/electrolyte interfaces. Moreover, the 1D nanowire array can accommodate the volume expansion and restrain the pulverization and deterioration of Co_3O_4/CoO during the repeated cycling process, resulting in enhanced cycling stability. Inspired by these interesting and fascinating results, new composites based on the HT-Co_3O_4 and HT-CoO nanowires have emerged and show noticeable and enhanced EES performance than the bare cobalt oxide nanowires. We developed several HT-Co_3O_4 and HT-CoO based core/shell nanowire arrays (e.g., Co_3O_4/C, Co_3O_4/MnO_2, Co_3O_4/NiO and Co_3O_4/$Co(OH)_2$, CoO/$Ni(OH)_2$, CoO/TiO_2, Co_3O_4/Fe_2O_3)[8, 31, 56, 98, 100-102, 118] and demonstrated their enhanced LIBs and supercapacitor performances with higher capacity and capacitances (even two times larger than the unmodified counterparts), and excellent cycling stability. Similar enhanced results have also been proven in other advanced composite nanowires such as Mo-decorated Co_3O_4, Co_3O_4@Pt@MnO_2, Co_3O_4@$NiCo_2O_4$, Co_3O_4@$Ni(OH)_2$, Co_9S//Co_3O_4@RuO_2 and CoO@Polypyrrole.[114, 119-123] The high capacity/capacitance and cycling stability in the core/shell systems are believed to benefit from the the unique architecture including the porous cobalt oxides core nanowire, nanostructured shell and ordered array configuration. (1)

The highly porous system shortens the transportation/diffusion path for both electrons and ions, thus leading to faster kinetics and high-rate capability; (2) High surface area of the mesoporous nanowire arrays favors the efficient contact between active materials and electrolytes, providing more active sites for electrochemical reactions; (3) The porous core/shell nanowire array architecture possess favorably morphological stability, which helps to alleviate the structure damage caused by volume expansion during the cycling process. In short, these characteristics would lead to fast ion/electron transfer, sufficient contact between active materials and electrolyte, and enhanced flexibility, finally resulting in enhanced electrochemical performance. In addition, we found that the active material deposited on 3D porous substrates (such as nickel foam) shows better electrochemical performance than their counterparts on the flat substrate, due to the fact that the 3D porous substrates provide higher active surface area and inner space for fast ion/electron transfer and higher energy conversion efficiency.

Notice that the cobalt oxides (Co_3O_4 or CoO) nanowires can also be prepared without NH_4F, but the obtained nanowires are much thinner and prone to be bending. The reactions of precursor are shown as follows:[112, 124-127]

$$H_2NCoNH_2 + H_2O \rightarrow 2NH_3 + CO_2 \quad (3.17)$$

$$NH_3{\cdot}H_2O \rightarrow NH_4 + OH^- \quad (3.18)$$

$$CO_2 + H_2O \rightarrow CO_3^{2-} + 2H^+ \quad (3.19)$$

$$2Co^{2+} + 2CO_3^{2-} + 2OH^- \rightarrow Co_2(OH)_2CO_3 \quad (3.20)$$

It is noteworthy that the chemical formula of $Co_2(OH)_2CO_3$ precursor is complex, sometimes it will contain the anions in the cobalt source (e. g., Cl^-, SO_4^- and NO_3^{2-}). Lot of cobalt oxides nanostructures (e.g., nanorod, echinus-like, emongrass-like, chrysanthemum-like, nanosphere, nanowire, nanoflake, nanoplate, nanocube, nanonet) and composites (Co_3O_4/graphene and Co_3O_4/carbon), [107, 111, 124, 126-137] have been fabricated by the HT method only with urea and cobalt sources, and showed high LIBs capacity of (700–100 mAh g^{-1}),[107,

[124, 130, 131] and delivered large specific capacitances (500–1124 F g^{-1}) at high charge/discharge rate.[111, 112, 125, 127-129]. Even so, researchers prefer the first HT method with NH_4F because the quality of the final cobalt oxides samples is much higher with better structural control and adhesion on the substrates and higher active materials load.

When the precipitant is hexamethylenetetramine (HMT), the reactions and precursor will be different, shown as follows.[138, 139]

$$(CH_2)_6N_4 + 10H_2O \rightarrow 6HCHO + 4OH^- + 4NH_4^+ \quad (3.21)$$

$$Co^{2+} + 2OH^- \rightarrow Co(OH)_2 \quad (3.22)$$

During the annealing process:

In air: $$6Co(OH)_2 + O_2 \rightarrow 2Co_3O_4 + 6H_2O \quad (3.23)$$

In argon: $$Co(OH)_2 \rightarrow CoO + H_2O \quad (3.24)$$

If the precipitant is ammonia or NaOH, the reactions of precursor are much easier as follow.[133, 140-142]

$$NH_3 \cdot H_2O \leftrightarrow NH_4^+ + OH^- \quad (3.25)$$

or $$NaOH \rightarrow Na^+ + OH^- \quad (3.26)$$

$$Co^{2+} + 2OH^- \rightarrow Co(OH)_2 \quad (3.27)$$

When the precipitant is oxalate, $(NH_4)_2C_2O_4$, the reactions of precursor are as follow.[143]

$$Co^{2+} + (NH_4)_2C_2O_4 \rightarrow CoC_2O_4 \cdot + 2NH_4^+ \quad (3.28)$$

Meanwhile, some other organic precipitants (e.g., ethylene glycol, ethanol, L-arginine, polyethylene glycol, lysine) are also used for the preparation of nanostructured cobalt oxides (nanoparticel, nanoflake, nanowire, nanosphere),[109, 117, 144-149] and composites with graphene and carbon.[109, 150] The specific reactions associated with the hydrolysis of these organic

precipitants, are still not clear and under investigation. Additionally, some HT reactions just utilize the hydrolysis of cobalt source such as $Co(NO_3)_2$ at high temperature to form precursor.[151, 152] This HT is always used to prepare composite materials, particularly with graphene or carbon.

After analysing the HT-cobalt oxides papers, we found that the HT-cobalt oxides (Co_3O_4 and CoO) nanowire arrays are very popular with researches and can be easily fabricated in controllable manner, which could not be realized by other solution synthesis method. Moreover, the obtained porous HT-cobalt oxides (Co_3O_4 and CoO) nanowire arrays exhibit good EES performance with high capacitance/capacity. Additionally, they are good templates or scaffolds for constructing new high-performance core/shell nanoarrays or composites. Nowadays, in order to further improve the EES performance, great efforts are focusing on the modification of HT-cobalt oxides (Co_3O_4 and CoO) nanowires by introducing graphene, metal, carbon nanotube and conducting polymers to get composite materials with new or improved functions. The introduction of conductive backbone or coating can improve the conductivity of the bare nanowires leading to enhanced electrochemical properties.

Solvothermal synthesis (ST) is the twin brother of HT. The literature of ST for the synthesis of cobalt oxides (Co_3O_4 and CoO) nanostructures is not as much as that of HT. Several cobalt oxides (Co_3O_4 and CoO) nanostructures (such as nanocapsules, nanosheets, nanpsheres and nanoflower) have been obtained in the organic solvents including methanol, ethanol and ethylene glycol.[153-159] Detailed reactions have not been studied and shown in these papers. The EES performances of the ST-cobalt oxides are comparable to those prepared by HT.

3.2 Chemical precipitation synthesis of cobalt oxides and cobalt oxides-based composites

The second-popular solution synthesis method of cobalt oxides (Co_3O_4 and CoO) is chemical precipitation (CP), which is regarded as the easiest chemical method for the

fabrication of metal oxides. CP only need to mix the cobalt sources ($Co(NO_3)_2$, $CoSO_4$, $CoCl_2$, etc.) and precipitants (ammonia, NaOH, KOH, Na_2CO_3, $K_2C_2O_4$, etc.) to produce precipitation under appropriate PH values. The involved reactions of precursors in CP are always very simple, expressed as follows.

$$Co^{2+} + 2OH^- \rightarrow Co(OH)_2 \quad (3.29)$$

or $$Co^{2+} + 2CO_3^{2-} \rightarrow CoCO_3 \quad (3.30)$$

or $$Co^{2+} + 2C_2O_4^{2-} \rightarrow Co\ C_2O_4 \quad (3.31)$$

Then the precursor converts into Co_3O_4 or CoO after annealing in different atmospheres. The CP process is very easy to process and suitable for large-scale preparation. The CP papers account for ~28 % in all the published solution-based papers of cobalt oxides for EES applications.

Common CP process is very fast and difficult to precisely control the morphology of metal oxides due to the fast precipitation. Though some unique nanostructured cobalt oxides (Co_3O_4 and CoO) have been realized by the CP, this controllable synthesis needs to be conducted with the help of some hard or soft templates (AAO, virus, carbon nanotube, surfactant, etc.).[116, 160, 161] Here, we first introduce a template-free method to fabricate cobalt oxide nanotubes developed by Lou's group.[162] Lou et al. used $Co(NO_3)_2$ and ammonia as the starting materials to form needle-like Co_3O_4 nanotubes in refluxed condition at 95–100 °C for 20 h. Firstly, a dense β-$Co(OH)_2$ nanowire will be formed according to the reaction:[162]

$$Co^{2+} + 2OH^- \rightarrow Co(OH)_2 \quad (3.32)$$

Then the $Co(OH)_2$ are oxidized into Co_3O_4 by O_2 in the solution: [162]

$$Co(OH)_2 + O_2 \rightarrow Co_3O_4 \quad (3.33)$$

The as-prepared needle-like nanotubes are cylindrical and constructed from Co_3O_4 building-blocks of less than 100 nm (Figure 7). As anode for LIBs, the needle-like Co_3O_4 nanotubes deliver a capacity of 918 mAh g^{-1}. The key point in this method is that the oxygen

must be sufficient to drive the reaction. Therefore, the reaction is conducted in refluxed condition to add the amount of oxygen in the solution. The samples are powder form, and can be scale-up deposition.

As for the template-assisted CP of cobalt oxides, Kim' group.[116, 163] and Du et al.[160] adopted M13 virus and carbon nanotube as the sacrificial templates for the fabrication of Co_3O_4 nanowire and nanotubes, respectively. The reactions are illustrated as below.[160]

$$Co_4(CO)_{12} \rightarrow 4Co + 12\ CO \qquad (3.34)$$

$$Co + xO_2 \rightarrow CoO_{x/2} \qquad (3.35)$$

The template-synthesized Co_3O_4 nanowire and nanotubes show high capacity of 900–200 mAh g^{-1} and good cycling stability for LIBs. These Co_3O_4 products are high quality, but the template-CP is tedious, requiring multiple synthetic steps, caustic chemical treatments, and long curing times. Meanwhile, the scale-up has also proven difficult and is not cost-effective due to the destruction of (relatively) expensive templates.

Meanwhile, numerous nanostructured cobalt oxides (e.g., nanowire, nanocage, nanoflake, nanorod, nanobox) are fabricated by other research groups and applied as active materials for EES by different CP methods. [108, 164-173] As cathode materials for supercapacitors, these CP-cobalt oxides present capacitances of 200–800 F g^{-1}, and the film samples show better performance. Furthermore, lots of cobalt oxides/graphene or cobalt oxides/carbon composites have been reported and showed enhanced EES performance than those pure materials due to the introduction of highly conductive carbon network.[161, 174-179] In recent years, this modification is mainly focused on graphene based composites, and the improvement is especially reflected in the improved cycling stability.

3.3 Electrochemical synthesis of cobalt oxides and cobalt oxides-based composites

Most of the published papers about ED of cobalt oxides for EES are based on a cathodic ED. The cathodic ED is mainly used for the synthesis of film samples, not powder form. This

cathodic ED can be performed in a standard three-electrode glass cell, with the conductive substrate as the working electrode, saturated calomel electrode (SCE) as the reference electrode and a Pt foil as the counter-electrode. In this configuation, the cobalt source must be $Co(NO_3)_2$, while other cobalt sources are not applicable due to the unique reaction mechanism. The ED process is expressed as follows.[57, 180-182]

$$NO_3^- + H_2O + 2e^- \rightarrow NO_2^- + 2OH^- \quad (3.36)$$

$$Co^{2+} + 2OH^- \rightarrow Co(OH)_2 \quad (3.37)$$

During the annealing process:[183-188]

In air: $$6Co(OH)_2 + O_2 \rightarrow 2Co_3O_4 + 6H_2O \quad (3.38)$$

In argon: $$Co(OH)_2 \rightarrow CoO + H_2O \quad (3.39)$$

Note that this ED process includes an electrochemical reaction and a precipitation reaction. In addition, metallic Co cannot form because the reaction potential of Co^{2+}/Co is much more negative than that of NO_3^-/NO_2^-during the electrochemical reduction process.[57] This ED is general, versatile and applicable to almost all conductive substrates. The thickness of the film is controlled by the reaction time and deposition current density. The as-electrodeposited precursor $Co(OH)_2$ film exhibits a porous structure consisting of randomly net-like arranged nanoflakes. This preferential growth is because that $Co(OH)_2$ crystal has a layered structure of the CdI_2 type, which shows weak interaction between layers and strong binding within the layered planes, and finally forms 2D nanoflake. After heat treatment, the cobalt oxide keeps the morphology of $Co(OH)_2$ precursor and shows nanoflake arrays architecture.

The ED-cobalt oxides (Co_3O_4 and CoO) are evaluated as cathode for supercapacitor and exhibit capacitances of 200–400 F g^{-1}. Our group prepared mesoporous Co_3O_4 monolayer hollow-sphere array by the above ED via a polystyrene (PS) sphere colloidal monolayer template (Figure 8).[186] The Co_3O_4 monolayer hollow-sphere array with mesoporous walls exhibits high pseudocapacitances of 358 F g^{-1} at 2 A g^{-1}, as well as excellent cycling stability

for application as pseudocapacitors. This ED can be easily combined with other methods to fabricate cobalt oxide based composites. For example, Li et al. reported Co_3O_4/$Ni(OH)_2$ composite mesoporous nanosheet networks and showed improved capacitance of 1144 F g^{-1}.[189] On the other hand, for LIBs application, the capacity of ED-cobalt oxides (Co_3O_4 and CoO) reaches to 500–900 mAh g^{-1}. Co_3O_4/TiO_2 and Co_3O_4/graphene composites are fabricated and also deliver enhanced capacities of about 1100 mAh g^{-1}.[182, 190]

The other cathodic ED is to deposit metallic Co which is then oxidized into CoO_x:[182, 191]

$$Co + 2/3\ O_2 \rightarrow 1/3\ Co_3O_4 \qquad (3.40)$$

In the metal based ED, the cobalt source is not limited to $Co(NO_3)_2$, other suitable sources can be $CoSO_4$, $Co(NO_3)_2$, $CoCl_2$, and $Co(CH_3COO)_2$.

3.4 Sol-gel and microwave synthesis and chemical bath deposition of cobalt oxides and cobalt oxides-based composites

Sol-gel synthesis is a facile method for the fabrication of cobalt oxides and cobalt oxides-based composites. We take the work of Lin et al. for example for the illustration of reaction mechanism of cobalt oxides nanoparticles.[192] $CoC1_2$, $NaOC_2H_5$ and dehydrated EtOH are used as the starting materials and solvent, and the main reactions are expressed as follow.[192]

$$CoC1_2 + 2NaOC_2H_5 \rightarrow Co(OC_2H_5)_2 + 2\ NaCl \qquad (3.41)$$

$$Co(OC_2H_5)_2 + 2H_2O \rightarrow Co(OH)_2 + 2HOC_2H_5 \qquad (3.42)$$

The above chemistry reactions lead to the formation of unique cobalt oxides via the hydrolysis and condensation of the cobalt alkoxide. The capacitance of the obtained cobalt oxides (Co_3O_4 and CoO) is not high, only ~175 F g^{-1}. In addition, Liu et al. reported sol-gel NiO/$NiCo_2O_4$/Co_3O_4 by using $CoCl_2$ and propylene and exhibited a high specific capacitance of 1717 F g^{-1}.[92]

Several Cobalt oxides nanoparticles and composites with carbon nanotube have been reported via different sol-gel techniques for LIBs. Generally, these sol-gel methods belong to

polymeric (or alkoxide) route with lots of organic solvents such as ethanol, isopropyl alcohol, cyclodextrin, citric acid, and polyvinyl pyrrolidone.[193-197] The specific sol-gel mechanism is different due to different solvents and starting materials. The sol-gel-cobalt oxide/CNT delivered much higher capacity than the pure ones, even two times larger.[194]

As for the microwave synthesis (MS) of cobalt oxides and cobalt oxides-based composites, it usually mix the cobalt sources ($CoSO_4$, $Co(NO_3)_2$, $CoCl_2$, and $Co(CH_3COO)_2$) and precipitants (ammonia, HMT, urea) together and then let the reactions take place under microwave oven. Cobalt oxide nanostructures (nanoparticles, nanorods, nanosheets and graphene composite) are fabricated and show a high capacity of 931 mAh g^{-1} and a capacitance of 519 F g^{-1}.[198-206]

In the following paragraphs, we focus on the CBD method for the synthesis of cobalt oxides and cobalt oxides-based composites. This CBD method was first proposed by Wu' group for the fabrication of free-standing Co_3O_4 nanowire arrays in 2006. The specific reactions are illustrated as follows.[207]

$$Co^{2+} + 6NH_3 \leftrightarrow [Co(NH_3)_6]^{2+} \quad (3.43)$$

$$[Co(NH_3)_6]^{2+} + 2OH^- \rightarrow Co(OH)_2 + 6NH_3 \quad (3.44)$$

$$6\,Co(OH)_2 + O_2 \rightarrow 2Co_3O_4 + 6H_2O \quad (3.45)$$

The formation of the hollow CBD-Co_3O_4 nanowire arrays is proposed to the synergy between axial screw dislocation and Kirkendall effect.[36, 56, 207] These CBD-Co_3O_4 nanowire arrays can be formed on arbitrary substrates. It should be mentioned that oxygen is indispensable for preparing vertically aligned Co_3O_4 nanowire arrays in this experiment. The oxygen in the solution helps to form $Co(OH)_2$ nanowire precursors. Without oxygen, only interconnected $Co(OH)_2$ nanowall films are formed on the substrate. The film quality is also related with the substrates position in the reaction solution. The substrates should be 2 mm away from the bottom of the vessel. Each nanowire is about 500 nm in diameter and about 15

μm in length (Figure 9). The nanowires on Ti foil show a capacity of 700 mAh g^{-1} for LIBS,[208] and the sample on nickel foam exhibited a high capacitance of 746 F g^{-1}.[209]

4. Copper oxides and copper oxides-based composites

Copper oxides are one of the most attractive classes of transition metal oxides with widely applications in energy conversion devices (anode material for LIBs or cathode material for supercapacitors) and optoelectronic devices. Copper forms two oxides in accordance with its two valences: cuprous oxide (Cu_2O) and cupric oxide (CuO). Both are semiconductors with band gaps of 2.0 eV and 1.2 eV, respectively. Their band gaps make them good candidates for photovoltaic devices (e.g. solar cells and water splitting), catalysts, sensors and optoelectronic devices.[210]

Cu_2O crystallizes in a simple cubic structure which can be considered as two sublattices, a facecentered cubic (fcc) sublattice of copper cations and a body-centered cubic (bcc) sublattice of oxygen anions (JCPDS 05-0667). The oxygen atoms occupy tetrahedral interstitial positions relative to the copper sublattice, so that oxygen is tetrahedrally coordinated by copper, whereas copper is linearly coordinated by two neighboring oxygens. These low coordination numbers are very unusual for metal oxides (only by two other substances, Ag_2O and Pb_2O, have the similar crystal structure). The other copper oxide, CuO, crystallizes with a monoclinic unit cell (JCPDS Card No. 41-0254), with a crystallographic point group of 2/m or C_{2h}. Its space group of its unit cell is $C_{2/c}$. The theoretic capacity of CuO and Cu_2O as Li-ion battery anode is 670 and 374 mAh g^{-1}, respectively. Various CuO and Cu_2O nanostructures have been prepared by different solution-based synthetic methods and applied as active materials for EES with enhanced electrochemical performances. We mainly focus on the mainstream solution-based synthesis methods of copper oxides for EES application.

4.1 Chemical precipitation synthesis of Copper Oxide and Copper Oxides-based composites

Among all the solution-based synthetic routes for the synthesis of copper oxides for EES, CP is the most popular solution synthesis method and the published CP papers account for ~50 % in all the published solution-based literature. Copper nitrate, copper chloride, copper sulfate and copper acetate are the most widely used copper sources. The adopted precipitants are common reagents such as ammonia and NaOH.[211-214] In the following section, we introduce some typical CP methods for the synthesis of hierarchical copper oxides with various morphologies.[215]

Previously, we fabricated various CuO nanostructures via a facile CP method by using $CuSO_4$ as the copper source and ammonia as the precipitant. The involved CP reactions can be illustrated as follows:[215]

$$Cu^{2+} + 2NH_3 \cdot H_2O \rightarrow Cu(OH)_2 + 2NH_4^+ \qquad (4.1)$$

$$Cu(OH)_2 \rightarrow CuO + H_2O \qquad (4.2)$$

The nanostructured CuO products are obtained after reacting for 12 h at 90 ^oC. In our case, the PH value has a great influence on the morphology of the CuO products because there is a competing reaction in the solution expressed as follows.[215]

$$Cu(OH)_2 + 4NH_3 + 2NH^+ \rightarrow [Cu(NH_3)_4]^{2+} + 2NH_3 \cdot H_2O \quad (4.3)$$

Obviously, the $Cu(OH)_2$ could be dissolved due to the complex reaction for the existence of excess NH^{4+} and free NH_3 in the solution. There is no doubt that different pH value will lead to different concentrations of $[Cu(NH_3)_4]^{2+}$ and OH^- in the solutions, and finally resulting in the formation of CuO with various morphologies such as leaf, shuttle, flower, dandelion, and caddice clew. These morphologies can be easily tailored by adjusting the pH value, indicating that the PH value is critical for the controllable growth of copper oxides in the CP method.

The PH effect is also demonstrated in other works. Park et al. reported a similar morphology evolution by changing the PH value in the CP solution.[211] It is found that the Cu_2O nanocubes could be converted to polycrystalline CuO hollow nanostructures through a sequential dissolution–precipitation process (Figure 10), by adding aqueous ammonia solutions in air. Increasing the pH of the solution leads to the formation of hollow cubes, hollow spheres, and urchin-like particles. The involved reactions are as follows.

$$Cu_2O + 0.5\ O_2 + 2H_2O + 8NH_3 \rightarrow 2[Cu(NH_3)_4]^{2+} + 4OH^- \quad (4.4)$$

$$[Cu(NH_3)_4]^{2+} + 2OH^- \rightarrow Cu(OH)_2 + 4NH_3 \quad (4.5)$$

$$Cu(OH)_2 + 2OH^- \rightarrow [Cu(OH)_4]^{2-} \quad (4.6)$$

$$[Cu(OH)_4]^{2-} \leftrightarrow CuO + 2OH^- + H_2O \quad (4.7)$$

The morphology of CP-copper oxides is also affected by other parameters such as the addition sequence of reagents. Tang's group found that the morphology of CP-CuO is also related with the order of addition of the reactive materials.[216] They reported CuO nanoribbons and nanoflowers from the same reaction system by varying the order of addition of the reactive materials.

For LIBs application, the copper oxides (CuO and Cu_2O) can reversibly react with Li ion to store electrochemical energy and the corresponding simplified reactions are expressed as follows:

Reactions for CuO with Li ion:[217, 218]

$$2CuO + 2Li^+ + 2e^- \leftrightarrow Cu_2O + Li_2O \quad (4.8)$$

$$Cu_2O + 2Li^+ + 2e^- \leftrightarrow 2Cu + Li_2O \quad (4.9)$$

As for Cu_2O, only the eqn. (4.9) occurs for LIBs. It is observed that the LIBs performance of copper oxides is tightly associated with the morphology of samples. CuO samples with different morphologies show distinct electrochemical performances. Taking our work for example, compared to others CuO nanostructures, dandelion-like and caddice clew-like CuO prepared by our group exhibit reversible discharge capacities of 385 mAh g^{-1} and 400 mAh

g^{-1} at 0.1 C, 340 mAh g^{-1} and 374 mAh g^{-1} at 0.5 C after 50 cycles, respectively.[215] The higher discharge capacities and better cycling performances are attributed to their larger surface area and porosity, leading to better contact between CuO and electrolyte and shorter diffusion length of lithium ions.

Inspired by the above works, we adopted a surfactant, cetyltrimethylammonium bromide (CTAB),[219] to modify the surface morphology of CuO spheres via a similar CP method. Ordered nano-needle arrays can be formed on the surface of the CuO spheres by the aid of CTAB. Each CuO sphere is about 2 μm in diameter and possesses a large number of nano-needles that are about 20–40 nm in width and more than 300 nm in length. The needle-like hierarchical structure can greatly increase the contact area between CuO and electrolyte, which provides more sites for Li^+ accommodation, shortens the diffusion length of Li^+ and enhances the reactivity of electrode reaction, especially at high rates. After 50 cycles, the reversible capacity of the prepared needle-like CuO can sustain a capacity of 441 mAh g^{-1}. Additionally, we used $N_2H_4{\cdot}H_2O$ to replace ammonia to prepare Cu_2O/Cu core/shell nanosphere composites. The corresponding reactions are described as below.[214]

$$N_2H_4 + 4Cu(OH)_4^{2-} \rightarrow 2Cu_2O + N_2 + 6H_2O + 8OH^- \quad (4.10)$$

$$N_2H_4 + Cu_2O \rightarrow 4Cu + N_2 + 2H_2O \quad (4.11)$$

The core/shell Cu_2O/Cu exhibits weaker polarization, better cycling life and higher coulombic efficiency than the pure octahedral Cu_2O due to the conductivity modification by Cu. Meanwhile, in order to further improve the LIBs performance of CuO, we prepared CuO/MWCNT nanocomposite by the CP method with CTAB.[218] The MWCNTs are incorporated into the leaf-like CuO nanoplates and build up a network to connect the CuO nanoleaves. The as-prepared CuO/MWCNT exhibits superior reversible Li-ion storage, the capacity maintains 627 mAh g^{-1} after 50 cycles. The improved capability is ascribed to the MWCNT conductive network in the composite. Graphene/CuO composites re also realized in the above CP method and enhance electrochemical performance is proved.[212, 220] Similar

enhancement was reported by Ko et al., who prepared CP-mesoporous CuO/CNTs with a capacity of 600 mAh g^{-1} at 5C (Figure 11).[221]

When CuO is applied for supercapacitors, the following redox reactions may be involved in the change between Cu(I) and Cu(II) species:[213, 222, 223]

$$CuO + 1/2H_2O + e^- \leftrightarrow 1/2Cu_2O + OH^- \quad (4.12)$$

Or $$CuO + H_2O + e^- \leftrightarrow CuOH + OH^- \quad (4.13)$$

But we have to point out that the copper oxides are not good active materials candidate for supercapacitors due to its poor electrochemical redox reactivity, and low discharge voltage in alkaline electrolyte, as compared to other metal oxides such as cobalt oxides and nickel oxides[3]. On the other hand, high-performance copper oxides based composites have attracted great attention, and great efforts are focusing on the modification of CP-copper oxides by introducing graphene,[212, 220, 222] metal[214], and carbon nanotube[213, 218, 221, 224] by CP method to further improve the EES performance. The introduction of conductive backbone or coating can improve the conductivity of the bare copper oxides leading to enhanced electrochemical properties.

4.2 Hydrothermal synthesis and solvothermal synthesis method of Copper Oxide and Copper Oxides-based composites

HT and ST are facial solution-based ways to synthesize copper oxides. According to the published papers of HT/ST-copper oxides, one kind of copper sources is directly from the oxidization of Cu foil substrate.[225-227] The other kind of copper sources comes from copper salt, such as nitrate, copper sulfate and copper acetate.[2, 228-230] For the first kind source, we synthesized nanoflower-like CuO and CuO/Ni composite films directly on the copper foil in the mixed solution of NaOH and $(NH_4)_2S_2O_8$. The reactions occurred in this process can be summarized as follows:[226, 231]

$$Cu + 4OH^- + (NH_4)_2S_2O_8 \rightarrow Cu(OH)_2 + 2SO_4^{2-} + 2NH_3 + 2H_2O \quad (4.14)$$

$$Cu(OH)_2 \rightarrow CuO + H_2O \quad (4.15)$$

The copper substrates are used not only as a source of copper but also as a support for the copper compound films. Note the fact that the pH value plays a vital role during the formation of the CuO film. When the reaction is carried out in acidic solution, no film is deposited on the copper surface. The copper will continuously be oxidized and dissolved, forming a blue solution. In pH range from 8 to 10, the copper foil loses its metallic luster, but there is still no perceptible solid deposit on it. When the molar ratio of $[NaOH]/[(NH_4)_2S_2O_8]$ is >10 and the concentration of NaOH is >1 M, the above reaction leads to the deposition of a blue precursor film on the copper foil. At elevated temperature and high pH value, the $Cu(OH)_2$ can be easily converted into CuO. The formation of $Cu(OH)_2$ and CuO nanostructures on copper surfaces involves inorganic polymerization (polycondensation) reactions under alkaline and oxidative conditions. Particle morphology may vary depending on synthetic conditions. Even aging in aqueous solution may bring about significant dimensional, morphological, and structural changes. As a brief summary, the growth of fiber and scroll films of $Cu(OH)_2$ and copper oxides can be controlled by varying the concentration of NaOH and the reaction time if $[NaOH]/[(NH_4)_2S_2O_8]$ is in the range of 10–40.[231] The obtained CuO/Ni composite film shows better LIBs performance than the pure CuO, and delivers a better capacity retention (96.3 %) than the pure CuO film (67.8 %).[226]

In addition, Zhang et al. synthesized gear-like CuO film directly on Cu substrate by ammonia. The formation mechanism from Cu to porous CuO nanoarrays can be interpreted as follows:[227]

$$Cu^{2+} + 4NH_3.H_2O \rightarrow Cu[NH_3]_4^{2+} + 2OH^- \quad (4.16)$$

$$Cu[NH_3]_4^{2+} + 2OH^- \rightarrow Cu(OH)_2 + 4NH_3 \quad (4.17)$$

$$Cu(OH)_2 \rightarrow CuO + H_2O \quad (4.18)$$

In the above reaction process, the HT parameters (such as the reaction time, concentration of ammonia solution and reaction temperature) have great influence on the reaction rate and morphology of the final CuO film. The as-prepared gear-like CuO delivers a capacitance of

348 F g^{-1} at 1 A g^{-1}.[227] But the discharge voltage is negative (–0.3 V), indicating that the CuO is not a suitable pseudocapacitive material due to the poor working voltage window.

As for the second HT-copper oxides, Gund et al. fabricated nanosheet clusters of caddice clew, yarn ball and cabbage slash-like microstructures of copper oxides in the presence of different surfactants. The possible chemical reactions in the solution can be supposed as follows.[230]

$$8CuSO_4 + 4H_2O + (NH_4)_2S_2O_8 \rightarrow CuO + 8H_2SO_4 + 2NH_4SO_4 \quad (4.19)$$

$$2Cu_2O + O_2 \rightarrow 4CuO \quad (4.20)$$

These CuO microstructures show good surface properties like uniform surface morphology, good surface area and a uniform pore size distribution. The obtained CuO samples present a high specific capacitance of 535 F g^{-1}. In addition, Gao et al. constructed complex CuO hollow micro/nanostructures with the use of $CuSO_4$, ammonia and tyrosine.[229] These structures consist of CuO nanosheets, which self-organize into hollow micrometer-sized monoliths with a hierarchical architecture. The hierarchically hollow structures enhance mass transport in macroscales, promote the accessibility of the nanomaterials, and greatly facilitate dispersion, transportation, separation, and recycling of nanomaterials. The synthesized hierarchical CuO hollow micro/nanostructures exhibit a high discharge/charge capacity of 560 mAh g^{-1} for LIBs.[229]

In the following section, we introduce an important ST work of Lou's group for the synthesis of ST-copper oxides nanostructures including nanorodrods and nanosheets (Figure 12).[225] They developed a facile ST method with $Cu(NO_3)_2$ source and 2-proponal or ethanol solvent, and the possible main reactions are expressed as follow:

$$2\ Cu(NO_3)_2 \cdot 3H_2O \rightarrow Cu_2(OH)_3NO_3 + 3HNO_3 + 6\ H_2O \quad (4.21)$$

During the annealing process:

$$Cu_2(OH)_3NO_3\ (s) \rightarrow 2CuO\ (s) + HNO_3\ (g) + H_2O\ (g) \quad (4.22)$$

The morphology of $Cu_2(OH)_3NO_3$ nanostructures can be readily controlled by using different solvents, in which precursor supersaturation for nucleation and crystal growth is determined by solvent polarity and solubility. In the above method, notice that the precise control of precursor concentration and supersaturation plays a prime role in the synthesis of $Cu_2(OH)_3NO_3$ nanostructures and the degree of supersaturation directly determines the crystal growth mode. Generally both the concentration and supersaturation of the precursor for the formation of low-dimensional $Cu_2(OH)_3NO_3$ nanostructures must be kept at a relatively low level to avoid overwhelming isotropic growth or even homogeneous nucleation in the solution. The above chemistry reactions lead to the formation of unique copper oxides, nanorods (in 2-proponal) and nanosheets (in ethanol). The unique nanostructural copper oxide films show excellent electrochemical performance as demonstrated by high capacities of 450–650 mAh g^{-1} at 0.5–2 C and almost 100% capacity retention over 100 cycles after the second cycle.[225]

4.3 Electrochemical synthesis of Copper Oxide and Copper Oxides-based composites

Most of the published papers on ED of copper oxides for EES are based on a cathodic ED. Similar to the ED used for other metal oxides, the cathodic ED is mainly used for the synthesis of copper oxide film samples, not powder form. This cathodic ED can be conducted in either or standard three-electrode or two-electrode glass cell. Copper sulfate or copper acetate is used as the copper source and the final ED-copper oxide is Cu_2O, not CuO. Cu_2O is electrodeposited by reactions given as follows:[214, 232]

$$2Cu^{2+} + 2e^- + 2OH^- \rightarrow 2CuOH \rightarrow Cu_2O+H_2O \qquad (4.23)$$

The electrolyte of the above ED reaction is alkaline. If the PH is low, the competing reaction of Cu^{2+} to metallic copper will occur:[233]

$$Cu^{2+} + 2\ e^- \rightarrow Cu \qquad (4.24)$$

Our group reported highly ordered porous Cu_2O film via the above ED on copper foil through a self-assembled polystyrene sphere template. Compared with the dense Cu_2O film,

the ordered porous Cu_2O film exhibits an improved electrochemical cycling stability. The capacity of the porous Cu_2O film can maintain a capacity 336 mAh g^{-1} and 213 mAh g^{-1} after 50 cycles at the rate of 0.1 C and 5 C, respectively.[234] Flexible ED-CNTs/Cu_2O hybrid electrodes synthesized by Ajayan et al. exhibit superior electrochemical performance compared with pure CNTs.[235] Deng et al. synthesized the three-dimensionally ordered macroporous Cu_2O/Ni inverse opal electrodes for electrochemical supercapacitors by the similar method. The calculated capacitance of the as-prepared 3D Cu_2O/Ni electrode is 502 F g^{-1} (Figure 13).[236] The improved electrochemical performances due to their porous structure film, which provides not only the direct contact of active material/current collector but also the sufficient contact of active material/electrolyte. Enhanced EES performances are also demonstrated in some other ED-Cu_2O/CNT and Cu_2O/Ni composites systems.[235, 236]

5. MnO_2 and MnO_2-based composites

Though manganese oxides have several different forms and phases (such as MnO_2, Mn_2O_3, MnO and Mn_3O_4), MnO_2 is the one of the most fascinating manganese oxides for EES applications due to its high capacity/capacitance, earth abundance, low cost and environmental friendliness. It is well known that MnO_2 can exist in different structural forms (e.g., α (JCPDS 44-0141), β (JCPDS 24-0735), γ (JCPDS 14-0644), δ (JCPDS 80-1098), ε (JCPDS 30-0820,), λ (JCPDS 44-0992) type), when the basic structural unit ([MnO_6] octahedron) is linked in different ways. The difference in the above polymorphs lies in the arrangement of the Mn^{4+} within the octahedral sites. Based on the different [MnO_6] links, MnO_2 can be divided into three categories: the chain-like tunnel structure such as α, β and γ type; the sheet or layered structure such as δ-MnO_2, and the 3D structure such as λ-MnO_2. MnO_2 usually crystallizes in the rutile crystal structure with three-coordinate oxide and octahedral metal centres. The band gap of MnO_2 is 0.26–0.7 eV depending on different polymorphs (β-MnO_2 is ~0.26 eV and γ-MnO_2 is ~0.6 eV).

MnO_2 have been extensively studied as active materials in EES systems since last century. The widely known example is the electrolytic manganese dioxides (EMD), which are the current commercial cathode materials for high-energy alkaline primary battery, which is not the focus of this review and will not be discussed here. Meanwhile, in recent years, great efforts are devoted to fabricating MnO_2-based high-performance EES devices such as LIBs and supercapacitors. In particular, the MnO_2 is considered as the most promising metal oxide electrode materials for supercapacitors owing to its high working voltage (near 2 V in aqueous system), low cost, high capacitance (theoretical capacitance of ~1370 F g^{-1}) and easy-processing.[237] So far, the published papers about MnO_2 and MnO_2-based composites for supercapacitors are more than 350. This number even surpasses cobalt oxides and nickel oxides in terms of their combined supercapacitor research. The electrochemical properties of MnO_2 are significantly affected by their phases and morphologies. A great many MnO_2-based nanostructures have been reported and fabricated by different solution-based synthesis methods, and enhanced electrochemical performances have been demonstrated in these systems with promising practical applications. In this section, we will introduce some typical solution-based synthetic methods (hydrothermal synthesis, chemical precipitation and electro-deposition methods) for MnO_2 and MnO_2-based composites and focus on the specific reaction mechanisms as well as their EES performances.

5.1 Hydrothermal synthesis of MnO_2 and MnO_2-based composites

HT is one of the three most popular solution-based methods (hydrothermal synthesis, chemical precipitation and electro-deposition methods) for the synthesis of MnO_2 and MnO_2-based composites for EES. According to the reaction mechanisms and reagents, basically, there are about three kinds of HT methods for the fabrication of MnO_2 and MnO_2-based composites for EES. Herein, we introduce these three HT methods of MnO_2 in detail in the following paragraphs.

5.1.1 HT reactions with oxidant ($KMnO_4$) and reducing agent (such as C, Cu and ethanol)

The first kind of HT method of MnO_2 involves the chemical reactions between oxidant ($KMnO_4$) and reducing agent (such as C, Cu, ethanol and polyethylene glycol).[6, 238-246] Previously, our group adopted this facile HT method to fabricate self-supported Co_3O_4/MnO_2 core/shell nanowire arrays on Ti foil.[98] In our case, we used the amorphous carbon as the reducing agent and the reactions are expressed as follows.[241, 242, 244]

$$4MnO_4^- + 3C + H_2O \rightarrow 4MnO_2 + CO_3^{2-} + 2HCO_3^- \quad (5.1)$$

$$4MnO_4^- + 2H_2O \rightarrow 4MnO_2 + 4OH^- + 3O_2 \quad (5.2)$$

For the above reactions, when the $KMnO_4$ solution is mixed with the carbon source at room temperature before the hydrothermal processing, the nanocrystalline MnO_2 will be formed on the surface of the carbon source due to the slow redox process according to eqn. (5.1).[241] When the solution is further treated in the hydrothermal reaction, the nanoflaky MnO_2 grows from the preformed nanocrystalline due to the decomposition of $KMnO_4$ in water according to eqn. (5.2), where MnO_2 nanoflakes will be formed. Except for the amorphous carbon, the carbon source can also be CNT, graphene, carbon cloth and so on. The reaction in eqn. (5.1) will promote the reaction in eqn. (5.2) to take place. This main problem in this HT method is that it will consume the carbon source and hard to precisely control the morphology of MnO_2/carbon. In view of these characteristics, MnO_2 hollow nanostructures can be formed when the HT reaction occurs deeply and sacrifice the carbon template. The key point in this HT is to use a reducing agent to trigger the reaction. If the reducing agent is Cu or ethanol, the reactions in eqn. (5.1) will be different as shown as below:[238, 246]

$$2MnO_4^- + 3Cu + 4H_2O \rightarrow 2MnO_2 + 3Cu(OH)_2 + 2OH^- \quad (5.3)$$

$$MnO_4^- + CH_3CH_2OH \rightarrow MnO_2 + CH_3COOH + OH^- + 0.5\ H_2 \quad (5.4)$$

The obtained HT-MnO_2 shows nanoflake structure. In our experiment, the MnO_2 nanoflake are well decorated on the surface of Co_3O_4 nanowire core forming core/shell nanowire arrays (Figure 14), which exhibit excellent supercapcitor performance with high capacitance of 480 F g^{-1} at 2.67 A g^{-1}, good cycle life with 2.7 % capacitance loss after 5000 cycles and remarkable rate capability.[98] It is reported that the pseudocapacitive (Faradic) reactions occurring on the surface and in the bulk of the electrode are the major charge storage mechanisms for manganese oxides. The surface Faradaic reaction involves the surface adsorption of electrolyte cations on the manganese oxide, illustrated as follows.[98, 237, 242]

$$(MnO_2)_{surface} + C^+ + e^- \rightarrow 2\ (MnOOC)_{surface}\ (C+ = H^+, Li^+, Na^+, K^+\ldots)\ (5.5)$$

The bulk Faradaic reaction relies on the intercalation or deintercalation of electrolyte cations in the bulk of the manganese oxide:[98, 237]

$$MnO_2 + C^+ + e^- \rightarrow 2\ (MnOOC)_{surface}\ (C+ = H^+, Li^+, Na^+, K^+\ldots) \quad (5.6)$$

In our work, the redox process is mainly governed by the insertion and deinsertion of Li^+ and from the electrolyte into the porous nanostructured MnO_2 matrix. In addition, hierarchical TiO_2 nanobelts@MnO_2 ultrathin nanoflakes core/shell arrays were reported by the same HT method and showed a specific capacitance of 557 F g^{-1} as cathode for supercapacitors.[240] Some other MnO_2 nanostructures (such as nanosphere, hollow sphere, and tubular nanostructure) have also been fabricated by this HT method and applied as electrode materials for EES.[238, 242-244] However, the above as-prepare pure MnO_2 nanostructures show a capacitance lower than 400 F g^{-1} due to the poor conductivity of MnO_2.[242-244, 246] To effectively utilize MnO_2 materials, MnO_2 composites with carbon (e.g., MnO_2/C nanosphere, MnO_2/CNT, MnO_2/Graphene) are constructed and exhibit improved electrochemical performances than the pure counterparts.[241, 245, 247] On the other hand, the MnO_2 is a potential active material (either cathode or anode) for LIBs. The theoretical capacity of MnO_2 as LIBs anode is ~1232 mAh g^{-1}, and the reactions are described as follows.[241, 245, 248]

$$MnO_2 + 4Li \leftrightarrow Mn + 2Li_2O \quad (5.7)$$

As anode for LIBs, the carbon/MnO_2 nano-urchins exhibit a reversible capacity of 628 mAh g^{-1}.[245] The nanoflaky MnO_2/CNT nanocomposite electrode exhibits a large reversible capacity of 801 mA h g^{-1}.[241] Moreover, Gu et al. prepared branched nanorods of MnO_2/Fe_2O_3 by the above HT method and presented a reversible specific capacity of 1028 mAh g^{-1} at 1000 mA g^{-1} up to 200 cycles, much higher than the MnO_2 alone.[6] The improved electrochemical performance is due to the synergistic effect such as enhanced stability, better conductivity and stain accommodation.

5.1.2 HT reactions with high-valence oxidant ($KMnO_4$ or persulfate) and low-valence manganese sources such as $MnSO_4$ or $MnCl_2$

The reaction between $KMnO_4$ and $MnSO_4$ is given as below.[249-252]

$$3MnSO_4 + 2KMnO_4 + 2H_2O \rightarrow 5MnO_2 + 2H_2SO_4 + K_2SO_4 \qquad (5.8)$$

It is believed that this HT method is especially suitable for the preparation of composite materials with carbon because the first HT method needs to consume reducing agent such as carbon source and this will not happen here. During the reaction, the $MnSO_4$ will preferentially react with $KMnO_4$ to form nanoflake MnO_2. Of course, the concentration ratio between $MnSO_4$ and $KMnO_4$ should be controlled. Hence, the carbon backbone is always kept and served as a support for the deposition of MnO_2. Moreover, the morphology of the MnO_2 can be tuned by the hydrothermal time. When the oxidant is persulfate such as $K_2S_2O_8$ or $(NH_4)_2S_2O_8$, the specific reactions are shown as below.[253-256]

$$MnSO_4 + (NH_4)_2S_2O_8 + 2H_2O \rightarrow MnO_2 + (NH_4)_2SO_4 + 2H_2SO_4 \qquad (5.9)$$

Lots of MnO_2 nanostructures including nanoflakes, nanorods, nanospheres have been obtained by this HT reaction and showed a capacitance of 168–455 F g^{-1} for supercapacitor application.[249, 250, 256-259] Meanwhile, other composites (e.g., MnO_2/graphene, MnO_2/CNT, MnO_2/ZnO, MnO_2/PPy, MnO_2/PANI) are reported and present enhanced capacitances of 516–873F g^{-1} attributed to the combination with conductive layers.[251-253, 260, 261] It should be mentioned that this HT reaction will not do harm to other conductive scaffold and favourable

for construction of MnO_2 based composite materials. Furthermore, this HT is applicable to co-synthesize conducting polymers with MnO_2 because the $KMnO_4$ or persulfate is also common oxidant for the chemical polymerization of conducting polymers.

5.1.3 Direct hydrolysis of $KMnO_4$ or $Mn(NO_3)_2$

The direct hydrolysis of $KMnO_4$ is the most facile and popular HT method for the preparation of MnO_2 and MnO_2-based composites illustrated as follows.[262, 263]

$$4MnO_4^- + 2H_2O \rightarrow 4MnO_2 + 4OH^- + 3O_2 \qquad (5.10)$$

The above HT reaction is very easy to control and process. It only needs to control the concentration of $KMnO_4$ and HT time. The problem in this HT is that the $KMnO_4$ may also react with other active materials leading to the formation of side products. In addition to the normal nanoflakes or nanosheets,[247, 264] by the aid of some templates or surfactants, MnO_2 nanospheres, nanourchins or nanorods and composites with, metal, carbon, conducting polymers, and metal oxides, are also fabricated and applied for LIBs and supercapacitors.[146, 227, 262, 264-271] The as-prepared MnO_2 nanostructures show a capacitance range of 200–528 F g^{-1} and a capacity range of 213–983 mAh g^{-1}. The electrochemical performance of composites is superior to the bare counterparts. On the other hand, the $Mn(NO_3)_2$ is another manganese source for the direct hydrolysis to prepare MnO_2 nanorods (Figure 15), expressed as below.[272]

$$Mn(NO_3)_2 \rightarrow MnO_2 + NO_2 \qquad (5.11)$$

But this method is not usual, and the side product NO_2 is toxic. The obtained MnO_2 nanorods are applied as the cathode for LIBs. The α-MnO_2 nanostructures shows a flat plateau between 3.0 and 2.5 V, and the discharge capacity is 204 mAh g^{-1} to an end voltage of 1.5 V. For γ-MnO_2 nanorods, the open-circuit potential was 3.43 V, and the discharge capacity exceeds 210 mAh g^{-1} indicating that a desirable amount of lithium inserted (in Lix-MnO_2, $x \approx 0.70$).[272] The reactions are expressed as follows. [272]

$$MnO_2 + xLi \leftrightarrow Lix\text{-}MnO_2 \qquad (5.12)$$

5.2 Chemical deposition of MnO_2 and MnO_2-based composites

To date, the CP-MnO_2 papers account for ~37 % in all the published literature about solution-based synthesis of MnO_2 for EES. The reactions in CP are almost the same as those of HT, but the CP is not conducted in sealed vessel, and usually does not need high reaction temperature. The manganese sources are $KMnO_4$, $MnCl_2$, $MnSO_4$, $Mn(NO_3)_2$ and $Mn(CH_3COO)_2$. Similar to HT, the CP-MnO_2 can also be classified into three kinds according to different reaction mechanisms. We will introduce different CP types of MnO_2 by taking some typical examples in the following and describe the corresponding mechanisms as well as EES performances.

5.2.1 CP reactions between oxidant ($KMnO_4$) and reducing agent (such as C, Cu, N_2H_4 and ethanol)

Lang et al. reported a facile CP method for the fabrication of nanoporous gold/MnO_2 hybrid electrodes by using $KMnO_4$ and N_2H_4 in alkaline electrolyte (Figure 16).[273] But they used the N_2H_4 gas as the reducing agent. The N_2H_4 gas is very active and the possible reactions are as follows.[273]

$$4MnO_4^- + 3N_2H_4 \rightarrow 4MnO_2 + 3N_2 + 4H_2O + 4OH^- \quad (5.13)$$

The as-fabricated nanoporous gold/MnO_2 hybrid electrodes show nanoporous structure and enhanced conductivity, resulting in a specific capacitance of the constituent MnO_2 (~1145 F g^{-1}). Although MnO_2 has intrinsically low conductivity that limits its charge/discharge rate, the charge-transfer-reaction pseudocapacitance of the nanoporous gold/MnO_2 electrode can be enhanced by the fast ion diffusion in the three-dimensional nanoporous architecture and highly electrical conductivity of the nanoporous gold skeleton as well as the epitaxial metal/oxide interfaces.

In the meantime, several MnO_2 nanostructures (nanorods and nanosheets) and composites (e.g., MnO_2/CNT, PANI/C/MnO_2, MnO_2/graphene, TiO_2/C/MnO_2) have been reported via

this CP reactions between carbon sources with $KMnO_4$ and applied for EES.[274-285] The involved reactions are the same as that of the eqn. (5.1) above. Though the CP-MnO_2 has the same reaction mechanism with that of HT, the CP reaction is conducted under mild condition and lower temperature, and the samples are all powder forms, not film. In other words, the CP is suitable for large-scale fabrication of MnO_2 and composites. Notice that the reactions between carbon sources and $KMnO_4$ are easier to control than that proposed by Lang et al. using N_2H_4 gas,[273] and more environmental friendliness. Additionally, Cu/MnO_2 superstructures and MnO_2 nanosheet/graphene flake composites are prepared by using Cu or ethanol as the reducing agent according to similar reaction of eqn. (5.3) and (5.4).[286, 287] Comparing the bare MnO_2 and their composites, it is found that the MnO_2-based composites show much higher capacitance and better cycling stability and high-rate capability due to the ion/electron transfer modification by introduction of conductive layers including graphene, CNT and conducting polymers. The PANI/C/MnO_2 shows a capacitance of 695 F g^{-1}, about two times larger than the pure MnO_2.[275] As cathode for LIBs, the MnO_2 on the GS affords an unprecedented high capacity of 230 mAh g^{-1} after 150 cycles, ~30 % higher than the bare MnO_2.[284]

5.2.2 CP reactions between oxidant ($KMnO_4$, persulfate or H_2O_2) and manganese sources such as $MnSO_4$, $MnCl_2$ or $Mn(CH_3COO)_2$.

The CP-MnO_2 prepared by reactions between ($KMnO_4$, persulfate or H_2O_2) and manganese sources (such as $MnSO_4$, $MnCl_2$ or $Mn(CH_3COO)_2$) is quite popular. This reaction is easy to control and more suitable for preparation of composites without sacrificing the needed conductive backbone. Peng et al. reported ultrathin 2D MnO_2/graphene hybrid nanostructures via the above method by using H_2O_2 and $MnCl_2$ as the starting materials.[288] The CP reactions are given as below.[288]

$$Mn^{2+} + H_2O_2 \rightarrow MnO_2 + 2H^+ \quad (5.14)$$

The whole reaction is very fast and exothermic. The MnO_2 is homogeneously grown on the graphene nanosheets and the obtained MnO_2/graphene nanosheets based planar supercapacitors demonstrate the impressive electrochemical performance with a high specific capacitance of 267 F g^{-1}, and excellent rate capability and cycling performance with capacitance retention of 92 % after 7000 charge/discharge cycles.[288]

The most widely used oxidant and reducing agent is $KMnO_4$ and $MnSO_4$, respectively. The involved reaction is the same as that shown in eqn. (5.8). Manganese source is not limited in $MnSO_4$, can also be $MnCl_2$ or $Mn(CH_3COO)_2$. The other common oxidant is $K_2S_2O_8$ or $(NH_4)_2S_2O_8$, like the reaction in eqn. (5.9). Based on these reactions, lots of MnO_2 nanostructures (e.g., nanorods, mesoporous MnO_2, clew-like, hollow urchin) and MnO_2-based composites (such as MnO_2 nanospheres/C/PEDOT-PST, MnO_2/graphene, MnO_2/CNT, MnO_2/graphene/CNT, MnO_2/RGO, Co_3O_4/Pt/MnO_2, SnO_2/ MnO_2, PANI/ MnO_2) have been reported and used as active materials for EES.[121, 289-304] It is observed that this CP-MnO_2 is help for fabrication of composites, and the CP process is not complex. When they are applied for EES, like other modification research, the composites with conductive backbone show much higher capacitance and capacity, and better rate capability and cycling performances.

5.2.3 CP reaction by direct hydrolysis of $KMnO_4$

The direct hydrolysis of $KMnO_4$ is another popular CP for the synthesis of MnO_2 electrode materials for EES. The reaction is shown in eqn. (5.10). Bao et al. prepared flexible Zn_2SnO_4/MnO_2 sore/shell hybrid composites by the direct hydrolysis of $KMnO_4$.[305] The MnO_2 resulting from hydrolysis of $KMnO_4$ is uniformly coated on the surface of Zn_2SnO_4 nanorod with a diameter of ~80 nm. This CP-MnO_2 shows a specific capacitance of 642 F/g at a current density of 1 A g^{-1} in 1 M Na_2SO aqueous solution as cathode for supercapacitors. This CP-MnO_2 is also widely adopted to prepared enhanced porous-structured MnO_2 composites for EES applications and improved electrochemical performances have been demonstrated in these systems such as MnO_2 nanowires/CoAl, Fe_2O_3/MnO_2 core/shell

nanowire, MnO_2/carbon, MnO_2/polypyrrole, graphene/MnO_2, MnO_2/PEDOT/graphene, and graphene/ MnO_2.[262, 263, 306-314] Foe this CP method, one point to be noticed is the concentration of $KMnO_4$, which will affect the morphology of the final samples.

5.3 Electrochemical synthesis of MnO_2 and MnO_2-based composites

Electro-deposition is always used to prepare MnO_2 film which can be easily combined with other conductive substrates or scaffold to form high-performance composites for EES. Up to now, most of the ED-MnO_2 nanostructures and composites are prepared by anodic ED with $Mn(CH_3COO)_2$ or $MnSO_4$ as the starting material. The support electrolyte is Na_2SO_4. The anodic ED reactions are proposed as follows.[315-317]

$$Mn^{2+} + 2H_2O - 2e^- \rightarrow MnO_2 + 4H^+ \quad (5.15)$$

The ED can be conducted in either two-electrode or three-electrode system. The substrates have a significant effect in this anodic ED. If the substrate is nickel foam or copper, the metal will dissolve at high potential. This phenomenon will not happen in carbon-based substrates.

Previously, Lu et al. reported a WO_{3-x}@Au@MnO_2 core/shell nanowires on carbon clothe by the above anodic ED and showed a capacitance of 588 F g^{-1} (Figure 17).[316] The ED-MnO_2 layer exhibits highly electrochemical reactivity leading to enhanced supercapacitor performance for the composite nanowires. Based on the anodic ED method, numerous MnO_2 nanostructured electrodes (e.g., nanorod, nanosheet, nanowire, nanotube) and composites (MnO_2/Pt, MnO_2/Metal, MnO_2/PEDOT-PST, MnO_2 nanosheet, MnO_2 nanorod, MnO_2/Au, MnO_2/PEDOT, MnO_2/CNT, MnO_2 nanopillars, MnO_2/graphene hydrogel, mesoporous MnO_2, MnO_2/TiN, MnO_2/PPY, IrO_2/MnO_2, MnO_2/RuO_2, etc.) have been fabricated for EES applications.[315, 317-349] The morphology of MnO_2 in the composites is related to the deposition time and deposition current density. The anodic ED-MnO_2 can deliver a high capacitance up to 1222 F g^{-1} at 5 A g^{-1},[329] and superior cycling life and rate capability are proven in the

composites with metal and graphene.[315-317, 338, 339] As anode of LIBs, the mesopoorus MnO_2 nanosheet arrays exhibit a reversible capacity as high as 1690 mAh g^{-1} after 100 cycles.[335]

The cathodic ED-MnO_2 mainly comes from two routes: (1) direct cathodic ED of MnO_2 in $Mn(NO_3)_2$ electrolyte and (2) conversion form metal Mn electrodeposited from an electrolyte containing a Mn^{2+} ion or $KMnO_4$. First, we introduce the work of Li and co-workers, who used the above two kind of cathodic ED for the construction of mesoporous MnO_2/carbon aerogel and ZnO/MnO_2 composites, respectively.[350, 351] The reactions in $Mn(NO_3)_2$ electrolyte are expressed as follows.[350]

$$NO_3^- + H_2O + 2e^- \rightarrow NO_2^- + 2OH^- \quad (5.16)$$

$$2Mn^{2+} + 4OH^- + O_2 \rightarrow 2MnO_2 + 2H_2O \quad (5.17)$$

The above mesoporous MnO_2/carbon aerogel composites show a high specific capacitance of 515.5 F g^{-1}. Meanwhile, they developed another cathodic ED using $Mn(CH_3COO)_2$ electrolyte, expressed as below.[351]

$$Mn^{2+} + 2e^- \rightarrow Mn \quad (5.18)$$

During the annealing process:

$$Mn + O_2 \rightarrow MnO_2 \quad (5.19)$$

These prepared single-crystal ZnO nanorod/amorphous and nanoporous MnO_2 shell composites have been employed as supercapacitor electrodes and give a high specific capacitance of 405 F g^{-1}. Similar cathodic ED-MnO_2 is also reported by other groups. [352, 353]

There is third kind of cathodic ED of MnO_2, which is realized by reduction of $KMnO_4$, shown as follows.[307, 354, 355]

$$MnO_4^- + 2H_2O + 3e^- \rightarrow MnO_2 + 4OH^- \quad (5.20)$$

MnO_2/CNT, Fe_2O_3/MnO_2 and amorphous MnO_2 films are prepared by this cathodic ED and high capacitances of 463–838 F g^{-1} are verified in the composite systems.[307, 354, 355]

In a nutshell, the anodic ED is most popular ED method for synthesis of MnO_2 and its deposition process is very easy to control. The MnO_2 of anodic ED exhibits the best EES performances among the ED-MnO_2 samples.

6. Iron oxides and iron oxides-based composites

Iron is the fourth most common element in the earth's crust (6.3 % by weight) and is usually oxidized into three kinds of oxides (Fe_2O_3, Fe_3O_4, and FeO), which are promising active materials for applications in photo-catalysis, EES and photo-electrochemical water splitting. Hematite Fe_2O_3 is the most thermodynamically stable form of iron oxide under ambient conditions and as such, it is also the most common form of crystalline iron oxide. The Fe_2O_3 have different polymorphs including α-Fe_2O_3 (rhombohedral structure, JCPDS 80-2377), β-Fe_2O_3 (orthorhombic structure, JCPDS 08-0093) and γ-Fe_2O_3 (cubic structure, JCPDS 89-5892) depending on the structure of $Fe(O)_6$ octahedra. The arrangement of cations produces pairs of $Fe(O)_6$ octahedra. Each octahedral shares edges with three neighboring $Fe(O)_6$ octahedra in the same plane and one face with an octahedral in an adjacent plane. Different combination of $Fe(O)_6$ octahedra will form different Fe_2O_3 polymorphs.[356] The band gap of Fe_2O_3 is about 1.9–2.2 eV depending on different polymorphs. Another important iron oxide is Fe_3O_4, whose crystal structure is similar to that of Co_3O_4. Fe_3O_4 has a face-centred cubic unit cell (JCPDS 65-3107). Fe_3O_4 differs from most other iron oxides in that it contains both divalent and trivalent iron. Its structure consists of octahedral and mixed tetrahedral/octahedral layers. Its band gap is ~0.1 eV. FeO has a defective NaCl structure and a band gap of ~2.4 eV. It consists of two interpenetrating face centred cubic structures of Fe^{II} and O^{2-} (JCPDS 43-1312). FeO is not stable in air and prone to be oxidized into Fe_3O_4 or Fe_2O_3. Over the past decades, numerous iron oxides and composites have been prepared by solution-based methods and applied as electrode materials for EES. In this section, we mainly

focus on the HT, ST, CP and ED methods for the synthesis of iron oxides and corresponding electrochemical performances.

6.1 Hydrothermal synthesis and solvothermal synthesis method of iron oxide and iron oxides-based composites

To date, the HT+ST papers account for ~32 % in all the published papers of solution synthesis of iron oxides for EES applications. $FeCl_3$, $FeSO_4$ and $Fe(NO_3)_3$ are the most widely used iron sources. The solvent includes water, ethanol and ethylene glycol.[357-362] As one of strong acid weak alkali salts, iron salt is very easy to hydrolyze into ferric hydroxide precipitation in water at high temperature. Then, ferric hydroxide precipitation decomposes into ferric oxide and water. The reactions are as following: [35]

$$Fe^{3+} + 6H_2O \rightarrow [Fe(H_2O)_6]^{3+} \quad (6.1)$$

$$[Fe(H_2O)_6]^{3+} \rightarrow FeOOH + 3H^+ + 4H_2O \quad (6.2)$$

$$2FeOOH \rightarrow Fe_2O_3 + H_2O \quad (6.3)$$

In order to accelerate the deposition process, some precipitants (such as urea,[363, 364] sodium hydroxide[357, 358, 364] and sodium acetate[365, 366]) are also used to promote the HT process. They could yield OH^- during the hydrolysis in the solution and consume the H^+ in eqn. (6.2) to accelerate the reaction. Previously, we prepared porous Fe_3O_4/C core/shell nanorods by the above HT reactions and demonstrated a high capacity of 762 mAh g^{-1} for LIBs application.[358] Additionally, Zhang et al. reported an interesting carbon coated Fe_3O_4 nanospindles by using $FeCl_3$ and NaH_2PO_4.[367] The main reactions are similar to those above. But the NaH_2PO_4 is important for controlling the morphology of the samples. The hydrolysis of NaH_2PO_4 produces OH^- as a precipitating agent. It controls the nucleation as well as growth of small iron oxide particles and finally forming Fe_3O_4 nanospindles (Figure 18). The obtained Fe_3O_4/C nanospindles show a high reversible capacity of 745 mAh g^{-1}. Meanwhile, we adopted $FeCl_3$ and Na_2SO_4 as the starting materials to fabricate Fe_2O_3 nanorod array on

carbon cloth.[35] The Na_2SO_4 is believed to be favorable for the formation of rods. The specific mechanism is still not clear.[35] Some other iron oxides nanostructures (such as nanorods, nanoparticles and spheroids) and iron oxides-based composites (e.g., Fe_3O_4/C, Fe_3O_4/graphene) have been reported by similar HT reactions.[357, 366, 368-370] The iron oxides grown on the carbon backbone show much better EES performance than the pure counterparts. As anode of LIBs, the ferric oxides (Fe_3O_4 and Fe_2O_3) can reversibly react with Li ion to store electrochemical energy and the corresponding simplified reactions are expressed as follows:[314, 371]

$$Fe_3O_4 + 8Li^+ \leftrightarrow 3Fe + 4Li_2O - 8e^- \quad (6.4)$$

And

$$Fe_2O_3 + 6Li^+ \leftrightarrow 2Fe + 3Li_2O - 6e^- \quad (6.5)$$

The iron oxides and composites are also investigated as cathode materials for supercapacitors. The Fe_3O_4/reduced graphene oxide delivers a capacitance of 480 F g^{-1}. As for the supercapacitor electrode, the capacitance mechanism of ferric oxides in aqueous electrolytes is still not clear yet. The possible reactions are given as follows.

In alkaline electrolyte such as KOH solution [372]

$$Fe_3O_4 + 4H^+ \leftrightarrow 2Fe^{3+} + Fe^{2+} + 4OH^- \quad (6.6)$$

$$Fe^{2+} \leftrightarrow Fe^{3+} + e^- \quad (6.7)$$

If the electrolyte is Na_2SO_3 solution[370, 373]

$$SO_3^{2-} + 3H_2O + 4\ e^- \leftrightarrow S_2O_6^{2-} + 6OH^- \quad (6.8)$$

$$S_2O_6^{2-} + 3H_2O + 8\ e^- \leftrightarrow 2S^- + 6OH^- \quad (6.9)$$

As the electrolyte is lithium perchlorate ($LiClO_4$) in ethylene carbonate (EC)/dimethyl carbonate (DMC) (in a volume ratio of 1:1):[374]

$$Fe_2O_3 + 2Li^+ + 2e^- \rightarrow Li_2(Fe_2O_3) \quad (6.10)$$

$$Li_2(Fe_2O_3) + 4Li^+ + 4e^- \rightarrow 2Fe^0 + 3Li_2O \quad (6.11)$$

$$2Fe^0 + 2Li_2O \leftrightarrow 2FeO + 4Li^+ + 4e^- \quad (6.12)$$

It is noteworthy that the solvent has great influence on the morphology of the final products, especially in organic solvents. Therefore, solvothermal synthesis (ST) is developed for the synthesis of iron oxides and composites. Zeng et al. reported flower-like α-Fe_2O_3 by using ethanol as solvent and proposed that the tentative solvothermal precursor could be a composition of $FeOC_2H_5O$, [362, 375] which converts into iron oxides after annealing. During the annealing process in air:[375]

$$2FeOC_2H_5O + 6O_2 \rightarrow Fe_2O_3 + 4CO_2 + 5H_2O \qquad (6.13)$$

In addition, they conducted a series of other investigations to further understand the effect of ethanol in the process. It is believed that ethanol may play important roles in at least three aspects: (i) acting as the solvent; (ii) acting as starting material to form the iron alkoxide precursor; and (iii) providing water molecules in the system by etherification. They also found that the rate of reaction has a strong impact on the morphology of products.

Ethylene glycol (EG) is another common solvent to synthesize ferric oxides in ST method[363, 365, 366, 368]. As a kind of reducing agent, EG is always used to synthesize Fe_3O_4 in most cases. Our group synthesized hierarchical hollow-structured single-crystalline magnetite (Fe_3O_4) microspheres as LIBs anode.[365] In our case, the solution is a mixture of ferric chloride, EG, polyvinylpyrrolidone (PVA) and NaAc, which is used as iron source, solvent and reducing agent, surfactant and precipitant, respectively. The possible reactions are shown as follows:[365]

$$CH_2OH–CH_2OH \rightarrow CH_3CHO + H_2O \qquad (6.14)$$

$$2CH_3CHO + Fe^{3+} \rightarrow Fe^{2+} + 2H^+ + CH_3COCOCH_3 \qquad (6.15)$$

Meanwhile, NaAc hydrolyze to offer OH^- in the ST system.[365]

$$Fe^{3+} + 3OH^- \rightarrow Fe(OH)_3 \qquad (6.16)$$

$$2Fe(OH)_3 + Fe(OH)_2 \rightarrow Fe_3O_4 + H_2O \qquad (6.17)$$

The as-prepared hierarchical hollow-structured Fe_3O_4 shows a high specific capacity and excellent cycle performance (851 mAh g^{-1} at 1 C and 750 mAh g^{-1} at 3 C up to 50 cycles).[365]

However, the poor intrinsic electrical conductivity of iron oxides hinders its practical applications for EES. There are different approaches to overcome these problems. One solution is to fabricate iron oxide nanostructures. Other strategies are to confine the iron oxide nanostructures with carbon to form a composite with the carbon host matrix. Fe_3O_4/C core/shell structure[358, 364, 367], ferric/graphene[363, 368] or CNTs composites [357, 373, 374] are synthesized to improve the conductivity of the integrate electrode.

6.2 Electrochemical synthesis of iron oxides and iron oxides-based composites

The electro-deposition (ED) methods for iron oxides and their composites are also classified into two types: cathodic ED and anodic ED. So far, there are three typical ED reactions for the fabrication of iron oxides nanostructures for EES applications. The obtained products are films, not powders. These three ED reactions have their own merits and demerits and will be discussed in detail in this section.

6.2.1 Anodic ED with $Fe(NH_4)_2(SO_4)_2$ or $FeSO_4$

The first ED developed for iron oxides and their composites is based on the anodic reaction of $Fe(NH_4)_2(SO_4)_2$. The precursor formation relies on the oxidation of Fe^{2+} to Fe^{3+}, which further reacts with the available OH^- from a slightly alkaline electrolyte to form insoluble FeOOH. In this reaction, a brown deposit can be observed at the beginning of anodic deposition, indicating the formation of FeOOH. The specific reactions are illustrated as follows.[376]

$$Fe^{2+} - e^- \rightarrow Fe^{3+} \quad (6.18)$$

$$Fe^{3+} + 3OH^- \rightarrow FeOOH + H_2O \quad (6.19)$$

During the annealing process in air atmosphere:[376]

$$2FeOOH \rightarrow Fe_2O_3 + H_2O \quad (6.20)$$

During the annealing process in H_2 atmosphere:

$$6FeOOH + H_2 \rightarrow 2Fe_3O_4 + 4H_2O \quad (6.21)$$

The as-prepared iron oxides always show a highly porous structure composed of nanosheets. Wu et al. prepred Fe_2O_3 nanosheets arrays by the above method and showd a capacitance of 146 F g^{-1}.[376] $FeSO_4$ is also used as the iron source to prepare iron oxides nanostructures via the same reaction mechanism. A big problem in this anodic ED is that the iron source $Fe(NH_4)_2(SO_4)_2$ or $FeSO_4$ is not stable and will be easily oxided by the O_2 in the electrolyte. So it is necessary to put some pure ion powder in the electrolyte to stablize the iron source. Several iron oxides-based composites (such as Fe_2O_3/carbon fibre, Fe_2O_3/MnO_2 and TiO_2/Fe_2O_3) have bee fabricated for EES via the above anodic ED by the aid of other templates including AAO, TiO_2 nanotube, and carbon fibre.[307, 377, 378] As cathode material of supercapacitors, the Fe_2O_3/MnO_2 presents a maximum specific capacitance of 838 F g^{-1}.[307] For LIBs application, the Fe_2O_3/carbon fibre and TiO_2/Fe_2O_3 exhibit a capacity of 970 mAh g^{-1} and 1190 mAh g^{-1}, respectively, much higher than the bare Fe_2O_3 (680 mAh g^{-1}).[377, 378]

6.2.2 Cathodic ED with $Fe_2(SO_4)_3$ and tri-ethanolamine (TEA) in alkaline electrolyte

In order to find a more stable and feasible ED for iron oxides, researchers have developed another facile cathodic ED using $Fe_2(SO_4)_3$ and tri-ethanolamine (TEA) as the starting materials. But this cathodic ED is usually adopted to fabricate Fe_3O_4 film. Previously, we prepared a 3D porous nano-Ni/Fe_3O_4 composite film by the cathodic ED.[379] The reactions are expressed as follow.[379, 380]

$$Fe(TEA)^{3+} + e^- \rightarrow Fe^{2+} + TEA \qquad (6.22)$$

$$Fe^{2+} + 2Fe(TEA)^{3+} + 8OH^- \rightarrow Fe_3O_4 + 4H_2O + 2TEA \qquad (6.23)$$

The electrolyte here is very stable and the deposition process is easy to control. The Fe_3O_4 nanoflakes are grown on the 3D Ni backbone forming a highly porous integrated electrode. The resultant 3D porous nano-Ni/Fe_3O_4 composite film shows a high capacity of 951mAh g^{-1} as well as enhanced rate capability. In addition, Tarascon' group used the same method to prepare Fe_3O_4-based Cu nano-architectured electrodes for LIBs with seperior high-rate

capability.[381] Similar Fe_3O_4/Cu core/shell nanorod arrays are reported by Duan et al. and deliver a capacity of 1003 mAh g^{-1}.[382]

6.2.3 Anodization of Fe foil.

The third ED of iron oxides is anodization of iron foils. This method originates from the well-known anodization of Ti foils towards TiO_2 nanotubes. The electrolyte is ammonium fluoride in an aqueous ethylene glycol solution. The working voltage is about 50 V. Xie et al. reported such an anodization method to fabricate Fe_3O_4/C nanotube arrays (Figure 19).[383] The involved precursor reactions are simply expressed as below.[383]

$$2Fe + 3H_2O - 6e^- \rightarrow Fe_2O_3 + 6H^+ \qquad (6.24)$$

$$Fe_2O_3 + 12F^- + 6H^+ \rightarrow 2FeF_6^{3-} + 2H_2O \qquad (6.25)$$

The Fe_3O_4 in the Fe_3O_4/C nanotube arrays is formed by the reduction of Fe_2O_3 via carbon. The NH_4F can accelerate the anodization reaction. The as-fabricated Fe_3O_4/C nanotubes grow vertically on the substrates and have average pore diameter of 100 nm. The Fe_3O_4/C nanotubes exhibit high capacity (1020 mAh cm^{-2} at 20 mA cm^{-2}) and high rate capability (176 mAh cm^{-2} at 1000 mA cm^{-2}). It is noteworthy that it is difficult to calculate the true load mass of active materials obtained by this method because the active materials directly come from the Fe foil.

6.3 Chemical precipitation of iron oxides and iron oxides-based composites

Generally, CP-Fe_2O_3 or CP-Fe_3O_4 is prepared by directly mixing iron sources (e.g., $FeCl_2$, $FeCl_3$, $Fe(NH_4)_2(SO_4)_2$, $MnSO_4$, $Fe(NO_3)_3$) with precipitants (e.g., NaOH, ammonia, Na_2CO_3, CH_3COONa). The iron sources usually react with the OH^- or CO_3^{2-} to form precursor, which converts into iron oxides after heat treatment. Meanwhile, there is a special CP based on hydrolysis of iron sources. We have investigated the hydrolysis reaction and prepared some high-performance iron oxides-based electrode materials for LIBs, including TiO_2 nanotube,

3D graphene foam and Co_3O_4 supported iron oxides.[324, 384-386] Herein, we take the TiO_2/ Fe_2O_3 core/shell nanoarrays as an example (Figure 20a) for discussion of the reaction process.[324] The $FeCl_3$ is unstable in the electrolyte and will hydrolyze into H^+ ions,

$$Fe^{3+} + 2H_2O \leftrightarrow FeOOH + 3H^+ . \quad (6.26)$$

When there exists a sacrificial template, $Co_2(OH)_2CO_3$ in this case, it will reacts with the above H^+ and this reaction accelerates the hydrolysis reaction according to[324]

$$4H^+ + Co_2(OH)_2CO_3 \rightarrow 2Co^{2+} + 3H_2O + CO_2 . \quad (6.27)$$

During the annealing process, $2FeOOH \rightarrow Fe_2O_3+H_2O$. (6.28)

The FeOOH product of hydrolysis can change into Fe_2O_3 after annealing in an air or oxygen ambient according to Eq. (6.28). The key point in this method is the sacrificial template to drive the hydrolysis reaction. The sacrificial template can be also metal oxides (such as ZnO, Al_2O_3) or metal hydroxides [$Ni(OH)_2$ or $Co(OH)_2$]. Using a similar method, we also obtained 3D GF-supported Fe_3O_4 nanoparticles with a homogeneous coverage, thanks to the uniform coating of ZnO by ALD (see Figure 20b).

Similar result is reported by other authors. Wang et al. reported a typical CP method for the synthesis of Fe_2O_3 nanorods by using $FeSO_4$ and CH_3COONa as the starting materials. The CH_3COONa is used as a source of hydroxide ions during the hydrolysis of iron salts to form FeOOH. The reactions are given as follow.[387]

$$CH_3COO^- + H_2O \rightarrow CH_3COOH + OH^- \quad (6.29)$$

$$4Fe^{2+} + 8OH^- + O_2 \rightarrow 4FeOOH + 2H_2O \quad (6.30)$$

In addition to above hydrolysis, other CP reactions in basic solutions are much easier, for example,[388-392]

$$4Fe^{2+} + 8OH^- + O_2 \rightarrow 4FeOOH + 2H_2O \quad (6.31)$$

or $$Fe^{3+} + 3OH^- \rightarrow FeOOH + H_2O \quad (6.32)$$

or $$Fe^{2+} + CO_3^{2-} \rightarrow FeCO_3 . \quad (6.33)$$

Then, the precursor converts into Fe_2O_3 or Fe_3O_4 after annealing in different atmosphere. Nonetheless, CP method based on a sacrificial template provides better control in nano morphology. A direct CP reaction with basic solution may be too fast and result in unwanted agglomerations.

The as-prepared CP-iron oxides are powders, not films. In order to have good EES performance, often the CP-Fe_2O_3 or CP-Fe_3O_4 will need further surface engineering or form composites with conductive host. For example, the Fe_3O_4/carbon nanotube composites can deliver a high discharge capacity of 656 mAh g^{-1} and stable cyclic retention.[388] The TiO_2/Fe_2O_3 core/shell nanoarrays, after a further step of carbon coating, exhibit a high reversible capacity of 840 mAh g^{-1} and evidently improved cycle stability (Figure 20a). With a homogeneous hybridization with 3D chemical-vapor-deposited graphene foam, the Fe_3O_4 nanoparticles LIB anode demonstrates an ultra-fast charging and discharging with a rate of 60 C within 500 cycles (Figure 20b).

7. Vanadium oxides and vanadium oxides-based composites

Vanadium oxides are typical multi-functional materials and have attracted strong interest over the past years for their unique electrical, optical, electrochemical properties. Two kinds of vanadium oxides, vanadium pentaoxide (V_2O_5) and vanadium dioxide (VO_2), are considered as promising active cathode materials for EES due to their high capacity/capacitance, high working voltage and excellent cycling stability. The V_2O_5 has an orthorhombic structure (JCPDS 41-1426) with lattice parameters a = 3.563 Å, b = 11.510 Å, c = 4.369 Å. The building block is a deformed VO_6 octahedron. The shortest V-O bond length corresponds to a double vanadyl bond ($V\text{-}O_1$ = 1.585 Å). The V_2O_5 has a layered structure with an easy cleavage plane (perpendicular to the c-axis) and a band gap of ~2.8 eV. The theoretical capacity of V_2O_5 is ~294 mAh g^{-1} between 4.0 and 2.0 V (vs. Li^+/Li), which is higher than those of $LiCoO_2$ (140 mAh g^{-1}), $LiMn_2O_4$ (148 mAh g^{-1}) and $LiFePO_4$ (170

mAh g^{-1}). The electrochemical reactions between V_2O_5 and Li ion between 4.0 and 2.0 V (vs. Li^+/Li) are expressed as follows:[49, 393-395]

$$V_2O_5 + 0.5\ Li^+ + 0.5e^- \rightarrow Li_{0.5}V_2O_5 \quad (7.1)$$

$$Li_{0.5}V_2O_5 + 0.5\ Li^+ + 0.5e^- \rightarrow LiV_2O_5 \quad (7.2)$$

$$LiV_2O_5 + Li^+ + e^- \rightarrow Li_2V_2O_5 \quad (7.3)$$

Another important vanadium oxide is VO_2, which is a typical binary compound with different polymorphs. The polymorphic varieties in this system include tetragonal rutile-type VO_2 (R), monoclinic VO_2 (M), and at least three metastable phases named as VO_2 (B), VO_2(A) and VO_2 (C). VO_2 can adopt different structures according to different synthesis methods. Generally speaking, the structures of the four VO_2 polymorphs, VO_2 (R), VO_2 (M), VO_2 (B), and VO_2 (A), are based on an oxygen bcc lattice with vanadium in the octahedral sites, the oxygen octahedra being more or less regular. They can be separated in two groups, depending on the mutual orientation of the fourfold axis of the oxygen octahedra. The oxygen octahedra can be aligned either along two perpendicular directions, as it is the case in the rutile structure. The band gap of VO_2 is 0.5–0.7 eV depending on different polymorphs. The theoretical capacity of VO_2 is ~340 mAh g^{-1} between 4.0 and 1.5 V (vs. Li^+/Li). The reaction can be written as[396, 397]

$$VO_2 + Li^+ + e^- \rightarrow LiVO_2\ . \quad (7.4)$$

In this section, we will briefly introduce some typical solution-based synthesis methods (mainly hydrothermal, solvothermal, electrodeposition and sol-gel) for the synthesis of vanadium oxides and composites for EES applications.

7.1 Hydrothermal synthesis and solvothermal synthesis of vanadium oxides and vanadium oxides-based composites

The HT and ST methods are popular with materials researchers and have been widely used for the fabrication of vanadium oxides and composites. Generally, there are two common

types of HT routes for the synthesis of V_2O_5 for EES. One HT method is to use the metavanadate ($NaVO_3$ or NH_4VO_3) and HCl as the starting materials and utilize the hydrolysis of ammonium metavanadate in the acid solution to form vanadium oxides after heat treatment.[115, 313, 394, 398-402] The other HT method is to utilize V_2O_5 sols precursor resulting from the reactions between commercial V_2O_5 powder and H_2O_2, and finally obtain V_2O_5 nanostructures after hydrothermal synthesis and annealing.[395, 403-405] Carbon sources (such as graphene, carbon nanotube and sucrose) and V_2O_5 are usually used as the starting materials to prepare HT-VO_2 and their composites.[406, 407]

First, we introduce the sol-based HT method for the synthesis of porous structured V_2O_5 for EES. Typically, the commercial powder V_2O_5 reacts with the H_2O_2 (30 wt. %) in deionized water and forms yellow slurry bubbled vigorously (note that this reaction is exothermic). Several parallel or sequential chemical reactions occur in the HT due to the decomposition of excess H_2O_2, expressed as follows.[395, 403, 408]

$$V_2O_5+4H_2O_2 \rightarrow 2[VO(O_2)_2(OH_2)]^- + 2H^+ + H_2O \quad (7.5)$$

$$V_2O_5 + 2H^+ + 2\ H_2O_2 + 3H_2O \rightarrow 2[VO(O_2)(OH_2)_3]^+ + O_2 \quad (7.6)$$

$$2[VO(O_2)_2(OH_2)]^- + 4H^+ + 2H_2O \rightarrow 2[VO(O_2)(OH_2)_3]^+ + O_2 \quad (7.7)$$

$$2[VO(O_2)(OH_2)_3]+ \rightarrow 2[VO_2]^+ + O_2 + 6H_2O \quad (7.8)$$

$$[VO_2]^+ + 2H_2O \leftrightarrow H^+ + VO(OH)_3 \quad (7.9)$$

During the annealing process:

$$2VO(OH)_3 \rightarrow V_2O_5 + 3H_2O \quad (7.10)$$

This sol-based HT route is very facile but needs to control the amount of H_2O_2. In this method, the peroxovanadates plays an important role in the formation of nanostructured V_2O_5 and composites such as nanobelt, 3D porous architecture V_2O_5 and V_2O_5/graphene.[395, 404, 405] Yan' group reported a 3D porous architecture V_2O_5 composed of nanosheets and showed a high specific capacitance of 451 F g^{-1} in a neutral aqueous Na_2SO_4 electrolyte for supercapacitors application (Figure 21).[395] In addition, the V_2O_5 nanobelt shows a high

reversible specific capacities of 163 mAh g^{-1} at 6.8 C.[405] All the above HT vanadium oxides are power materials, not films.

The other HT of V_2O_5 is associated with the hydrolysis of metavanadate. For example:

$$2NH_4VO_3 + H_2O \rightarrow NH_3{\cdot}H_2O + HVO_3 \qquad (7.11)$$

During the annealing process:

$$2HVO_3 \rightarrow V_2O_5 + H_2O \qquad (7.12)$$

The metavanadate based HT method have been used for fabrication of V_2O_5 nanomaterials (tarfruit-like, nanowire), and composites (e.g., V_2O_5/graphene, V_2O_5/CNT, V_2O_5/PPY, V_2O_5/SnO_2) by the aid of some surfactants and copolymers.[115, 313, 394, 398-402] These V_2O_5 composites exhibit a high capacitance up to 500 F g^{-1} and a capacity of 200 mAh g^{-1} at high working current of 1000 mA g^{-1}.

The HT-VO_2 nanostructures could be prepared by a reduction reaction between V_2O_5 and carbon sources such as graphene and sucrose, simply expressed as below.[406, 407]

$$V_2O_5 + C \rightarrow 2VO_2 + CO \qquad (7.13)$$

or

$$2V_2O_5 + C \rightarrow 4VO_2 + CO_2 \qquad (7.14)$$

VO_2/graphene nanoribbon and nanobelts reported by Yan's group and Yang et al. exhibit a capacity of 160–300 mAh g^{-1}.[406, 407] The nanobelt and nanoribbon is very thin and favourable for fast ion/ electron transfer. The introduction of graphene improves the conductivity of composite leading to enhanced properties and cycling stability.

In parallel with HT, solvothermal synthesis (ST) of vanadium oxides are also extensively studied to construct vanadium oxides nanostructures including rod-like, nanosphere, urchin-like and hollow microflower.[40, 393, 396, 397, 409-411] The vanadium sources of ST are different from those for HT. Most of the vanadium sources are vanadium based organic solvents, such as vanadium oxytripropoxide,[409] and vanadium isopropoxide.[412] Usually, the solvents are ethylene glycol, ethanol or N-methylpyrrolidone. The specific reactions are still not fully clear and need further investigation. The ST-vanadium oxides nanostructures could deliver a

higher specific capacitance of 537 F g^{-1} at a current density of 1 A g^{-1} in neutral aqueous electrolytes.[409] The ST-V_2O_5 hollow microflowers exhibit a remarkable reversible capacity of 211 mAh g^{-1} and good cycling stabilities and excellent rate capabilities.[393]

7.2 Sol-gel synthesis and electrochemical synthesis of vanadium oxides and vanadium oxides-based composites

Here we focus on the sol-gel and electro-deposition methods of vanadium oxides and composites for EES. According to formation mechanism of sols, there are three basic kinds of sol-gel for the synthesis of vanadium oxides for EES. The first kind of sol-gel sol is the same as that of the sol-based HT methods. The vanadium bulks or commercial V_2O_5 powders are dissolved in H_2O_2 to form sol containing $[VO_2]^+$.[413, 414] The second type is to use vanadium oxy tripropoxide, which hydrolyses to form V_2O_5 sol.[415, 416] The last one is to obtain HVO_3 sol by ion exchange method using $NaVO_3$ as the starting material.[417] Several nanoscale sol-gel-vanadium oxides (such as nanoporous V_2O_5, nanoparticle and nanotube),[413, 415, 418] and composites (V_2O_5/graphene and V_2O_5/CNT),[414, 416-419] have been fabricated and delivered a high LIBs capacity of >200 mAh g^{-1}, and a pseudocapacitance of 200–316 F g^{-1}. But the nanosized morphologies of sol-gel-vanadium oxides are often prepared via other hard or soft templates.

In addition to the sol-gel method, electro-deposition synthesis is another facile way to the fabrication of vanadium oxides and composites, mainly for film samples. We note that the ED-V_2O_5 is often prepared by anodic ED method with the $VOSO_4$ as the vanadium source and Na_2SO_4 as the supporting electrolyte. The plausible involved reactions may be as follows:

$$2VOSO_4 + 2H_2O - 2e^- \rightarrow 2[VO_2]^+ + 2SO_4^{2-} + 4\,H^+ \quad (7.15)$$

$$[VO_2]^+ + 2H_2O \leftrightarrow H^+ + VO(OH)_3 \quad (7.16)$$

$$2VO(OH)_3 \rightarrow V_2O_5 + 3H_2O \quad (7.17)$$

Nanoporous ED-V_2O_5 films and composites films (e. g., V_2O_5/CNT, V_2O_5/TiO_2, V_2O_5/graphene, V_2O_5/PANI),[420-424] have been synthesized by the above ED method and applied as cathodes for LIBs and supercapacitors. The ED-V_2O_5/graphene cathode delivered a discharge capacity of 208 mAh g^{-1} during the 100th cycle.[420] The aligned mixed V_2O_5–TiO_2 nanotube arrays exhibit a capacitance of 220 F g^{-1}.[425]

In addition, it is found that the chemical precipitation and microwave synthesis of vanadium oxides and composites for EES are not the research focus and the corresponding papers are quite few, so we do not introduce them here.

8. Tungsten oxides and tungsten oxides-based composites

Tungsten oxide (WO_3), also known as tungsten trioxide, has attracted extensive attention because of its distinctive physical and chemical properties, making it suitable for applications in electrochromic devices, photo-catalysis, gas sensing and EES.[2, 179, 405, 426-433] The simplest crystal structure of WO_3 is referred to the ‘‘ideal’’ cubic type and described as the three-dimensional networks of corner-sharing WO_6 octahedra. However, cubic WO_3 is seldom observed experimentally. The common WO_3 displays a little distorted structures compared with cubicWO_3, classified into following five forms: tetragonal (α-WO_3), orthorhombic (β-WO_3), monoclinic I (γ-WO_3), triclinic (δ-WO_3), monoclinic II (ε-WO_3) and hexagonal (h-WO_3). The different phases of WO_3 depend on different synthesis methods and ambient temperature. The γ-WO_3 (JCPDS 72-1465) and h-WO_3 (JCPDS 85-2459) are the most stable phases at room temperature. The band gap of WO_3 is ~ 2.7 eV. WO_3 is stable in the acid solution and will dissolve in the alkaline electrolyte.

In the past decades, the research of WO_3 mainly focused on the field of electrochromics and photocatalysis. Over recent years, scientific researchers have found that WO_3 is also an active material for EES as the new findings deepened our knowledge of electrochromics, which is an electrochemical process associated with ion/electron transfer in nature. Compared

to other metal oxides, the published literature of WO_3 is still not much, but a growing number of papers are dedicated to the solution-based synthetic methods for the synthesis of WO_3 and its composites for EES.

8.1 Hydrothermal synthesis of tungsten oxides and tungsten oxides-based composites

To date, most of the nanostructured WO_3 for EES have been fabricated by HT method, which is classified into two types according to different mechanism and tungsten sources: Na_2WO_4 and metal W. For the first one, the HT-WO_3 uses Na_2WO_4 and HC as the starting materials and the WO_3 precipitation from a in a concentrated acid solution containing tungsten ion. The reactions are described as follows:[179, 434]

$$WO_4^{2-} + 2H^+ + nH_2O \leftrightarrow H_2WO_4 \cdot nH_2O \qquad (8.1)$$

$$H_2WO_4 \cdot nH_2O \leftrightarrow WO_3 + (n+1)\,H_2O \qquad (8.2)$$

Different WO_3 nanostructures and composites such as nanoflake, nanowire, nanoplate, nanoflowers WO_3/SnO_2 and WO_3/graphene have been prepared by this HT method and applied as active materials for EES.[435-439] It is noteworthy that the WO_3 nanowires can be formed with the help of $(NH_4)_2SO_4$ and each nanowire is a hexagonal single crystal and their long axes are oriented toward the [0001] direction. in the presence of an appropriate amount of ammonium sulfate in the solution, WO_3 primary particles aggregate along the [0001] direction of the h-WO_3 unit cell via self-assembly, because sulfate ions preferentially adsorb on the faces parallel to the c-axis of the WO_3 nanocrystal and thus 1D single crystal nanowires are finally formed.[179, 435] These WO_3 based nanostructures show quite good electrochemical performances. The ordered WO_3 nanowire arrays on carbon cloth exhibit a high specific capacitance of 521 F g^{-1} at 1 A g^{-1} (Figure 22).[435] The WO_3/graphene nanocomposite electrode delivers a reversible lithium storage capacity of 656 mAh g^{-1} after 100 cycle at100 mA g^{-1} and an enhanced cyclability compared with the bare WO_3 nanowires electrode.[439] The obtained capacitance and capacity are comparable to those of other metal oxides.[3, 4, 440]

The other HT can be called sol-based HT method, which first prepares WO_3 sols by reacting metal W with H_2O_2. Then the WO_3 sols are treated in HT condition to form WO_3 nanomaterials. The possible reactions about is very complex, may be as below.[441-443]

$$W + 10\ H_2O_2 \leftrightarrow [W_2(O)_3(O_2)_4(H_2O_2)]^{2-} + 2H^+ + 6H_2O \quad (8.3)$$

The hexagonal WO_3 nanostructures are fabricated by the sol-based HT and show a discharge capacity of 215 mAh g^{-1}.[442, 443] The first HT method is much easier than the second one, which is tedious and difficult for the preparation of sols.

8.2 Other solution-based synthesis of tungsten oxides and tungsten oxides-based composites

Though lots of papers about WO_3 have been reported for electrochromic and catalytic applications, there are only a few papers about WO_3 prepared by other solution-based methods (such as sol-gel, electro-deposition and microwave synthesis) for EES. Therefore, we will introduce them together in this section.

Zou et al. reported a WO_3/Polyaniline composite prepared by a cathodic electro-deposition method and a specific capacitance of 168 F g^{-1}.[444] The W sources are usually tungstic acid or tungstate such as Na_2WO_4. The formed precursor in the ED is HWO_3 with blue color with reactions shown as below.

$$WO_4^{2-} + e^- + H+ \rightarrow HWO_3 \quad (8.4)$$

The precursor HWO_3 will change into amorphous WO_3 after dehydrogenation under anodic potential. The reaction mechanism of Sol-gel WO_3 is similar to that of above sol-based HT, but the W source is not limited in metal W, can also be other tungstate. V_2O_5–WO_3 and RuO–WO_3 composites have been fabricated and showed enhance LIBs and supercapcitor performances due to the synergistic effect between V_2O_5, RuO andWO_3.[445, 446] Additionally, a crystalline tungsten oxide mixtures, WO_3–$WO_3 \cdot 0.5H_2O$ is prepared by a microwave synthesis for supercapacitor with a capacitance of 290 F g^{-1}.[447]

9. Conclusions and perspectives

Electrochemical energy storage devices and systems are playing an important role in developing a secure and green energy future of human society. The performance of EES systems, both lithium ion batteries and supercapacitors, is mainly determined by the electrode materials. Among the electrode materials studied so far, metal oxides based electrodes can provide high energy density with Faradic reaction, thus have drawn much attention for next-generation high-performance EES devices. In the past decades, the nanoscale metal oxides and their composites have elicited much interest due to their distinctive structural features and intriguing properties. Generally, compared to bulk materials, nanostructured metal oxides can provide many merits, including enlarged electrode/electrolyte contact area for reactions, short ion diffusion distance and better charge transfer kinetics.

Methods	**Applicable objects**	**Merits**	**Demerits**
Electro-deposition (ED)	Nanostructured films	Easy control in morphology, Relatively fast	Unsuitable for large-scale production
Chemical precipitation (CP)	Powders, colloidal nanostructures	Fast deposition, Large-scale production	Difficult in morphology control
Microwave synthesis (MS)	Powders, colloidal nanostructures	Much faster than CP, Large-scale production	Difficult in morphology control
Sol-gel	Nanostructured film and powders	Large-scale production	Unwanted dense film without using template, so difficult in producing porous films
Hydrothermal and solvothermal synthesis (HT, ST)	Nanostructured film and powders	Easy control in morphology, Large-scale production	High temperature, Slow growth

Chemical bath deposition (CBD)	Nanostructured film and powders	Easy control in morphology, Large-scale production, Faster than HT and ST	Limited to a few metal oxides

Table 1 Merits and demerits of different solution-based methods

To date, a wide range of solution-based synthesis methods have been developed to prepare high-quality metal oxides and metal oxide-based composites for EES applications. Each method has its own advantages and disadvantages (**Table 1**). These solution-based synthesis methods usually can be combined smartly to construct non-conventional nanostructures with tailored morphologies and functions. ED is usually used to prepare film samples and the deposition process is easy to control, but ED is not favorable for large-scale production. In contrast to ED, CP is suitable for fabrication of powder products and easy for large-scale deposition, but the morphology of samples is difficult to precisely control due to the fast CP reaction. MS can be considered a special CP method, which is conducted in microwave oven. Its reaction rate is much faster than the common CP. Similar to CP, sol-gel is also a method for large-scale production, but sol-gel is not limited in powder products and can be extended to prepare film samples. However, the sol-gel-film always shows a dense and flat morphology without other porous templates. EPD is only used for the preparation of films, while it usually needs organic solvents and high working voltage above 50 V. HT and ST can be for both powder and film samples, but they need high reaction temperature and the reactions are required to be conducted in sealed vessels.

After analysing the published literature, notice the fact that heavy research is focused on metal oxides based composites with CNT, graphene, porous metal, conducting polymers. These modifications are aiming at improving the ion/electron transportation characteristic of metal oxides and obtaining high energy and power densities. It is well accepted that the EES systems involve electrochemical process with charge transfer and ion diffusion.

Unfortunately, most of the active electrode materials (e.g., NiO, MnO_2, Co_3O_4 and Fe_2O_3) are p-type semiconductors whose electric conductivity is too low to support fast electron transport required by high rates. Therefore, great efforts are dedicated to ameliorating the electrochemical activity and kinetic feature of metal oxides by designing composite materials with other highly conductive layers or scaffolds.

In view of such context, it becomes necessary to think about this question: What are the general principles or guidelines for designing advanced electrode materials? Of course, the rules for supercapacitors and LIBs are kind of different due to their different electrochemical reactions. In the following, we propose the basic rules for designing high-performance electrodes of supercapacitors (see also Figure 23),[3, 5, 448] which can be summarized as four and elaborated as follows.

Rule 1: High power density. This is the most important rule and the prerequisite for high-performance supercapacitors. Supercapacitors are unique because of their high power density, fast recharge capability and long cycle life. The power density is controlled by the kinetic feature of the electrodes, which is tightly related to the transport characteristics of ions and electrons in electrodes and at the electrode/electrolyte interfaces.[448] Therefore, electrodes with porous nanostructures and good conductivity are highly desirable, especially the combination of these two is indispensable for high power density. Porous nanostructures are favorable for fast ion/electron transfer and facilitate the sufficient contact between electrolyte and active materials leading to fast reaction kinetics. As for the conductivity issue, the active materials with high conductivity will show low polarization and accelerate reaction kinetics. In this regard, researchers generally adopt conductive scaffolds or conductive coatings to improve the conductivity of the whole electrode to obtain faster reaction kinetics and enhanced performances.

Rule 2: High capacitance and high working voltage. The energy density (E) of a supercapacitor is governed by the equation: $E = \frac{1}{2}CV^2$ (where C and V represent the

capacitance of the electrode and the potential across the electrode, respectively).[3, 448] In this context, an effective way to boost energy density is to develop electrode materials with high capacitance and high working voltage. To achieve high capacitances, firstly, we have to select active materials with high capacitances. Previous research about active materials of supercapacitors is heavily focused on pure carbon materials, but their specific capacitances are not high enough and encumber the energy density. Then the scientific community shifts its attention to pseudocapacitive materials (such as metal oxides/hydroxides, metal sulfides and conducting polymers),[5, 7, 237] whose specific capacitances are several times larger than carbon materials. Nevertheless, most of pseudocapacitive materials are p-type semiconductors whose conductivity is low and not kinetically favorable for fast electron transfer in high-rate capability. Fortunately, it is found that the two design strategies for high power density in Rule 1 are also applicable for improving capacitance. The porous nanostructure design (porous construction of pseudocapacitive materials) and conductivity modification (combination between pseudocapacitive materials and highly conductive backbones) can effectively improve the utilization of active materials resulting in higher capacitance. As for the working voltage, it depends on several factors including the intrinsic electrochemical reactions of active materials, electrolyte species and macroscopic structure of supercapacitors. Generally, asymmetric supercapacitors exhibit higher working voltage than the symmetric ones.

Rule 3: Lighter the better. The mass unit of energy density and power density is Wh/kg and W/kg, respectively. This means that the energy density and power density will be much higher if the weight of the electrode is low. In commercial supercapacitors, the conductive substrates are metal foams or foils (such as nickel foam or aluminum foil) that do not contribute to the capacitance, but just as a support for active materials. Their weight will account for a large portion in the device and decrease the overall energy density and power density. Fortunately, benefiting from the advancement of superlight graphene/graphite

technologies,[8, 270] three-dimensional (3D) porous graphene or graphite foams have attracted great attention and become promising new light-weight substrates with high conductivity and chemical stability.[449]

Rule 4: High structural stability. A supercapacitor requires a long cycling life more than 10^4 times, so the electrode materials must have strong mechanical and structural stability to reach high cycling life. It has been demonstrated that nanoarrays grown directly on substrates possess good mechanical and structural stability during cycling compared to powders. Particularly, a core/shell nanowire array not only has the merits of porous structure, but also possesses good strain accommodation during cycles resulting in high cycling life.[101, 450]

Based on the rules above, the ideal electrode materials for supercapacitors should be highly porous, conductive, light, highly active and stable. Most of the rules are also applicable for LIBs expect the Rule 1. It is noteworthy that the energy density of LIBs is the core characteristics, not the power density. Any design strategy should not sacrifice the energy density of LIBs. Last but not least, experimental and theoretical fundamental studies on ion/electron transport behavior at the surface and cross-electrode under device working conditions can be of also great help in both electrode design and device configuration.

Acknowledgements

H. J. Fan thanks the financial support by SERC Public Sector Research Funding (Grant number 1121202012), Agency for Science, Technology, and Research (A*STAR) and MOE AcRF Tier 1 (RG 66/11). Support from the Energy Research Institute @NTU (ERI@N) is also great appreciated. J. P. Tu thanks the financial supported by the National Science and Technology Support Program (2012BAK30B04-05) and Key Science and Technology Innovation Team of Zhejiang Province (2010R50013).

Notes and References

1. J. M. Tarascon and M. Armand, *Nature*, 2001, **414**, 359-367.
2. X. Xia, D. Chao, X. Qi, Q. Xiong, Y. Zhang, J. Tu, H. Zhang and H. J. Fan, *Nano Lett.*, 2013, **13**, 4562-4568.
3. J. R. Miller and P. Simon, *Science*, 2008, **321**, 651-652.
4. P. Poizot, S. Laruelle, S. Grugeon, L. Dupont and J. M. Tarascon, *Nature*, 2000, **407**, 496-499.
5. G. P. Wang, L. Zhang and J. J. Zhang, *Chem. Soc. Rev.*, 2012, **41**, 797-828.
6. Q. Zhang, E. Uchaker, S. L. Candelaria and G. Cao, *Chem. Soc. Rev.*, 2013, **42**, 3127-3171.
7. Y. Zhang, H. Feng, X. B. Wu, L. Z. Wang, A. Q. Zhang, T. C. Xia, H. C. Dong, X. F. Li and L. S. Zhang, *Int. J. Hydrogen. Energ*, 2009, **34**, 4889-4899.
8. C. H. Xu, B. H. Xu, Y. Gu, Z. G. Xiong, J. Sun and X. S. Zhao, *Energy Environ. Sci.*, 2013, **6**, 1388-1414.
9. E. Frackowiak and F. Beguin, *Carbon*, 2001, **39**, 937-950.
10. B. Sakintuna, F. Lamari-Darkrim and M. Hirscher, *Int. J. Hydrogen. Energ*, 2007, **32**, 1121-1140.
11. R. Dash, J. Chmiola, G. Yushin, Y. Gogotsi, G. Laudisio, J. Singer, J. Fischer and S. Kucheyev, *Carbon*, 2006, **44**, 2489-2497.
12. D. Choi, G. E. Blomgren and P. N. Kumta, *Adv. Mater.*, 2006, **18**, 1178-1182.
13. A. S. Arico, P. Bruce, B. Scrosati, J. M. Tarascon and W. Van Schalkwijk, *Nat. Mater.*, 2005, **4**, 366-377.
14. C. W. Cheng and H. J. Fan, *Nano Today*, 2012, **7**, 327-343.
15. X. L. Ji, K. T. Lee and L. F. Nazar, *Nat. Mater.*, 2009, **8**, 500-506.
16. J. Hassoun and B. Scrosati, *Angew. Chem. Int. Edit.*, 2010, **49**, 2371-2374.
17. C. K. Chan, H. L. Peng, G. Liu, K. McIlwrath, X. F. Zhang, R. A. Huggins and Y. Cui, *Nat. Nanotech.*, 2008, **3**, 31-35.
18. L. F. Cui, Y. Yang, C. M. Hsu and Y. Cui, *Nano Lett.*, 2009, **9**, 3370-3374.
19. L. F. Cui, R. Ruffo, C. K. Chan, H. L. Peng and Y. Cui, *Nano Lett.*, 2009, **9**, 491-495.
20. H. Nagayama, H. Honda and H. Kawahara, *J. Electrochem. Soc.*, 1988, **135**, 2013-2016.
21. X. H. Xia, J. P. Tu, J. Zhang, X. L. Wang, W. K. Zhang and H. Huang, *Electrochim. Acta*, 2008, **53**, 5721-5724.
22. X. H. Xia, J. P. Tu, J. Zhang, X. L. Wang, W. K. Zhang and H. Huang, *Sol. Energ. Mat. Sol. C.*, 2008, **92**, 628-633.
23. X. H. Huang, J. P. Tu, X. H. Xia, X. L. Wang, J. Y. Xiang and L. Zhang, *J. Power Sources*, 2010, **195**, 1207-1210.
24. X. H. Huang, J. P. Tu, X. H. Xia, X. L. Wang, J. Y. Xiang, L. Zhang and Y. Zhou, *J. Power Sources*, 2009, **188**, 588-591.
25. X. H. Huang, J. P. Tu, Z. Y. Zeng, J. Y. Xiang and X. B. Zhao, *J. Electrochem. Soc.*, 2008, **155**, A438-A441.
26. X. H. Huang, J. P. Tu, X. H. Xia, X. L. Wang and J. Y. Xiang, *Electrochem. Commun.*, 2008, **10**, 1288-1290.
27. X. H. Xia, J. P. Tu, X. L. Wang, C. D. Gu and X. B. Zhao, *J. Mater. Chem.*, 2011, **21**, 671-679.
28. X. H. Xia, J. P. Tu, Y. J. Mai, R. Chen, X. L. Wang, C. D. Gu and X. B. Zhao, *Chem-eur. J.*, 2011, **17**, 10898-10905.
29. X. Y. Yan, X. L. Tong, J. Wang, C. W. Gong, M. G. Zhang and L. P. Liang, *Mater. Lett.*, 2013, **95**, 1-4.
30. J. B. Wu, Z. G. Li and Y. Lin, *Electrochim. Acta*, 2011, **56**, 2116-2121.
31. X. H. Xia, J. P. Tu, Y. Q. Zhang, X. L. Wang, C. D. Gu, X. B. Zhao and H. J. Fan, *ACS Nano*, 2012, **6**, 5531-5538.
32. J. B. Wu, R. Q. Guo, X. H. Huang and Y. Lin, *J. Power Sources*, 2013, **243**, 317-322.
33. Y. J. Mai, X. H. Xia, R. Chen, C. D. Gu, X. L. Wang and J. P. Tu, *Electrochim. Acta*, 2012, **67**, 73-78.
34. J. Fang, Y. F. Yuan, L. K. Wang, H. L. Ni, H. L. Zhu, J. S. Gui, J. L. Yang, Y. B. Chen and S. Y. Guo, *Mater. Lett.*, 2013, **111**, 1-4.
35. Q. Q. Xiong, J. P. Tu, X. H. Xia, X. Y. Zhao, C. D. Gu and X. L. Wang, *Nanoscale*, 2013, **5**, 7906-7912.
36. Y. G. Li, B. Tan and Y. Y. Wu, *Chem. Mater.*, 2008, **20**, 2602-2602.

37. Y. Q. Zhang, X. H. Xia, J. P. Tu, Y. J. Mai, S. J. Shi, X. L. Wang and C. D. Gu, *J. Power Sources*, 2012, **199**, 413-417.
38. J. Zhong, X. L. Wang, X. H. Xia, C. D. Gu, J. Y. Xiang, J. Zhang and J. P. Tu, *J. Alloy. Compd.*, 2011, **509**, 3889-3893.
39. J. H. Zhu, J. A. Jiang, J. P. Liu, R. M. Ding, H. Ding, Y. M. Feng, G. M. Wei and X. T. Huang, *J. Solid State Chem.*, 2011, **184**, 578-583.
40. A. Pan, H. B. Wu, L. Yu, T. Zhu and X. W. Lou, *ACS Appl. Mater. Interfaces*, 2012, **4**, 3874-3879.
41. Y. Z. Zheng, H. Y. Ding and M. L. Zhang, *Mater. Res. Bull.*, 2009, **44**, 403-407.
42. L. Fan, L. Tang, H. F. Gong, Z. H. Yao and R. Guo, *J. Mater. Chem.*, 2012, **22**, 16376-16381.
43. Y. Q. Zou and Y. Wang, *Nanoscale*, 2011, **3**, 2615-2620.
44. S. B. Ni, T. Li, X. H. Lv, X. L. Yang and L. L. Zhang, *Electrochim. Acta*, 2013, **91**, 267-274.
45. C. H. Luo, W. L. Lu, Y. Li, Y. Y. Feng, W. Feng, Y. H. Zhao and X. Y. Yuan, *Appl. Phys. A-mater.*, 2013, **113**, 683-692.
46. M. M. Liu, J. Chang, J. Sun and L. Gao, *RSC Adv.*, 2013, **3**, 8003-8008.
47. Y. G. Zhu, G. S. Cao, C. Y. Sun, J. Xie, S. Y. Liu, T. J. Zhu, X. B. Zhao and H. Y. Yang, *RSC Adv.*, 2013, **3**, 19409-19415.
48. Q. Li, Y. J. Chen, T. Yang, D. N. Lei, G. H. Zhang, L. Mei, L. B. Chen, Q. H. Li and T. H. Wang, *Electrochim. Acta*, 2013, **90**, 80-89.
49. H. Liu and W. Yang, *Energy Environ. Sci.*, 2011, **4**, 4000.
50. J. M. Ma, J. Q. Yang, L. F. Jiao, Y. H. Mao, T. H. Wang, X. C. Duan, J. B. Lian and W. J. Zheng, *CrystEngComm*, 2012, **14**, 453-459.
51. A. K. Mondal, D. W. Su, Y. Wang, S. Q. Chen, Q. Liu and G. X. Wang, *J. Alloy. Compd.*, 2014, **582**, 522-527.
52. Q. F. Wu, Z. H. Hu and Y. F. Liu, *J. Mater. Eng. Perform.*, 2013, **22**, 2398-2402.
53. Z. H. Zhu, J. Ping, X. P. Huang, J. G. Hu, Q. Y. Chen, X. B. Ji and C. E. Banks, *J. Mater. Sci.*, 2012, **47**, 503-507.
54. D. W. Wang, F. Li and H. M. Cheng, *J. Power Sources*, 2008, **185**, 1563-1568.
55. Q. F. Wu, Y. F. Liu and Z. H. Hu, *J. Solid State Electr.*, 2013, **17**, 1711-1716.
56. Y. G. Li and Y. Y. Wu, *Chem. Mater.*, 2010, **22**, 5537-5542.
57. X. H. Xia, J. P. Tu, J. Y. Xiang, X. H. Huang, X. L. Wang and X. B. Zhao, *J. Power Sources*, 2010, **195**, 2014-2022.
58. D. W. Su, H. S. Kim, W. S. Kim and G. X. Wang, *Chem-eur. J.*, 2012, **18**, 8224-8229.
59. X. H. Wang, L. Qiao, X. L. Sun, X. W. Li, D. K. Hu, Q. Zhang and D. Y. He, *J. Mater. Chem. A*, 2013, **1**, 4173-4176.
60. J. T. Zai, C. Yu, L. Q. Tao, M. Xu, Y. L. Xiao, B. Li, Q. Y. Han, K. X. Wang and X. F. Qian, *CrystEngComm*, 2013, **15**, 6663-6671.
61. Z.-l. Wang, D. Xu, L.-m. Wang and X.-b. Zhang, *ChemPlusChem*, 2012, **77**, 124-128.
62. M. M. Liu, J. Chang, J. Sun and L. Gao, *Electrochim. Acta*, 2013, **107**, 9-15.
63. M. S. Wu and C. H. Yang, *Appl. Phys. Lett.*, 2007, **91**, 033109 - 033109-033103
64. M. S. Wu and Y. P. Lin, *Electrochim. Acta*, 2011, **56**, 2068-2073.
65. M. S. Wu and H. H. Hsieh, *Electrochim. Acta*, 2008, **53**, 3427-3435.
66. M. S. Wu, Y. A. Huang, C. H. Yang and H. H. Jow, *Int. J. Hydrogen. Energ*, 2007, **32**, 4153-4159.
67. M. S. Wu and M. J. Wang, *Electrochem. Solid St*, 2010, **13**, A1-A3.
68. M. S. Wu, M. J. Wang and J. J. Jow, *J. Power Sources*, 2010, **195**, 3950-3955.
69. Y. F. Yuan, X. H. Xia, J. B. Wu, J. L. Yang, Y. B. Chen and S. Y. Guo, *Electrochem. Commun.*, 2010, **12**, 890-893.
70. X. H. Wang, Z. B. Yang, X. L. Sun, X. W. Li, D. S. Wang, P. Wang and D. Y. He, *J. Mater. Chem.*, 2011, **21**, 9988-9990.
71. S. G. Hwang, G. O. Kim, S. R. Yun and K. S. Ryu, *Electrochim. Acta*, 2012, **78**, 406-411.
72. K. Liang, X. Z. Tang and W. C. Hu, *J. Mater. Chem.*, 2012, **22**, 11062-11067.
73. M. S. Wu, D. S. Chan, K. H. Lin and J. J. Jow, *Mater. Chem. Phys.*, 2011, **130**, 1239-1245.
74. M. S. Wu, C. Y. Huang and K. H. Lin, *J. Power Sources*, 2009, **186**, 557-564.
75. U. M. Patil, R. R. Salunkhe, K. V. Gurav and C. D. Lokhande, *Appl. Surf. Sci.*, 2008, **255**, 2603-2607.
76. M. W. Xu, S. J. Bao and H. L. Li, *J. Solid State Electr.*, 2007, **11**, 372-377.

77. M. P. Yeager, D. Su, N. S. Marinkovic and X. W. Teng, *J. Electrochem. Soc.*, 2012, **159**, A1598-A1603.
78. F. B. Zhang, Y. K. Zhou and H. L. Li, *Mater. Chem. Phys.*, 2004, **83**, 260-264.
79. L. Yuan, Z. P. Guo, K. Konstantinov, P. Munroe and H. K. Liu, *Electrochem. Solid St*, 2006, **9**, A524-A528.
80. D. D. Han, P. C. Xu, X. Y. Jing, J. Wang, D. L. Song, J. Y. Liu and M. L. Zhang, *J. Solid State Chem.*, 2013, **203**, 60-67.
81. D. D. Han, P. C. Xu, X. Y. Jing, J. Wang, P. P. Yang, Q. H. Shen, J. Y. Liu, D. L. Song, Z. Gao and M. L. Zhang, *J. Power Sources*, 2013, **235**, 45-53.
82. Q. Li, H. F. Ni, Y. Cai, X. Y. Cai, Y. J. Liu, G. Chen, L. Z. Fan and Y. D. Wang, *Mater. Res. Bull.*, 2013, **48**, 3518-3526.
83. C. Z. Yuan, L. R. Hou, Y. L. Feng, S. L. Xiong and X. G. Zhang, *Electrochim. Acta*, 2013, **88**, 507-512.
84. S. M. Abbas, S. T. Hussain, S. Ali, K. S. Munawar, N. Ahmad and N. Ali, *Mater. Lett.*, 2013, **107**, 158-161.
85. L. Q. Tao, J. T. Zai, K. X. Wang, Y. H. Wan, H. J. Zhang, C. Yu, Y. L. Xiao and X. F. Qian, *RSC Adv.*, 2012, **2**, 3410-3415.
86. M. S. Wu and H. W. Chang, *J. Phys. Chem. C*, 2013, **117**, 2590-2599.
87. X. J. Zhu, J. Hu, H. L. Dai, L. Ding and L. Jiang, *Electrochim. Acta*, 2012, **64**, 23-28.
88. A. S. Adekunle, K. I. Ozoemena, B. B. Mamba, B. O. Agboola and O. S. Oluwatobi, *International Journal of Electrochemical Science*, 2011, **6**, 4760-4774.
89. J. Xu, X. F. Gu, J. Y. Cao, W. C. Wang and Z. D. Chen, *J. Solid State Electr.*, 2012, **16**, 2667-2674.
90. X. H. Huang, J. P. Tu, C. Q. Zhang and F. Zhou, *Electrochim. Acta*, 2010, **55**, 8981-8985.
91. S. I. Kim, J. S. Lee, H. J. Ahn, H. K. Song and J. H. Jang, *ACS Appl. Mater. Interfaces*, 2013, **5**, 1596-1603.
92. M. C. Liu, L. B. Kong, C. Lu, X. M. Li, Y. C. Luo and L. Kang, *ACS Appl. Mater. Interfaces*, 2012, **4**, 4631-4636.
93. A. K. Rai, L. T. Anh, C. J. Park and J. Kim, *Ceram. Int.*, 2013, **39**, 6611-6618.
94. N. Behm, D. Brokaw, C. Overson, D. Peloquin and J. C. Poler, *J. Mater. Sci.*, 2013, **48**, 1711-1716.
95. C. Y. Cao, W. Guo, Z. M. Cui, W. G. Song and W. Cai, *J. Mater. Chem.*, 2011, **21**, 3204-3209.
96. Y. Ren and L. A. Gao, *J. Am. Ceram. Soc.*, 2010, **93**, 3560-3564.
97. S. Vijayakumar, S. Nagamuthu and G. Muralidharan, *ACS Appl. Mater. Interfaces*, 2013, **5**, 2188-2196.
98. J. P. Liu, J. Jiang, C. W. Cheng, H. X. Li, J. X. Zhang, H. Gong and H. J. Fan, *Adv. Mater.*, 2011, **23**, 2076-2081.
99. X. H. Xia, J. P. Tu, Y. Q. Zhang, J. Chen, X. L. Wang, C. D. Gu, C. Guan, J. S. Luo and H. J. Fan, *Chem. Mater.*, 2012, **24**, 3793-3799.
100. C. Guan, J. P. Liu, C. W. Cheng, H. X. Li, X. L. Li, W. W. Zhou, H. Zhang and H. J. Fan, *Energy Environ. Sci.*, 2011, **4**, 4496-4499.
101. C. Guan, X. H. Xia, N. Meng, Z. Y. Zeng, X. H. Cao, C. Soci, H. Zhang and H. J. Fan, *Energy Environ. Sci.*, 2012, **5**, 9085-9090.
102. J. Chen, X. H. Xia, J. P. Tu, Q. Q. Xiong, Y. X. Yu, X. L. Wang and C. D. Gu, *J. Mater. Chem.*, 2012, **22**, 15056-15061.
103. X. H. Xia, J. P. Tu, Y. Q. Zhang, Y. J. Mai, X. L. Wang, C. D. Gu and X. B. Zhao, *RSC Adv.*, 2012, **2**, 1835-1841.
104. J. Jiang, J. P. Liu, R. M. Ding, X. X. Ji, Y. Y. Hu, X. Li, A. Z. Hu, F. Wu, Z. H. Zhu and X. T. Huang, *J. Phys. Chem. C*, 2010, **114**, 929-932.
105. X. Y. Xue, S. A. Yuan, L. L. Xing, Z. H. Chen, B. He and Y. J. Chen, *Chem. Commun.*, 2011, **47**, 4718-4720.
106. J. H. Kwak, Y. W. Lee and J. H. Bang, *Mater. Lett.*, 2013, **110**, 237-240.
107. F. D. Wu and Y. Wang, *J. Mater. Chem.*, 2011, **21**, 6636-6641.
108. D. Fang, L. C. Li, W. L. Xu, G. Z. Li, G. Li, N. F. Wang, Z. P. Luo, J. Xu, L. Liu, C. L. Huang, C. W. Liang and Y. S. Ji, *J. Mater. Chem. A*, 2013, **1**, 13203-13208.

109. J. Liu, Y. C. Zhou, C. P. Liu, J. B. Wang, Y. Pan and D. F. Xue, *CrystEngComm*, 2012, **14**, 2669-2674.
110. L. Li, K. H. Seng, Z. X. Chen, Z. P. Guo and H. K. Liu, *Nanoscale*, 2013, **5**, 1922-1928.
111. X. C. Dong, H. Xu, X. W. Wang, Y. X. Huang, M. B. Chan-Park, H. Zhang, L. H. Wang, W. Huang and P. Chen, *ACS Nano*, 2012, **6**, 3206-3213.
112. L. Yang, S. Cheng, Y. Ding, X. B. Zhu, Z. L. Wang and M. L. Liu, *Nano Lett.*, 2012, **12**, 321-325.
113. X. H. Xia, J. P. Tu, Y. J. Mai, X. L. Wang, C. D. Gu and X. B. Zhao, *J. Mater. Chem.*, 2011, **21**, 9319-9325.
114. C. Zhou, Y. W. Zhang, Y. Y. Li and J. P. Liu, *Nano Lett.*, 2013, **13**, 2078-2085.
115. G. M. Wang, X. H. Lu, Y. C. Ling, T. Zhai, H. Y. Wang, Y. X. Tong and Y. Li, *ACS Nano*, 2012, **6**, 10296-10302.
116. K. T. Nam, D. W. Kim, P. J. Yoo, C. Y. Chiang, N. Meethong, P. T. Hammond, Y. M. Chiang and A. M. Belcher, *Science*, 2006, **312**, 885-888.
117. H. Qiao, L. F. Xiao, Z. Zheng, H. W. Liu, F. L. Jia and L. Z. Zhang, *J. Power Sources*, 2008, **185**, 486-491.
118. C. Guan, Z. Zeng, X. Li, X. Cao, Y. Fan, X. Xia, G. Pan, H. Zhang and H. J. Fan, *Small*, 2013, n/a-n/a.
119. J. Xu, Q. F. Wang, X. W. Wang, Q. Y. Xiang, B. Hang, D. Chen and G. Z. Shen, *ACS Nano*, 2013, **7**, 5453-5462.
120. H. N. Zhang, Y. J. Chen, W. W. Wang, G. H. Zhang, M. Zhuo, H. M. Zhang, T. Yang, Q. H. Li and T. H. Wang, *J. Mater. Chem. A*, 2013, **1**, 8593-8600.
121. H. Xia, D. D. Zhu, Z. T. Luo, Y. Yu, X. Q. Shi, G. L. Yuan and J. P. Xie, *Scientific Reports*, 2013, **3**, 2978.
122. G. H. Zhang, T. H. Wang, X. Z. Yu, H. N. Zhang, H. G. Duan and B. A. Lu, *Nano Energy*, 2013, **2**, 586-594.
123. C. H. Tang, X. S. Yin and H. Gong, *ACS Appl. Mater. Interfaces*, 2013, **5**, 10574-10582.
124. Y. J. Fu, X. W. Li, X. L. Sun, X. H. Wang, D. Q. Liu and D. Y. He, *J. Mater. Chem.*, 2012, **22**, 17429-17431.
125. S. L. Xiong, C. Z. Yuan, M. F. Zhang, B. J. Xi and Y. T. Qian, *Chem-eur. J.*, 2009, **15**, 5320-5326.
126. G. X. Wang, X. P. Shen, J. Horvat, B. Wang, H. Liu, D. Wexler and J. Yao, *J. Phys. Chem. C*, 2009, **113**, 4357-4361.
127. H. T. Wang, L. Zhang, X. H. Tan, C. M. B. Holt, B. Zahiri, B. C. Olsen and D. Mitlin, *J. Phys. Chem. C*, 2011, **115**, 17599-17605.
128. H. Pang, F. Gao, Q. Chen, R. M. Liu and Q. Y. Lu, *Dalton T.*, 2012, **41**, 5862-5868.
129. F. Zhang, C. Z. Yuan, X. J. Lu, L. J. Zhang, Q. Che and X. G. Zhang, *J. Power Sources*, 2012, **203**, 250-256.
130. H. Y. Sun, M. Ahmad and J. Zhu, *Electrochim. Acta*, 2013, **89**, 199-205.
131. S. B. Zhou, G. Wang, Y. Z. Xie, H. Wang and J. B. Bai, *J Nanopart. Res.*, 2013, **15**.
132. Y. Liu and X. G. Zhang, *Solid State Ionics*, 2013, **231**, 63-68.
133. S. W. Bian and L. Zhu, *RSC Adv.*, 2013, **3**, 4212-4215.
134. X. W. Wang, S. Q. Liu, H. Y. Wang, F. Y. Tu, D. Fang and Y. H. Li, *J. Solid State Electr.*, 2012, **16**, 3593-3602.
135. X. M. Liu, Q. Long, C. H. Jiang, B. B. Zhan, C. Li, S. J. Liu, Q. Zhao, W. Huang and X. C. Dong, *Nanoscale*, 2013, **5**, 6525-6529.
136. L. J. Xie, K. X. Li, G. H. Sun, Z. A. Hu, C. X. Lv, J. L. Wang and C. M. Zhang, *J. Solid State Electr.*, 2013, **17**, 55-61.
137. S. K. Meher and G. R. Rao, *J. Phys. Chem. C*, 2011, **115**, 15646-15654.
138. B. R. Duan and Q. Cao, *Electrochim. Acta*, 2012, **64**, 154-161.
139. Y. Liu, C. H. Mi, L. H. Su and X. G. Zhang, *Electrochim. Acta*, 2008, **53**, 2507-2513.
140. Y. Wang, H. Xia, L. Lu and J. Y. Lin, *ACS Nano*, 2010, **4**, 1425-1432.
141. W. L. Yao, J. Yang, J. L. Wang and Y. Nuli, *J. Electrochem. Soc.*, 2008, **155**, A903-A908.
142. C. Z. Yuan, L. Yang, L. R. Hou, J. Y. Li, Y. X. Sun, X. G. Zhang, L. F. Shen, X. J. Lu, S. L. Xiong and X. W. Lou, *Adv. Funct. Mater.*, 2012, **22**, 2560-2566.
143. W. W. Yuan, D. Xie, Z. M. Dong, Q. M. Su, J. Zhang, G. H. Du and B. S. Xu, *Mater. Lett.*, 2013, **97**, 129-132.

144. G. M. Zhou, L. Li, Q. Zhang, N. Li and F. Li, *Phys. Chem. Chem. Phys.*, 2013, **15**, 5582-5587.
145. C. C. Li, Q. H. Li, L. B. Chen and T. H. Wang, *J. Mater. Chem.*, 2011, **21**, 11867-11872.
146. A. M. Hashem, A. M. Abdel-Latif, H. M. Abuzeid, H. M. Abbas, H. Ehrenberg, R. S. Farag, A. Mauger and C. M. Julien, *J. Alloy. Compd.*, 2011, **509**, 9669-9674.
147. M. X. Liao, Y. F. Liu, Z. H. Hu and Q. Yu, *J. Alloy. Compd.*, 2013, **562**, 106-110.
148. T. Zhu, J. S. Chen and X. W. Lou, *J. Mater. Chem.*, 2010, **20**, 7015-7020.
149. L. R. Hou, C. Z. Yuan, L. Yang, L. F. Shen, F. Zhang and X. G. Zhang, *RSC Adv.*, 2011, **1**, 1521-1526.
150. Q. Wang, C. Y. Zhang, X. B. Xia, L. L. Xing and X. Y. Xue, *Mater. Lett.*, 2013, **112**, 162-164.
151. L. H. Zhuo, Y. Q. Wu, J. Ming, L. Y. Wang, Y. C. Yu, X. B. Zhang and F. Y. Zhao, *J. Mater. Chem. A*, 2013, **1**, 1141-1147.
152. G. X. Wang, X. P. Shen, J. N. Yao, D. Wexler and J. Ahn, *Electrochem. Commun.*, 2009, **11**, 546-549.
153. Y. H. Xiao, S. J. Liu, F. Li, A. Q. Zhang, J. H. Zhao, S. M. Fang and D. Z. Jia, *Adv. Funct. Mater.*, 2012, **22**, 4052-4059.
154. D. H. Zhang and W. B. Zou, *Curr. Appl. Phys.*, 2013, **13**, 1796-1800.
155. K. Deori, S. K. Ujjain, R. K. Sharma and S. Deka, *ACS Appl. Mater. Interfaces*, 2013, **5**, 10665-10672.
156. J. Liu, H. Xia, L. Lu and D. F. Xue, *J. Mater. Chem.*, 2010, **20**, 1506-1510.
157. L. Q. Tao, J. T. Zai, K. X. Wang, H. J. Zhang, M. Xu, J. Shen, Y. Z. Su and X. F. Qian, *J. Power Sources*, 2012, **202**, 230-235.
158. Y. Wang, F. Yan, S. W. Liu, A. Y. S. Tan, H. H. Song, X. W. Sun and H. Y. Yang, *J. Mater. Chem. A*, 2013, **1**, 5212-5216.
159. Z. G. Wen, F. Zheng, Z. R. Jiang, M. X. Li and Y. X. Luo, *J. Mater. Sci.*, 2013, **48**, 342-347.
160. N. Du, H. Zhang, B. Chen, J. B. Wu, X. Y. Ma, Z. H. Liu, Y. Q. Zhang, D. Yang, X. H. Huang and J. P. Tu, *Adv. Mater.*, 2007, **19**, 4505-4509.
161. L. Y. Pan, H. B. Zhao, W. C. Shen, X. W. Dong and J. Q. Xu, *J. Mater. Chem. A*, 2013, **1**, 7159-7166.
162. X. W. Lou, D. Deng, J. Y. Lee, J. Feng and L. A. Archer, *Adv. Mater.*, 2008, **20**, 258-262.
163. H. W. Shim, A. H. Lim, J. C. Kim, E. Jang, S. D. Seo, G. H. Lee, T. D. Kim and D. W. Kim, *Scientific Reports*, 2013, **3**, 2325.
164. X. Zhu, G. Q. Ning, X. L. Ma, Z. J. Fan, C. G. Xu, J. S. Gao, C. M. Xu and F. Wei, *J. Mater. Chem. A*, 2013, **1**, 14023-14030.
165. J. Sun, H. M. Liu, X. Chen, D. G. Evans and W. S. Yang, *Nanoscale*, 2013, **5**, 7564-7571.
166. S. Vijayanand, R. Kannan, H. S. Potdar, V. K. Pillai and P. A. Joy, *J. Appl. Electrochem.*, 2013, **43**, 995-1003.
167. R. Xu, J. W. Wang, Q. Y. Li, G. Y. Sun, E. B. Wang, S. H. Li, J. M. Gu and M. L. Ju, *J. Solid State Chem.*, 2009, **182**, 3177-3182.
168. Y. M. Sun, X. L. Hu, W. Luo and Y. H. Huang, *J. Mater. Chem.*, 2012, **22**, 13826-13831.
169. C. H. Chen, B. J. Hwang, J. S. Do, J. H. Weng, M. Venkateswarlu, M. Y. Cheng, R. Santhanam, K. Ragavendran, J. F. Lee, J. M. Chen and D. G. Liu, *Electrochem. Commun.*, 2010, **12**, 496-498.
170. J. Zhi, S. Deng, Y. X. Zhang, Y. F. Wang and A. G. Hu, *J. Mater. Chem. A*, 2013, **1**, 3171-3176.
171. W. Du, R. M. Liu, Y. W. Jiang, Q. Y. Lu, Y. Z. Fan and F. Gao, *J. Power Sources*, 2013, **227**, 101-105.
172. S. G. Kandalkar, C. D. Lokhande, R. S. Mane and S. H. Han, *Appl. Surf. Sci.*, 2007, **253**, 3952-3956.
173. S. G. Kandalkar, J. L. Gunjakar and C. D. Lokhande, *Appl. Surf. Sci.*, 2008, **254**, 5540-5544.
174. B. J. Li, H. Q. Cao, J. Shao, G. Q. Li, M. Z. Qu and G. Yin, *Inorg. Chem.*, 2011, **50**, 1628-1632.
175. G. L. Wang, J. C. Liu, S. Tang, H. Y. Li and D. X. Cao, *J. Solid State Electr.*, 2011, **15**, 2587-2592.
176. Y. F. Wang and L. J. Zhang, *J. Power Sources*, 2012, **209**, 20-29.
177. M. Zhang, M. Q. Jia, Y. H. Jin and X. R. Shi, *Appl. Surf. Sci.*, 2012, **263**, 573-578.
178. W. W. Zhou, J. P. Liu, T. Chen, K. S. Tan, X. T. Jia, Z. Q. Luo, C. X. Cong, H. P. Yang, C. M. Li and T. Yu, *Phys. Chem. Chem. Phys.*, 2011, **13**, 14462-14465.

179. J. Zhang, J. P. Tu, X. H. Xia, X. L. Wang and C. D. Gu, *J. Mater. Chem.*, 2011, **21**, 5492-5498.
180. H. C. Liu and S. K. Yen, *J. Power Sources*, 2007, **166**, 478-484.
181. S. L. Chou, J. Z. Wang, H. K. Liu and S. X. Dou, *J. Power Sources*, 2008, **182**, 359-364.
182. G. P. Kim, I. Nam, N. D. Kim, J. Park, S. Park and J. Yi, *Electrochem. Commun.*, 2012, **22**, 93-96.
183. V. Srinivasan and J. W. Weidner, *J. Power Sources*, 2002, **108**, 15-20.
184. C. Z. Yuan, L. Yang, L. R. Hou, L. F. Shen, X. G. Zhang and X. W. Lou, *Energy Environ. Sci.*, 2012, **5**, 7883-7887.
185. Y. F. Yuan, X. H. Xia, J. B. Wu, X. H. Huang, Y. B. Pei, J. L. Yang and S. Y. Guo, *Electrochem. Commun.*, 2011, **13**, 1123-1126.
186. X. H. Xia, J. P. Tu, X. L. Wang, C. D. Gu and X. B. Zhao, *Chem. Commun.*, 2011, **47**, 5786-5788.
187. J. B. Wu, Y. Lin, X. H. Xia, J. Y. Xu and Q. Y. Shi, *Electrochim. Acta*, 2011, **56**, 7163-7170.
188. C. W. Kung, H. W. Chen, C. Y. Lin, R. Vittal and K. C. Ho, *J. Power Sources*, 2012, **214**, 91-99.
189. J. H. Zhong, A. L. Wang, G. R. Li, J. W. Wang, Y. N. Ou and Y. X. Tong, *J. Mater. Chem.*, 2012, **22**, 5656-5665.
190. N. A. Kyeremateng, C. Lebouin, P. Knauth and T. Djenizian, *Electrochim. Acta*, 2013, **88**, 814-820.
191. C. Wang, D. L. Wang, Q. M. Wang and L. Wang, *Electrochim. Acta*, 2010, **55**, 6420-6425.
192. C. Lin, J. A. Ritter and B. N. Popov, *J. Electrochem. Soc.*, 1998, **145**, 4097-4103.
193. B. Guo, C. S. Li and Z. Y. Yuan, *J. Phys. Chem. C*, 2010, **114**, 12805-12817.
194. W. L. Yao, J. Q. Chen and H. W. Cheng, *J. Solid State Electr.*, 2011, **15**, 183-188.
195. Y. X. Gu, F. F. Jian and X. Wang, *Thin Solid Films*, 2008, **517**, 652-655.
196. Y. H. Ding, P. Zhang, Z. L. Long, Y. Jiang, J. N. Huang, W. J. Yan and G. Liu, *Mater. Lett.*, 2008, **62**, 3410-3412.
197. J. Park, W. G. Moon, G. P. Kim, I. Nam, S. Park, Y. Kim and J. Yi, *Electrochim. Acta*, 2013, **105**, 110-114.
198. G. Chen, E. G. Fu, M. Zhou, Y. Xu, L. Fei, S. G. Deng, V. Chaitanya, Y. Q. Wang and H. M. Luo, *J. Alloy. Compd.*, 2013, **578**, 349-354.
199. Y. Lu, Y. Wang, Y. Q. Zou, Z. Jiao, B. Zhao, Y. Q. He and M. H. Wu, *Electrochem. Commun.*, 2010, **12**, 101-105.
200. J. Q. Wang, B. Niu, G. D. Du, R. Zeng, Z. X. Chen, Z. P. Guo and S. X. Dou, *Mater. Chem. Phys.*, 2011, **126**, 747-754.
201. S. Q. Chen and Y. Wang, *J. Mater. Chem.*, 2010, **20**, 9735-9739.
202. J. Q. Wang, G. D. Du, R. Zeng, B. Niu, Z. X. Chen, Z. P. Guo and S. X. Dou, *Electrochim. Acta*, 2010, **55**, 4805-4811.
203. C. T. Hsieh, J. S. Lin, Y. F. Chen and H. S. Teng, *J. Phys. Chem. C*, 2012, **116**, 15251-15258.
204. S. Vijayakumar, A. K. Ponnalagi, S. Nagamuthu and G. Muralidharan, *Electrochim. Acta*, 2013, **106**, 500-505.
205. L. Cui, J. Li and X. G. Zhang, *J. Appl. Electrochem.*, 2009, **39**, 1871-1876.
206. J. Yan, T. Wei, W. M. Qiao, B. Shao, Q. K. Zhao, L. J. Zhang and Z. J. Fan, *Electrochim. Acta*, 2010, **55**, 6973-6978.
207. Y. G. Li, B. Tan and Y. Y. Wu, *J. Am. Chem. Soc.*, 2006, **128**, 14258-14259.
208. Y. G. Li, B. Tan and Y. Y. Wu, *Nano Lett.*, 2008, **8**, 265-270.
209. Y. Y. Gao, S. L. Chen, D. X. Cao, G. L. Wang and J. L. Yin, *J. Power Sources*, 2010, **195**, 1757-1760.
210. G. Filipic and U. Cvelbar, *Nanotechnology*, 2012, **23**.
211. J. C. Park, J. Kim, H. Kwon and H. Song, *Adv. Mater.*, 2009, **21**, 803-807.
212. B. Wang, X.-L. Wu, C.-Y. Shu, Y.-G. Guo and C.-R. Wang, *J. Mater. Chem.*, 2010, **20**, 10661-10664.
213. X. Zhang, W. Shi, J. Zhu, D. J. Kharistal, W. Zhao, B. S. Lalia, H. H. Hng and Q. Yan, *ACS Nano*, 2011, **5**, 2013-2019.
214. J. Xiang, J. Tu, Y. Yuan, X. Huang, Y. Zhou and L. Zhang, *Electrochem. Commun.*, 2009, **11**, 262-265.

215. J. Xiang, J. Tu, L. Zhang, Y. Zhou, X. Wang and S. Shi, *J. Power Sources*, 2010, **195**, 313-319.
216. B. Heng, C. Qing, D. Sun, B. Wang, H. Wang and Y. Tang, *RSC Adv.*, 2013, **3**, 15719-15726.
217. J. Xiang, J. Tu, X. Huang and Y. Yang, *J. Solid State Electr.*, 2008, **12**, 941-945.
218. J. Xiang, J. Tu, J. Zhang, J. Zhong, D. Zhang and J. Cheng, *Electrochem. Commun.*, 2010, **12**, 1103-1107.
219. J. Xiang, J. Tu, L. Zhang, Y. Zhou, X. Wang and S. Shi, *Electrochim. Acta*, 2010, **55**, 1820-1824.
220. Y. J. Mai, X. L. Wang, J. Y. Xiang, Y. Q. Qiao, D. Zhang, C. D. Gu and J. P. Tu, *Electrochim. Acta*, 2011, **56**, 2306-2311.
221. S. Ko, J. I. Lee, H. S. Yang, S. Park and U. Jeong, *Adv. Mater.*, 2012, **24**, 4451-4456.
222. J. Y. Lin, J. H. Liao and S. W. Chou, *Electrochim. Acta*, 2011, **56**, 8818-8826.
223. B. Zhao, P. Liu, H. Zhuang, Z. Jiao, T. Fang, W. Xu, B. Lu and Y. Jiang, *J. Mater. Chem. A*, 2013, **1**, 367-373.
224. X. Y. Shen, S. Chen, D. B. Mu, B. R. Wu and F. Wu, *J. Power Sources*, 2013, **238**, 173-179.
225. Z. Wang, F. Su, S. Madhavi and X. W. Lou, *Nanoscale*, 2011, **3**, 1618-1623.
226. J. Xiang, J. Tu, Y. Yuan, X. Wang, X. Huang and Z. Zeng, *Electrochim. Acta*, 2009, **54**, 1160-1165.
227. L. Yu, Y. Jin, L. Li, J. Ma, G. Wang, B. Geng and X. Zhang, *CrystEngComm*, 2013, **15**, 7657-7662.
228. A. Banerjee, U. Singh, V. Aravindan, M. Srinivasan and S. Ogale, *Nano Energy*, 2013, **2**, 1158-1163.
229. S. Gao, S. Yang, J. Shu, S. Zhang, Z. Li and K. Jiang, *J. Phys. Chem. C*, 2008, **112**, 19324-19328.
230. G. S. Gund, D. P. Dubal, D. S. Dhawale, S. S. Shinde and C. D. Lokhande, *RSC Adv.*, 2013, **3**, 24099-24107.
231. W. X. Zhang, X. G. Wen and S. H. Yang, *Inorg. Chem.*, 2003, **42**, 5005-5014.
232. Y. Lee, I. Leu, C. Liao, S. Chang, M. Wu, J. Yen and K. Fung, *Electrochem. Solid St.*, 2006, **9**, A207-A210.
233. X. M. Liu and Y. C. Zhou, *Appl. Phys. A-mater.*, 2005, **81**, 685-689.
234. J. Xiang, X. Wang, X. Xia, L. Zhang, Y. Zhou, S. Shi and J. Tu, *Electrochim. Acta*, 2010, **55**, 4921-4925.
235. A. Goyal, A. L. M. Reddy and P. M. Ajayan, *Small*, 2011, **7**, 1709-1713.
236. M. J. Deng, C. Z. Song, P. J. Ho, C. C. Wang, J. M. Chen and K. T. Lu, *Phys. Chem. Chem. Phys.*, 2013, **15**, 7479-7483.
237. W. F. Wei, X. W. Cui, W. X. Chen and D. G. Ivey, *Chem. Soc. Rev.*, 2011, **40**, 1697-1721.
238. J. L. Liu, L. Z. Fan and X. H. Qu, *Electrochim. Acta*, 2012, **66**, 302-305.
239. Y. Liu, D. Yan, R. F. Zhuo, S. K. Li, Z. G. Wu, J. Wang, P. Y. Ren, P. X. Yan and Z. R. Geng, *J. Power Sources*, 2013, **242**, 78-85.
240. Y. S. Luo, D. Z. Kong, J. S. Luo, S. Chen, D. Y. Zhang, K. W. Qiu, X. Y. Qi, H. Zhang, C. M. Li and T. Yu, *RSC Adv.*, 2013, **3**, 14413-14422.
241. H. Xia, M. O. Lai and L. Lu, *J. Mater. Chem.*, 2010, **20**, 6896-6902.
242. S. W. Bian, Y. P. Zhao and C. Y. Xian, *Mater. Lett.*, 2013, **111**, 75-77.
243. J. X. Zhu, W. H. Shi, N. Xiao, X. H. Rui, H. T. Tan, X. H. Lu, H. H. Hng, J. Ma and Q. Y. Yan, *ACS Appl. Mater. Interfaces*, 2012, **4**, 2769-2774.
244. Z. C. Yang, C. H. Tang, H. Gong, X. Li and J. Wang, *J. Power Sources*, 2013, **240**, 713-720.
245. Y. Wang, Z. J. Han, S. F. Yu, R. R. Song, H. H. Song, K. Ostrikov and H. Y. Yang, *Carbon*, 2013, **64**, 230-236.
246. M. Xu, L. Kong, W. Zhou and H. Li, *J. Phys. Chem. C*, 2007, **111**, 19141-19147.
247. Y. Huang, Y. Y. Li, Z. Q. Hu, G. M. Wei, J. L. Guo and J. P. Liu, *J. Mater. Chem. A*, 2013, **1**, 9809-9813.
248. X. D. Liu, C. Z. Chen, Y. Y. Zhao and B. Jia, *J. Nanomater.*, 2013.
249. V. Subramanian, H. W. Zhu, R. Vajtai, P. M. Ajayan and B. Q. Wei, *J. Phys. Chem. B*, 2005, **109**, 20207-20214.
250. B. Ming, J. Li, F. Kang, G. Pang, Y. Zhang, L. Chen, J. Xu and X. Wang, *J. Power Sources*, 2012, **198**, 428-431.

251. A. Bahloul, B. Nessark, E. Briot, H. Groult, A. Mauger, K. Zaghib and C. M. Julien, *J. Power Sources*, 2013, **240**, 267-272.
252. A. Sumboja, C. Y. Foo, J. Yan, C. Y. Yan, R. K. Gupta and P. S. Lee, *J. Mater. Chem.*, 2012, **22**, 23921-23928.
253. W. Tang, Y. Y. Hou, X. J. Wang, Y. Bai, Y. S. Zhu, H. Sun, Y. B. Yue, Y. P. Wu, K. Zhu and R. Holze, *J. Power Sources*, 2012, **197**, 330-333.
254. X. Wang and Y. D. Li, *J. Am. Chem. Soc.*, 2002, **124**, 2880-2881.
255. P. Yu, X. Zhang, D. L. Wang, L. Wang and Y. W. Ma, *Crst. Growth. Des.*, 2009, **9**, 528-533.
256. Z. J. Sun, H. Y. Chen, D. Shu, C. He, S. Q. Tang and J. Zhang, *J. Power Sources*, 2012, **203**, 233-242.
257. R. S. Kalubarme, H. S. Jadhav and C. J. Park, *Electrochim. Acta*, 2013, **87**, 457-465.
258. D. L. Yan, Z. L. Guo, G. S. Zhu, Z. Z. Yu, H. R. Xu and A. B. Yu, *J. Power Sources*, 2012, **199**, 409-412.
259. X. Zhang, P. Yu, H. T. Zhang, D. C. Zhang, X. Z. Sun and Y. W. Ma, *Electrochim. Acta*, 2013, **89**, 523-529.
260. X. M. Feng, Z. Z. Yan, N. N. Chen, Y. Zhang, Y. W. Ma, X. F. Liu, Q. L. Fan, L. H. Wang and W. Huang, *J. Mater. Chem. A*, 2013, **1**, 12818-12825.
261. Y. Zhao, P. Jiang and S. S. Xie, *J. Power Sources*, 2013, **239**, 393-398.
262. W. Yao, H. Zhou and Y. Lu, *J. Power Sources*, 2013, **241**, 359-366.
263. C. Z. Yuan, L. R. Hou, L. Yang, D. K. Li, L. F. Shen, F. Zhang and X. G. Zhang, *J. Mater. Chem.*, 2011, **21**, 16035-16041.
264. N. A. Tang, X. K. Tian, C. Yang and Z. B. Pi, *Mater. Res. Bull.*, 2009, **44**, 2062-2067.
265. W. Y. Li, Q. Liu, Y. G. Sun, J. Q. Sun, R. J. Zou, G. Li, X. H. Hu, G. S. Song, G. X. Ma, J. M. Yang, Z. G. Chen and J. Q. Hu, *J. Mater. Chem.*, 2012, **22**, 14864-14867.
266. Y. X. Zhang, F. Li and M. Huang, *Mater. Lett.*, 2013, **112**, 203-206.
267. B. J. Zhang, W. Y. Li, J. Q. Sun, G. J. He, R. J. Zou, J. Q. Hu and Z. G. Chen, *Mater. Lett.*, 2014, **114**, 40-43.
268. L. Yu, G. Q. Zhang, C. Z. Yuan and X. W. Lou, *Chem. Commun.*, 2013, **49**, 137-139.
269. W. M. Chen, L. Qie, Q. G. Shao, L. X. Yuan, W. X. Zhang and Y. H. Huang, *ACS Appl. Mater. Interfaces*, 2012, **4**, 3047-3053.
270. J. Jiang, J. H. Zhu, Y. M. Feng, J. P. Liu and X. T. Huang, *Chem. Commun.*, 2012, **48**, 7471-7473.
271. J. Wang, J. Liu, Y. C. Zhou, P. Hodgson and Y. C. Li, *RSC Adv.*, 2013, **3**, 25937-25943.
272. F. Y. Cheng, J. Z. Zhao, W. Song, C. S. Li, H. Ma, J. Chen and P. W. Shen, *Inorg. Chem.*, 2006, **45**, 2038-2044.
273. X. Y. Lang, A. Hirata, T. Fujita and M. W. Chen, *Nat. Nanotech.*, 2011, **6**, 232-236.
274. H. J. Wang, C. Peng, J. D. Zheng, F. Peng and H. Yu, *Mater. Res. Bull.*, 2013, **48**, 3389-3393.
275. Y. F. Yan, Q. L. Cheng, V. Pavlinek, P. Saha and C. Z. Li, *Electrochim. Acta*, 2012, **71**, 27-32.
276. Z. X. Song, W. Liu, M. Zhao, Y. J. Zhang, G. C. Liu, C. Yu and J. S. Qiu, *J. Alloy. Compd.*, 2013, **560**, 151-155.
277. H. J. Huang and X. Wang, *Nanoscale*, 2011, **3**, 3185-3191.
278. Z. S. Wu, W. C. Ren, D. W. Wang, F. Li, B. L. Liu and H. M. Cheng, *ACS Nano*, 2010, **4**, 5835-5842.
279. X. Zhao, L. L. Zhang, S. Murali, M. D. Stoller, Q. H. Zhang, Y. W. Zhu and R. S. Ruoff, *ACS Nano*, 2012, **6**, 5404-5412.
280. X. Y. Xie, C. Zhang, M. B. Wu, Y. Tao, W. Lv and Q. H. Yang, *Chem. Commun.*, 2013, **49**, 11092-11094.
281. V. Subramanian, H. W. Zhu and B. Q. Wei, *Electrochem. Commun.*, 2006, **8**, 827-832.
282. S. J. He, C. X. Hu, H. Q. Hou and W. Chen, *J. Power Sources*, 2014, **246**, 754-761.
283. H. Lai, J. X. Li, Z. G. Chen and Z. G. Huang, *ACS Appl. Mater. Interfaces*, 2012, **4**, 2325-2328.
284. J. X. Li, Y. Zhao, N. Wang, Y. H. Ding and L. H. Guan, *J. Mater. Chem.*, 2012, **22**, 13002-13004.
285. J. Y. Liao, D. Higgins, G. Lui, V. Chabot, X. C. Xiao and Z. W. Chen, *Nano Lett.*, 2013, **13**, 5467-5473.

286. H. Pang, S. M. Wang, G. C. Li, Y. H. Ma, J. Li, X. X. Li, L. Zhang, J. S. Zhang and H. H. Zheng, *J. Mater. Chem. A*, 2013, **1**, 5053-5060.
287. Q. X. Chu, J. Du, W. B. Lu, G. H. Chang, Z. C. Xing, H. Y. Li, C. J. Ge, L. Wang, Y. L. Luo, A. M. Asiri, A. O. Al-Youbi and X. P. Sun, *Chempluschem*, 2012, **77**, 872-876.
288. L. L. Peng, X. Peng, B. R. Liu, C. Z. Wu, Y. Xie and G. H. Yu, *Nano Lett.*, 2013, **13**, 2151-2157.
289. Y. Hou, Y. W. Cheng, T. Hobson and J. Liu, *Nano Lett.*, 2010, **10**, 2727-2733.
290. Q. T. Qu, P. Zhang, B. Wang, Y. H. Chen, S. Tian, Y. P. Wu and R. Holze, *J. Phys. Chem. C*, 2009, **113**, 14020-14027.
291. B. You, N. Li, H. Y. Zhu, X. L. Zhu and J. Yang, *Chemsuschem*, 2013, **6**, 474-480.
292. S. Chen, J. W. Zhu, X. D. Wu, Q. F. Han and X. Wang, *ACS Nano*, 2010, **4**, 2822-2830.
293. M. Kim, Y. Hwang and J. Kim, *J. Power Sources*, 2013, **239**, 225-233.
294. H. J. Zheng, J. X. Wang, Y. Jia and C. A. Ma, *J. Power Sources*, 2012, **216**, 508-514.
295. A. Sumboja, C. Y. Foo, X. Wang and P. S. Lee, *Adv. Mater.*, 2013, **25**, 2809-2815.
296. T. Brousse, P. L. Taberna, O. Crosnier, R. Dugas, P. Guillemet, Y. Scudeller, Y. Zhou, F. Favier, D. Belanger and P. Simon, *J. Power Sources*, 2007, **173**, 633-641.
297. S. Devaraj, G. S. Gabriel, S. R. Gajjela and P. Balaya, *Electrochem. Solid St*, 2012, **15**, A57-A59.
298. C. Y. Wan, M. Cheng, Q. S. Zhang and N. Q. Jia, *Powder Technol.*, 2013, **235**, 706-711.
299. S. Chen, J. W. Zhu, Q. F. Han, Z. J. Zheng, Y. Yang and X. Wang, *Crst. Growth. Des.*, 2009, **9**, 4356-4361.
300. A. M. Hashem, H. M. Abuzeid, A. E. Abdel-Ghany, A. Mauger, K. Zaghib and C. M. Julien, *J. Power Sources*, 2012, **202**, 291-298.
301. Q. Li, J. M. Anderson, Y. Q. Chen and L. Zhai, *Electrochim. Acta*, 2012, **59**, 548-557.
302. L. Chen, Z. X. Song, G. C. Liu, J. S. Qiu, C. Yu, J. W. Qin, L. Ma, F. Q. Tian and W. Liu, *J. Phys. Chem. Solids*, 2013, **74**, 360-365.
303. B. X. Li, G. X. Rong, Y. Xie, L. F. Huang and C. Q. Feng, *Inorg. Chem.*, 2006, **45**, 6404-6410.
304. X. L. Li, H. F. Song, H. Wang, Y. L. Zhang, K. Du, H. Y. Li and J. M. Huang, *J. Appl. Electrochem.*, 2012, **42**, 1065-1070.
305. L. H. Bao, J. F. Zang and X. D. Li, *Nano Lett.*, 2011, **11**, 1215-1220.
306. J. W. Zhao, Z. Z. Lu, M. F. Shao, D. P. Yan, M. Wei, D. G. Evans and X. Duan, *RSC Adv.*, 2013, **3**, 1045-1049.
307. D. Sarkar, G. G. Khan, A. K. Singh and K. Mandal, *J. Phys. Chem. C*, 2013, **117**, 15523-15531.
308. J. F. Zang and X. D. Li, *J. Mater. Chem.*, 2011, **21**, 10965-10969.
309. A. J. Roberts, A. F. D. de Namor and R. C. T. Slade, *Phys. Chem. Chem. Phys.*, 2013, **15**, 3518-3526.
310. M. Kim, Y. Hwang and J. Kim, *J. Mater. Sci.*, 2013, **48**, 7652-7663.
311. M. P. He, Y. Y. Zheng and Q. F. Du, *Mater. Lett.*, 2013, **104**, 48-52.
312. L. L. Xing, C. X. Cui, C. H. Ma and X. Y. Xue, *Mater. Lett.*, 2011, **65**, 2104-2106.
313. C. X. Guo, M. Wang, T. Chen, X. W. Lou and C. M. Li, *Adv. Energy. Mater.*, 2011, **1**, 736-741.
314. A. Pan, D. Liu, X. Zhou, B. B. Garcia, S. Liang, J. Liu and G. Cao, *J. Power Sources*, 2010, **195**, 3893-3899.
315. J. L. Kang, A. Hirata, L. J. Kang, X. M. Zhang, Y. Hou, L. Y. Chen, C. Li, T. Fujita, K. Akagi and M. W. Chen, *Angew. Chem. Int. Edit.*, 2013, **52**, 1664-1667.
316. X. H. Lu, T. Zhai, X. H. Zhang, Y. Q. Shen, L. Y. Yuan, B. Hu, L. Gong, J. Chen, Y. H. Gao, J. Zhou, Y. X. Tong and Z. L. Wang, *Adv. Mater.*, 2012, **24**, 938-944.
317. L. Y. Chen, J. L. Kang, Y. Hou, P. Liu, T. Fujita, A. Hirata and M. W. Chen, *J. Mater. Chem. A*, 2013, **1**, 9202-9207.
318. D. D. Zhao, Y. Q. Zhao, X. Zhang, C. L. Xu, Y. Peng, H. L. Li and Z. Yang, *Mater. Lett.*, 2013, **107**, 115-118.
319. Z. J. Su, C. Yang, C. J. Xu, H. Y. Wu, Z. X. Zhang, T. Liu, C. Zhang, Q. H. Yang, B. H. Li and F. Y. Kang, *J. Mater. Chem. A*, 2013, **1**, 12432-12440.
320. M. Kundu and L. F. Liu, *J. Power Sources*, 2013, **243**, 676-681.

321. J. W. Xiao, S. X. Yang, L. Wan, F. Xiao and S. Wang, *J. Power Sources*, 2014, **245**, 1027-1034.
322. X. H. Lu, D. Z. Zheng, T. Zhai, Z. Q. Liu, Y. Y. Huang, S. L. Xie and Y. X. Tong, *Energy Environ. Sci.*, 2011, **4**, 2915-2921.
323. X. Zhang, D. D. Zhao, Y. Q. Zhao, P. Y. Tang, Y. L. Shen, C. L. Xu, H. L. Li and Y. Xiao, *J. Mater. Chem. A*, 2013, **1**, 3706-3712.
324. J. S. Luo, X. H. Xia, Y. S. Luo, C. Guan, J. L. Liu, X. Y. Qi, C. F. Ng, T. Yu, H. Zhang and H. J. Fan, *Adv. Energy. Mater.*, 2013, **3**, 737-743.
325. H. C. Gao, F. Xiao, C. B. Ching and H. W. Duan, *ACS Appl. Mater. Interfaces*, 2012, **4**, 2801-2810.
326. J. W. Liu, J. Essner and J. Li, *Chem. Mater.*, 2010, **22**, 5022-5030.
327. M. H. Yu, T. Zhai, X. H. Lu, X. J. Chen, S. L. Xie, W. Li, C. L. Liang, W. X. Zhao, L. P. Zhang and Y. X. Tong, *J. Power Sources*, 2013, **239**, 64-71.
328. C. L. Xu, Y. Q. Zhao, G. W. Yang, F. S. Li and H. L. Li, *Chem. Commun.*, 2009, 7575-7577.
329. P. Y. Tang, Y. Q. Zhao, Y. M. Wang and C. L. Xu, *Nanoscale*, 2013, **5**, 8156-8163.
330. R. Liu and S. B. Lee, *J. Am. Chem. Soc.*, 2008, **130**, 2942-2943.
331. S. M. Dong, X. Chen, L. Gu, X. H. Zhou, L. F. Li, Z. H. Liu, P. X. Han, H. X. Xu, J. H. Yao, H. B. Wang, X. Y. Zhang, C. Q. Shang, G. L. Cui and L. Q. Chen, *Energy Environ. Sci.*, 2011, **4**, 3502-3508.
332. J. Duay, S. A. Sherrill, Z. Gui, E. Gillette and S. B. Lee, *ACS Nano*, 2013, **7**, 1200-1214.
333. M. S. Wu and P. C. J. Chiang, *Electrochem. Commun.*, 2006, **8**, 383-388.
334. S. L. Chou, Y. X. Wang, J. T. Xu, J. Z. Wang, H. K. Liu and S. X. Dou, *Electrochem. Commun.*, 2013, **31**, 35-38.
335. M. Kundu, C. C. A. Ng, D. Y. Petrovykh and L. F. Liu, *Chem. Commun.*, 2013, **49**, 8459-8461.
336. M. S. Wu, P. C. J. Chiang, J. T. Lee and J. C. Lin, *J. Phys. Chem. B*, 2005, **109**, 23279-23284.
337. W. F. Wei, X. W. Cui, W. X. Chen and D. G. Ivey, *J. Power Sources*, 2009, **186**, 543-550.
338. S. L. Chou, J. Z. Wang, S. Y. Chew, H. K. Liu and S. X. Dou, *Electrochem. Commun.*, 2008, **10**, 1724-1727.
339. Y. M. He, W. J. Chen, X. D. Li, Z. X. Zhang, J. C. Fu, C. H. Zhao and E. Q. Xie, *ACS Nano*, 2013, **7**, 174-182.
340. Y. Jin, H. Y. Chen, M. H. Chen, N. Liu and Q. W. Li, *ACS Appl. Mater. Interfaces*, 2013, **5**, 3408-3416.
341. Z. P. Sun, S. Firdoz, E. Y. X. Yap, L. Li and X. M. Lu, *Nanoscale*, 2013, **5**, 4379-4387.
342. S. Park, I. Nam, G. P. Kim, J. W. Han and J. Yi, *ACS Appl. Mater. Interfaces*, 2013, **5**, 9908-9912.
343. H. Xia, J. K. Feng, H. L. Wang, M. O. Lai and L. Lu, *J. Power Sources*, 2010, **195**, 4410-4413.
344. Y. L. Chen, P. C. Chen, T. L. Chen, C. Y. Lee and H. T. Chiu, *J. Mater. Chem. A*, 2013, **1**, 13301-13307.
345. Z. G. Ye, G. W. Liu, G. B. Huang, K. Wang and G. J. Qiao, *ECS Electrochem. Lett.*, 2013, **2**, A118-A120.
346. J. Y. Tao, N. S. Liu, W. Z. Ma, L. W. Ding, L. Y. Li, J. Su and Y. H. Gao, *Scientific Reports*, 2013, **3**, 2286.
347. J. C. Chou, Y. L. Chen, M. H. Yang, Y. Z. Chen, C. C. Lai, H. T. Chiu, C. Y. Lee, Y. L. Chueh and J. Y. Gan, *J. Mater. Chem. A*, 2013, **1**, 8753-8758.
348. W. F. Wei, X. W. Cui, W. X. Chen and D. G. Ivey, *J. Phys. Chem. C*, 2008, **112**, 15075-15083.
349. M. S. Wu and Y. H. Fu, *Carbon*, 2013, **60**, 236-245.
350. G. R. Li, Z. P. Feng, Y. N. Ou, D. C. Wu, R. W. Fu and Y. X. Tong, *Langmuir.*, 2010, **26**, 2209-2213.
351. Y. B. He, G. R. Li, Z. L. Wang, C. Y. Su and Y. X. Tong, *Energy Environ. Sci.*, 2011, **4**, 1288-1292.
352. W. Xiao, H. Xia, J. Y. H. Fuh and L. Lu, *J. Electrochem. Soc.*, 2009, **156**, A627-A633.
353. D. W. Liu, Q. F. Zhang, P. Xiao, B. B. Garcia, Q. Guo, R. Champion and G. Z. Cao, *Chem. Mater.*, 2008, **20**, 1376-1380.
354. H. Zhao, G. Y. Han, Y. Z. Chang, M. Y. Li and Y. P. Li, *Electrochim. Acta*, 2013, **91**, 50-57.

355. D. D. Zhao, Z. Yang, L. Y. Zhang, X. L. Feng and Y. F. Zhang, *Electrochem. Solid St*, 2011, **14**, A93-A96.
356. K. Sivula, F. Le Formal and M. Gratzel, *Chemsuschem*, 2011, **4**, 432-449.
357. C. Ban, Z. Wu, D. T. Gillaspie, L. Chen, Y. Yan, J. L. Blackburn and A. C. Dillon, *Adv. Mater.*, 2010, **22**, E145-E149.
358. Q. Xiong, Y. Lu, X. Wang, C. Gu, Y. Qiao and J. Tu, *J. Alloy. Compd.*, 2012, **536**, 219-225.
359. W. Zhang, X. Wang, H. Zhou, J. Chen and X. Zhang, *J. Alloy. Compd.*, 2012, **521**, 39-44.
360. Y. Zhao, J. Li, Y. Ding and L. Guan, *Chem. Commun.*, 2011, **47**, 7416-7418.
361. B. Wang, J. S. Chen, H. B. Wu, Z. Wang and X. W. Lou, *J. Am. Chem. Soc.*, 2011, **133**, 17146-17148.
362. S. Jin, H. Deng, D. Long, X. Liu, L. Zhan, X. Liang, W. Qiao and L. Ling, *J. Power Sources*, 2011, **196**, 3887-3893.
363. D. Chen, G. Ji, Y. Ma, J. Y. Lee and J. Lu, *ACS Appl. Mater. Interfaces*, 2011, **3**, 3078-3083.
364. Y. Lu, J. P. Tu, C. D. Gu, X. L. Wang and S. X. Mao, *J. Mater. Chem.*, 2011, **21**, 17988-17997.
365. Q. Q. Xiong, J. P. Tu, Y. Lu, J. Chen, Y. X. Yu, Y. Q. Qiao, X. L. Wang and C. D. Gu, *J. Phys. Chem. C*, 2012, **116**, 6495-6502.
366. S. Wang, J. Zhang and C. Chen, *J. Power Sources*, 2010, **195**, 5379-5381.
367. W. M. Zhang, X. L. Wu, J. S. Hu, Y. G. Guo and L. J. Wan, *Adv. Funct. Mater.*, 2008, **18**, 3941-3946.
368. W. Shi, J. Zhu, D. H. Sim, Y. Y. Tay, Z. Lu, X. Zhang, Y. Sharma, M. Srinivasan, H. Zhang and H. H. Hng, *J. Mater. Chem.*, 2011, **21**, 3422-3427.
369. Y. Ma, G. Ji and J. Y. Lee, *J. Mater. Chem.*, 2011, **21**, 13009-13014.
370. L. Wang, H. Ji, S. Wang, L. Kong, X. Jiang and G. Yang, *Nanoscale*, 2013, **5**, 3793-3799.
371. Y. Chen, H. Xia, L. Lu and J. Xue, *J. Mater. Chem.*, 2012, **22**, 5006-5012.
372. P. M. Hallam, M. Gómez-Mingot, D. K. Kampouris and C. E. Banks, *RSC Adv.*, 2012, **2**, 6672-6679.
373. S.-Y. Wang, K.-C. Ho, S.-L. Kuo and N.-L. Wu, *J. Electrochem. Soc.*, 2006, **153**, A75-A80.
374. X. Zhao, C. Johnston and P. S. Grant, *J. Mater. Chem.*, 2009, **19**, 8755-8760.
375. S. Zeng, K. Tang, T. Li, Z. Liang, D. Wang, Y. Wang, Y. Qi and W. Zhou, *J. Phys. Chem. C*, 2008, **112**, 4836-4843.
376. M. S. Wu and R. H. Lee, *J. Electrochem. Soc.*, 2009, **156**, A737-A743.
377. G. F. Ortiz, I. Hanzu, P. Lavela, J. L. Tirado, P. Knauth and T. Djenizian, *J. Mater. Chem.*, 2010, **20**, 4041-4046.
378. M. S. Wu, Y. H. Ou and Y. P. Lin, *Electrochim. Acta*, 2010, **55**, 3240-3244.
379. Q. Q. Xiong, J. P. Tu, Y. Lu, J. Chen, Y. X. Yu, X. L. Wang and C. D. Gu, *J. Mater. Chem.*, 2012, **22**, 18639-18645.
380. S. Mitra, P. Poizot, A. Finke and J. M. Tarascon, *Adv. Funct. Mater.*, 2006, **16**, 2281-2287.
381. L. Taberna, S. Mitra, P. Poizot, P. Simon and J. M. Tarascon, *Nat. Mater.*, 2006, **5**, 567-573.
382. H. Duan, J. Gnanaraj and J. Y. Liang, *J. Power Sources*, 2011, **196**, 4779-4784.
383. K. Y. Xie, Z. G. Lu, H. T. Huang, W. Lu, Y. Q. Lai, J. Li, L. M. Zhou and Y. X. Liu, *J. Mater. Chem.*, 2012, **22**, 5560-5567.
384. J. P. Liu, Y. Y. Li, H. J. Fan, Z. H. Zhu, J. Jiang, R. M. Ding, Y. Y. Hu and X. T. Huang, *Chem. Mater.*, 2009, **22**, 212-217.
385. J. S. Luo, J. L. Liu, Z. Y. Zeng, C. F. Ng, L. J. Ma, H. Zhang, J. Y. Lin, Z. X. Shen and H. J. Fan, *Nano Lett.*, 2013, **13**, 6136-6143.
386. Y. S. Luo, J. S. Luo, J. Jiang, W. W. Zhou, H. P. Yang, X. Y. Qi, H. Zhang, H. J. Fan, D. Y. W. Yu, C. M. Li and T. Yu, *Energy Environ. Sci.*, 2012, **5**, 6559-6566.
387. Y. Wang, J. L. Cao, S. R. Wang, X. Z. Guo, J. Zhang, H. J. Xia, S. M. Zhang and S. H. Wu, *J. Phys. Chem. C*, 2008, **112**, 17804-17808.
388. Y. He, L. Huang, J. S. Cai, X. M. Zheng and S. G. Sun, *Electrochim. Acta*, 2010, **55**, 1140-1144.
389. P. Tartaj and J. M. Amarilla, *J. Power Sources*, 2011, **196**, 2164-2170.
390. J. Z. Wang, C. Zhong, D. Wexler, N. H. Idris, Z. X. Wang, L. Q. Chen and H. K. Liu, *Chem-eur. J.*, 2011, **17**, 661-667.
391. J. Y. Zhong, C. B. Cao, Y. Y. Liu, Y. A. Li and W. S. Khan, *Chem. Commun.*, 2010, **46**, 3869-3871.

392. B. J. Li, H. Q. Cao, J. Shao, M. Z. Qu and J. H. Warner, *J. Mater. Chem.*, 2011, **21**, 5069-5075.
393. A. Q. Pan, H. B. Wu, L. Zhang and X. W. Lou, *Energy Environ. Sci.*, 2013, **6**, 1476.
394. J. W. Lee, S. Y. Lim, H. M. Jeong, T. H. Hwang, J. K. Kang and J. W. Choi, *Energy Environ. Sci.*, 2012, **5**, 9889.
395. J. Zhu, L. Cao, Y. Wu, Y. Gong, Z. Liu, H. E. Hoster, Y. Zhang, S. Zhang, S. Yang, Q. Yan, P. M. Ajayan and R. Vajtai, *Nano Lett.*, 2013, **13**, 5408-5413.
396. A. Pan, H. B. Wu, L. Yu and X. W. D. Lou, *Angewandte Chemie*, 2013, **125**, 2282-2286.
397. J. Xie, C. Wu, S. Hu, J. Dai, N. Zhang, J. Feng, J. Yang and Y. Xie, *Phys. Chem. Chem. Phys.*, 2012, **14**, 4810-4816.
398. M. Jayalakshmi, M. M. Rao, N. Venugopal and K. B. Kim, *J. Power Sources*, 2007, **166**, 578-583.
399. S. D. Perera, A. D. Liyanage, N. Nijem, J. P. Ferraris, Y. J. Chabal and K. J. Balkus, *J. Power Sources*, 2013, **230**, 130-137.
400. S. D. Perera, B. Patel, N. Nijem, K. Roodenko, O. Seitz, J. P. Ferraris, Y. J. Chabal and K. J. Balkus, *Adv. Energy. Mater.*, 2011, **1**, 936-945.
401. Q. T. Qu, Y. S. Zhu, X. W. Gao and Y. P. Wu, *Adv. Energy. Mater.*, 2012, **2**, 950-955.
402. J. Shao, X. Y. Li, Q. T. Qu and H. H. Zheng, *J. Power Sources*, 2012, **219**, 253-257.
403. Y. Y. Liu, M. Clark, Q. F. Zhang, D. M. Yu, D. W. Liu, J. Liu and G. Z. Cao, *Adv. Energy. Mater.*, 2011, **1**, 194-202.
404. G. Du, K. H. Seng, Z. Guo, J. Liu, W. Li, D. Jia, C. Cook, Z. Liu and H. Liu, *RSC Adv.*, 2011, **1**, 690.
405. X. Rui, J. Zhu, W. Liu, H. Tan, D. Sim, C. Xu, H. Zhang, J. Ma, H. H. Hng, T. M. Lim and Q. Yan, *RSC Adv.*, 2011, **1**, 117.
406. S. Yang, Y. Gong, Z. Liu, L. Zhan, D. P. Hashim, L. Ma, R. Vajtai and P. M. Ajayan, *Nano Lett.*, 2013, **13**, 1596-1601.
407. X. H. Rui, D. H. Sim, C. Xu, W. L. Liu, H. T. Tan, K. M. Wong, H. H. Hng, T. M. Lim and Q. Y. Yan, *RSC Adv.*, 2012, **2**, 1174-1180.
408. C. J. Fontenot, J. W. Wiench, M. Pruski and G. L. Schrader, *J. Phys. Chem. B*, 2000, **104**, 11622-11631.
409. M. L. Li, G. Y. Sun, P. P. Yin, C. P. Ruan and K. L. Ai, *ACS Appl. Mater. Interfaces*, 2013, **5**, 11462-11470.
410. J. Yang, T. B. Lan, J. D. Liu, Y. F. Song and M. D. Wei, *Electrochim. Acta*, 2013, **105**, 489-495.
411. Y. L. Cheah, V. Aravindan and S. Madhavi, *ACS Appl. Mater. Interfaces*, 2013, **5**, 3475-3480.
412. X. H. Rui, J. X. Zhu, D. Sim, C. Xu, Y. Zeng, H. H. Hng, T. M. Lim and Q. Y. Yan, *Nanoscale*, 2011, **3**, 4752-4758.
413. B. Saravanakumar, K. K. Purushothaman and G. Muralidharan, *ACS Appl. Mater. Interfaces*, 2012, **4**, 4484-4490.
414. H. Yamada, K. Tagawa, M. Komatsu, I. Moriguchi and T. Kudo, *J. Phys. Chem. C*, 2007, **111**, 8397-8402.
415. N. A. Galiote, M. N. Camargo, R. M. Iost, F. Crespilho and F. Huguenin, *Langmuir.*, 2011, **27**, 12209-12217.
416. M. Sathiya, A. S. Prakash, K. Ramesha, J. M. Tarascon and A. K. Shukla, *J. Am. Chem. Soc.*, 2011, **133**, 16291-16299.
417. T. Kudo, Y. Ikeda, T. Watanabe, M. Hibino, M. Miyayama, H. Abe and K. Kajita, *Solid State Ionics*, 2002, **152**, 833-841.
418. J. S. Bonso, A. Rahy, S. D. Perera, N. Nour, O. Seitz, Y. J. Chabal, K. J. Balkus, J. P. Ferraris and D. J. Yang, *J. Power Sources*, 2012, **203**, 227-232.
419. A. Kuwahara, S. Suzuki and M. Miyayama, *Solid State Ionics*, 2008, **179**, 1890-1896.
420. W. Y. Zhang, Y. Zeng, N. Xiao, H. H. Hng and Q. Y. Yan, *J. Mater. Chem.*, 2012, **22**, 8455-8461.
421. A. M. Engstrom and F. M. Doyle, *J. Power Sources*, 2013, **228**, 120-131.
422. C. C. Hu, C. M. Huang and K. H. Chang, *J. Power Sources*, 2008, **185**, 1594-1597.
423. I. H. Kim, J. H. Kim, B. W. Cho, Y. H. Lee and K. B. Kim, *J. Electrochem. Soc.*, 2006, **153**, A989-A996.

424. K. I. Park, H. M. Song, Y. Kim, S. I. Mho, W. I. Cho and I. H. Yeo, *Electrochim. Acta*, 2010, **55**, 8023-8029.
425. Q. H. Wang, L. F. Jiao, H. M. Du, J. Q. Yang, Q. N. Huan, W. X. Peng, Y. C. Si, Y. J. Wang and H. T. Yuan, *CrystEngComm*, 2011, **13**, 6960-6963.
426. G. F. Cai, X. L. Wang, D. Zhou, J. H. Zhang, Q. Q. Xiong, C. D. Gu and J. P. Tu, *RSC Adv.*, 2013, **3**, 6896-6905.
427. G. F. Cai, D. Zhou, Q. Q. Xiong, J. H. Zhang, X. L. Wang, C. D. Gu and J. P. Tu, *Sol. Energ. Mat. Sol. C.*, 2013, **117**, 231-238.
428. J. Zhang, J. P. Tu, G. H. Du, Z. M. Dong, Q. M. Su, D. Xie and X. L. Wang, *Electrochim. Acta*, 2013, **88**, 107-111.
429. J. Zhang, J. P. Tu, G. H. Du, Z. M. Dong, Y. S. Wu, L. Chang, D. Xie, G. F. Cai and X. L. Wang, *Sol. Energ. Mat. Sol. C.*, 2013, **114**, 31-37.
430. J. Zhang, J. P. Tu, X. H. Xia, Y. Qiao and Y. Lu, *Sol. Energ. Mat. Sol. C.*, 2009, **93**, 1840-1845.
431. J. Zhang, X. L. Wang, Y. Lu, Y. Qiao, X. H. Xia and J. P. Tu, *J. Solid State Electr.*, 2011, **15**, 2213-2219.
432. J. Zhang, X. L. Wang, X. H. Xia, C. D. Gu and J. P. Tu, *Sol. Energ. Mat. Sol. C.*, 2011, **95**, 2107-2112.
433. J. Zhang, X. L. Wang, X. H. Xia, C. D. Gu, Z. J. Zhao and J. P. Tu, *Electrochim. Acta*, 2010, **55**, 6953-6958.
434. X. X. Li, G. Y. Zhang, F. Y. Cheng, B. Guo and J. Chen, *J. Electrochem. Soc.*, 2006, **153**, H133-H137.
435. L. N. Gao, X. F. Wang, Z. Xie, W. F. Song, L. J. Wang, X. Wu, F. Y. Qu, D. Chen and G. Z. Shen, *J. Mater. Chem. A*, 2013, **1**, 7167-7173.
436. Y. C. Qiu, G. L. Xu, Q. Kuang, S. G. Sun and S. H. Yang, *Nano Research*, 2012, **5**, 826-832.
437. X. Y. Xue, B. He, S. Yuan, L. L. Xing, Z. H. Chen and C. H. Ma, *Nanotechnology*, 2011, **22**.
438. J. Q. Yang, L. F. Jiao, Q. Q. Zhao, Q. H. Wang, H. Y. Gao, Q. N. Huan, W. J. Zheng, Y. J. Wang and H. T. Yuan, *J. Mater. Chem.*, 2012, **22**, 3699-3701.
439. M. P. Yu, H. T. Sun, X. Sun, F. Y. Lu, T. Hu, G. K. Wang, H. Qiu and J. Lian, *Mater. Lett.*, 2013, **108**, 29-32.
440. B. Dunn, H. Kamath and J. M. Tarascon, *Science*, 2011, **334**, 928-935.
441. C. Y. Kim, M. Lee, S. H. Huh and E. K. Kim, *J. Sol-gel. Sci. Techn.*, 2010, **53**, 176-183.
442. K. Huang and Q. Zhang, *Nano Energy*, 2012, **1**, 172-175.
443. K. Huang, Q. Pan, F. Yang, S. Ni, X. Wei and D. He, *J. Phys. D. Appl. Phys.*, 2008, **41**.
444. B. X. Zou, Y. Liang, X. X. Liu, D. Diamond and K. T. Lau, *J. Power Sources*, 2011, **196**, 4842-4848.
445. C. A. Cai, D. S. Guan and Y. Wang, *J. Alloy. Compd.*, 2011, **509**, 909-915.
446. Y. U. Jeong and A. Manthiram, *J. Electrochem. Soc.*, 2001, **148**, A189-A193.
447. K. H. Chang, C. C. Hu, C. M. Huang, Y. L. Liu and C. I. Chang, *J. Power Sources*, 2011, **196**, 2387-2392.
448. X. B. Ren, H. Y. Lu, H. B. Lin, Y. N. Liu and Y. Xing, *Russ. J. Electrochem+*. 2010, **46**, 77-80.
449. Z. P. Chen, W. C. Ren, L. B. Gao, B. L. Liu, S. F. Pei and H. M. Cheng, *Nat. Mater.*, 2011, **10**, 424-428.
450. C. Guan, X. L. Li, Z. L. Wang, X. H. Cao, C. Soci, H. Zhang and H. J. Fan, *Adv. Mater.*, 2012, **24**, 4186-4190.

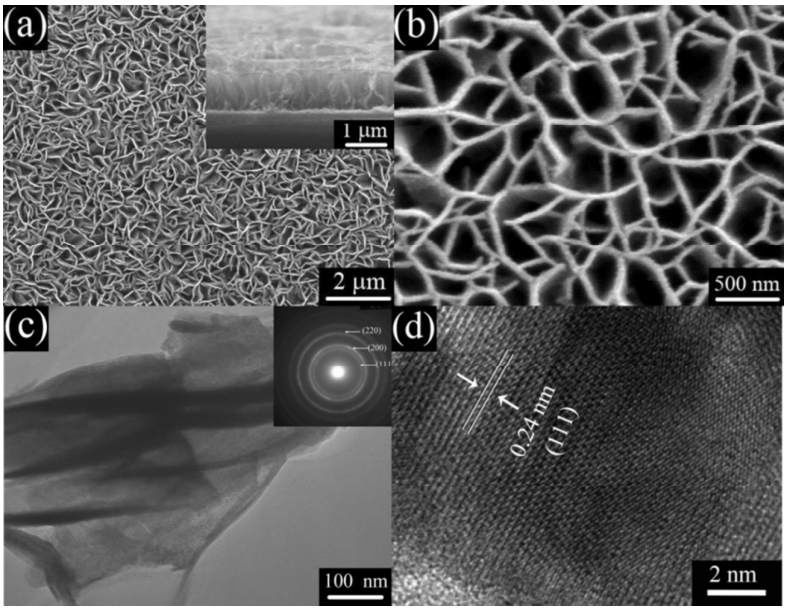

Figure 1 Film of NiO nanoflakes obtained by chemical bath deposition. Reproduced with permission from Ref. 27.

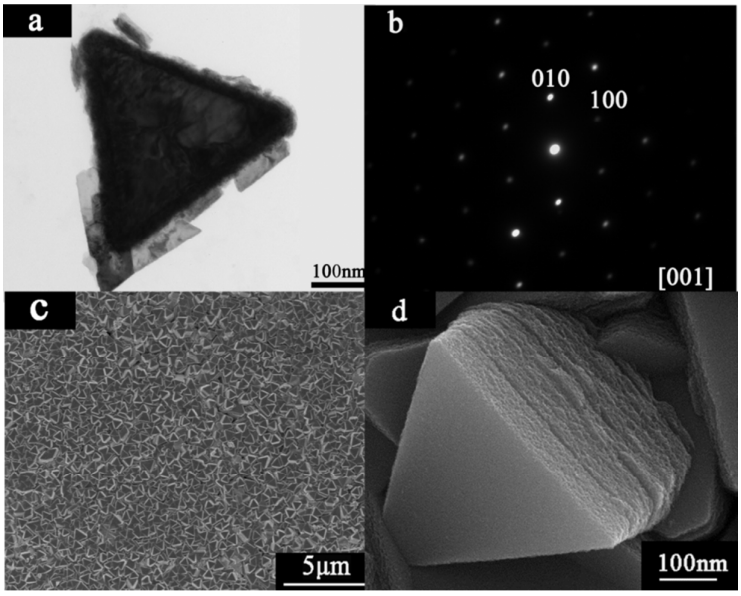

Figure 2 (a) TEM image and (b) SAED pattern of chemical bath deposited NiO triangular prism. (c, d) SEM images of the film composed of NiO triangular prisms. Reproduced with permission from Ref. 38.

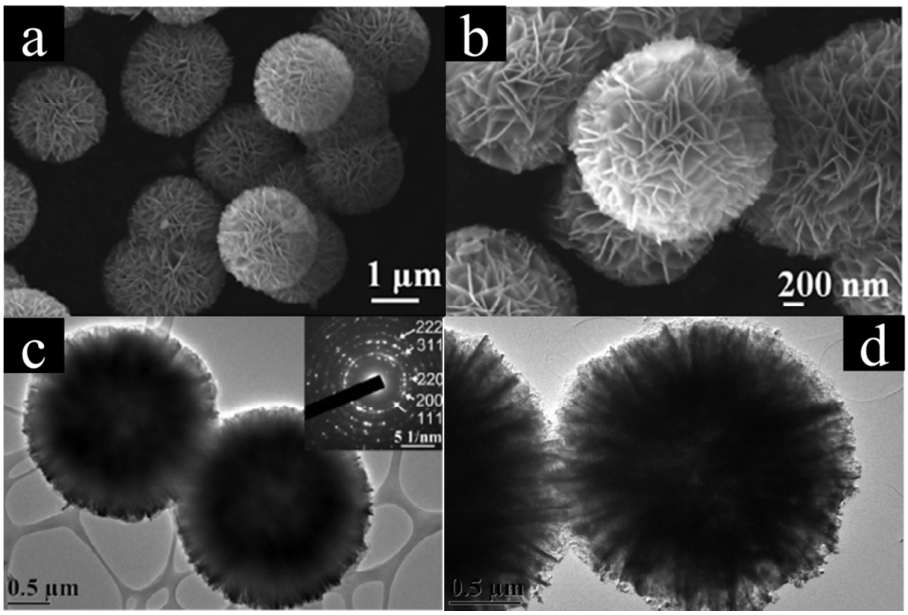

Figure 3 NiO spheres composed of nanoflakes obtained by hydrothermal synthesis. Reproduced with permission from Ref. 51.

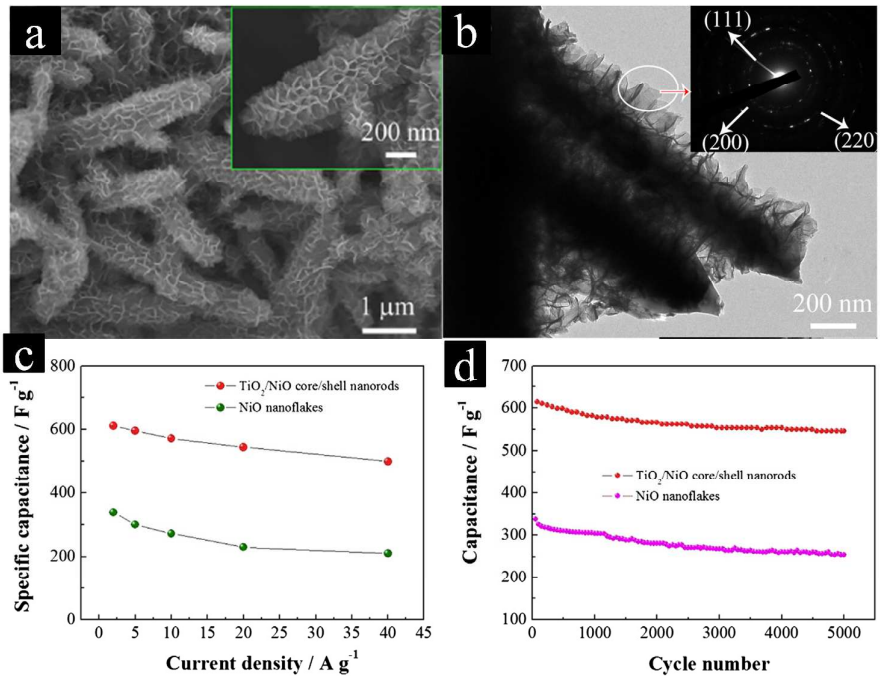

Figure 4 (a, b) SEM-TEM images and (c, d) pseudocapacitive performances TiO_2/NiO core/shell nanorod arrays on carbon cloth. The NiO nanoflakes are obtained by electro-deposition method. Reproduced with permission from Ref. 32.

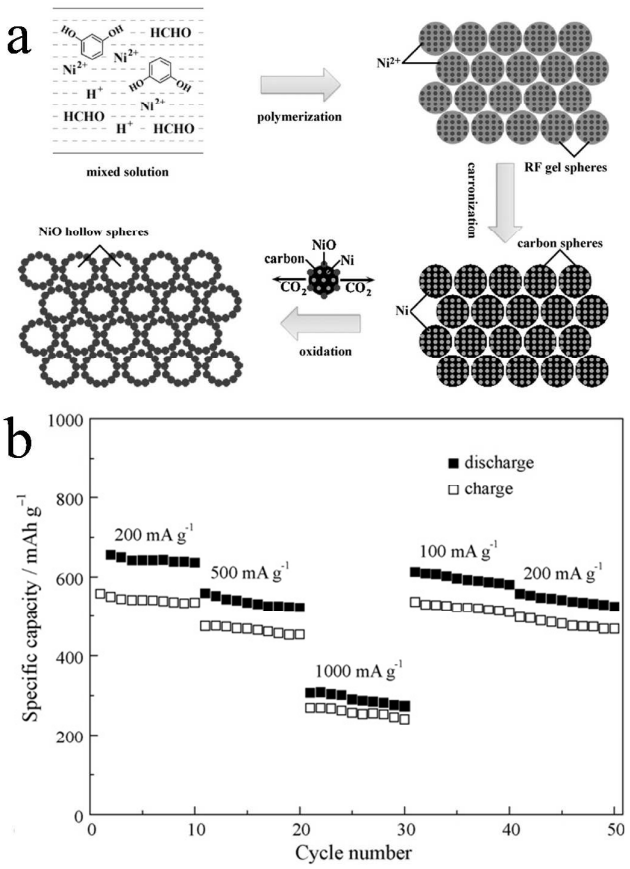

Figure 5. (a) Schematics of the sol-gel synthesis procedure of hollow NiO spheres. (b) Rate capability as the Li-ion battery electrode. Reproduced with permission from Ref. 90.

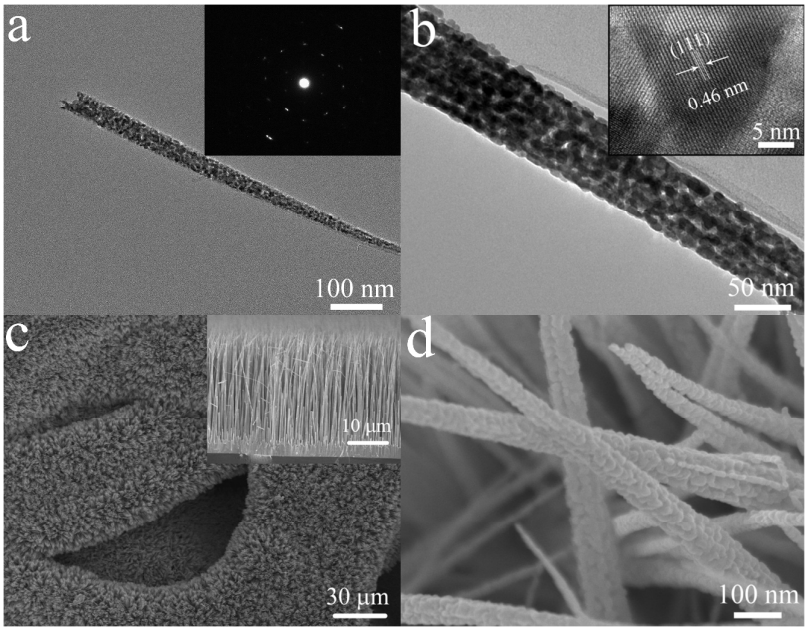

Figure 6 Porous Co_3O_4 nanowires by hydrothermal synthesis method. (a, b) TEM and HRTEM images of individual Co_3O_4 nanowire; (c, d) SEM images of Co_3O_4 nanowire array grown on nickel foam. Reproduced with permission from Ref. 103.

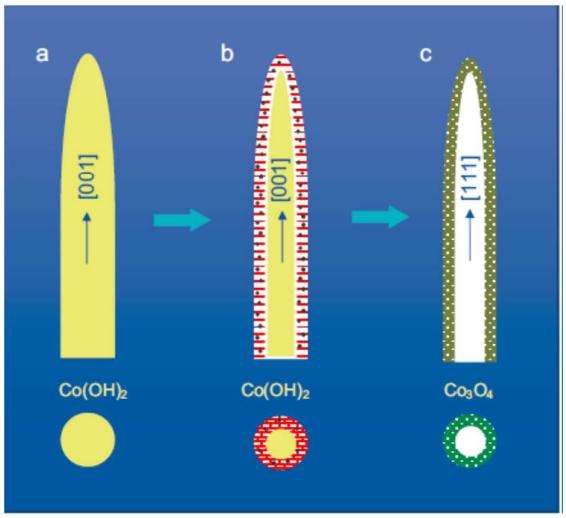

Figure 7. Schematic illustration of Co_3O_4 needle-like nanotubes obtained by chemical precipitation method. (a) Single-crystalline β-$Co(OH)_2$ nanoneedles along [001] direction. (b) $Co(OH)_2$ with loose platelet-walls. (c) Co_3O_4 needle-like nanotubes. Reproduced with permission from Ref. 162.

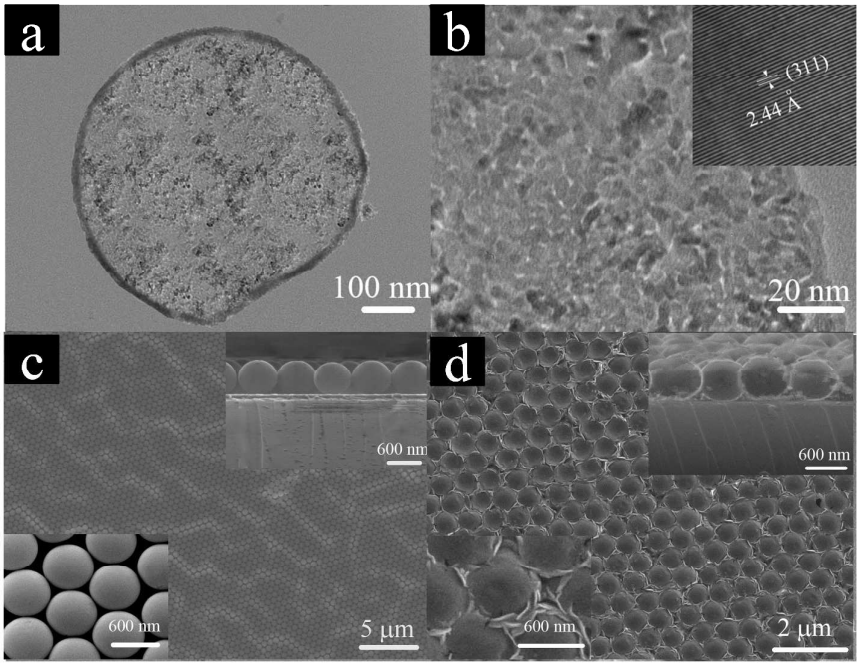

Figure 8 Co_3O_4 hollow sphere layers by electro-deposition on polystyrene sphere templates. TEM (a) and HRTEM (b) images of individual Co_3O_4 hollow sphere. SEM images of (c) monolayer PS sphere template and (d) Co_3O_4 monolayer hollow-sphere array. Reproduced with permission from Ref. 186.

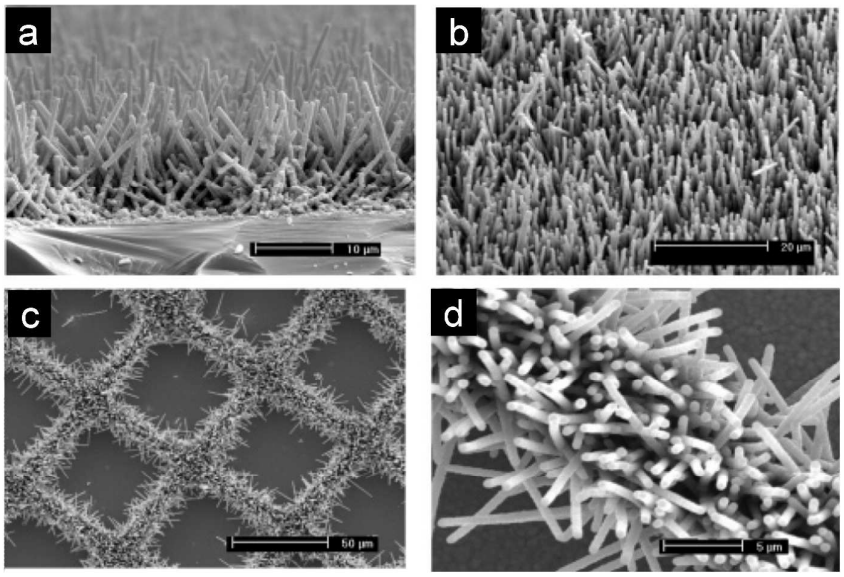

Figure 9 Co_3O_4 nanowire arrays by chemical bath deposition. Reproduced with permission from Ref. 207.

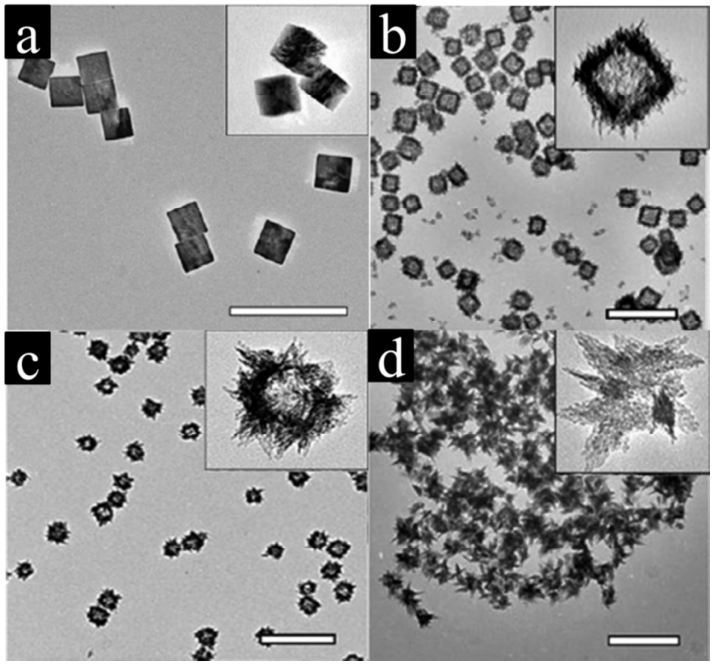

Figure 10 Copper oxide colloidal nanoparticles by chemical precipitation method. (a) Cu_2O nanocubes; (c) CuO hollow cubes; (c) hollow spheres; (d) urchin-like particles. Reproduced with permission from Ref. 211.

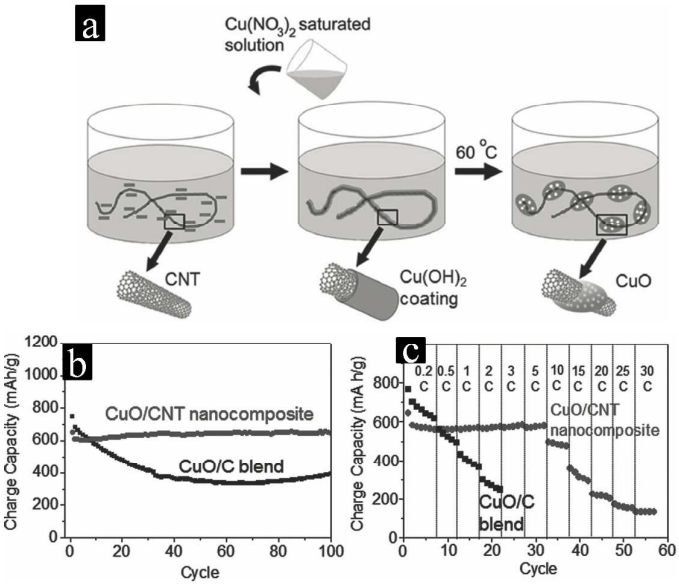

Figure 11 (a) Preparation of the CuO/CNT composites by chemical precipitation. (b, c) cycling performances and rate capability of the CuO/CNT composites. Reproduced with permission from Ref. 221.

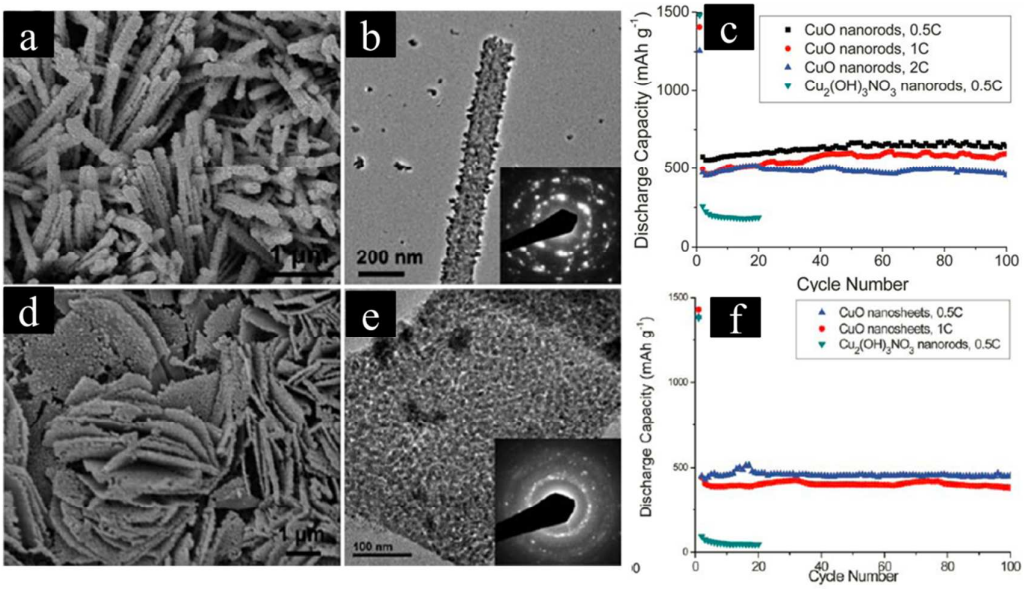

Figure 12 (a, b) SEM-TEM images and (c) cycling stability of CuO nanorods obtained by hydrothermal synthesis; (d, e) SEM-TEM images and (f) cycling stability of CuO nanosheets obtained by hydrothermal synthesis. Reproduced with permission from Ref. 225.

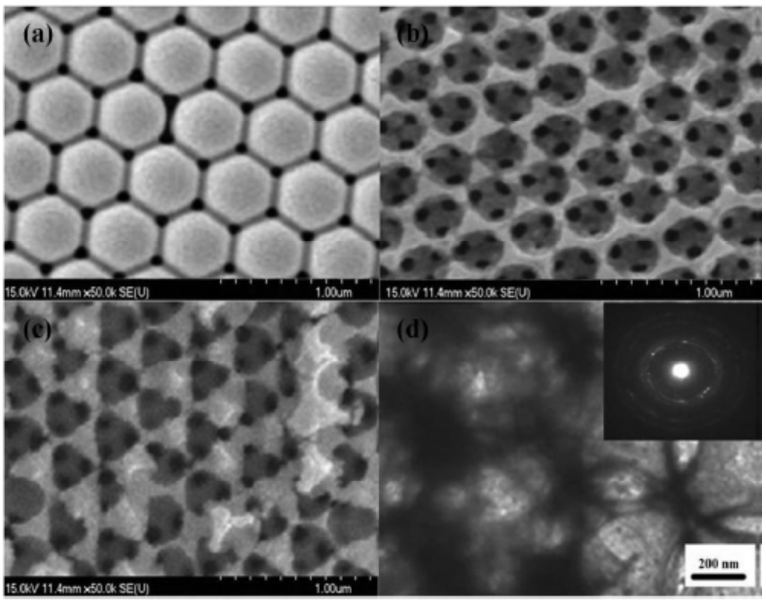

Figure 13 3D porous composite nanostructures obtained by electrode-deposition on polystyrene opals template. (a) Polystyrene opals template, (b) Ni inverse opals structure after first deposition, (c) Cu_2O/Ni structure after second deposition, and (d) TEM image of the Cu_2O/Ni structure. Reproduced with permission from Ref. 236.

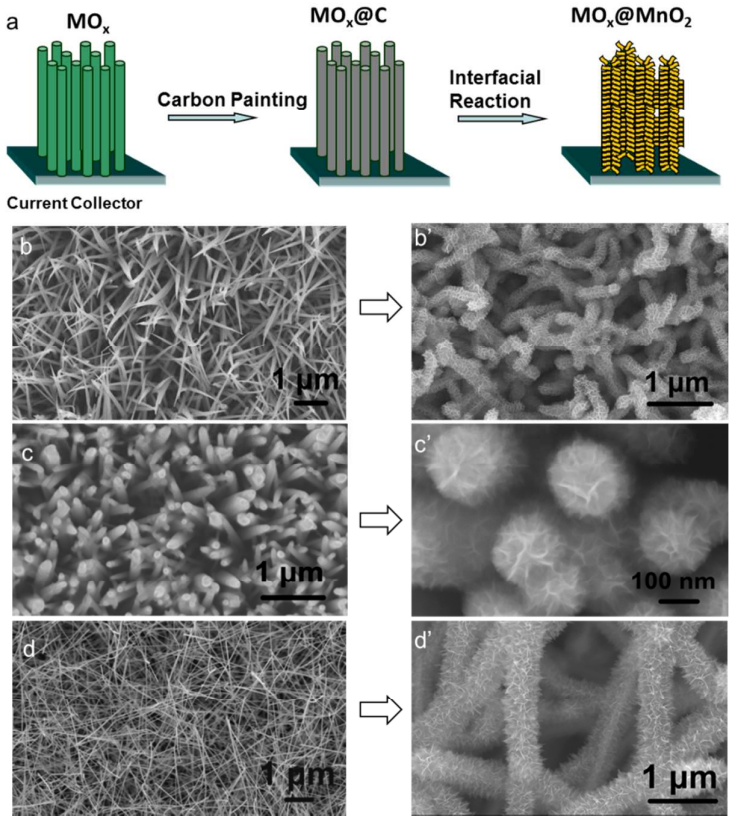

Figure 14. MnO2 nanosheets by hydrothermal synthesis via the chemical reaction between $KMnO_4$ with carbon. (a) Schematics of the fabrication procedure for the MnO^2 nanosheet branches on various metal oxide core nanowires. (b) Co_3O_4 nanowire array, (c) ZnO nanowires, and (d) SnO_2 nanowires. SEM images in the right column show the corresponding nanowire arrays with MnO_2 nanomembrane branches. Reproduced with permission from Ref. 98.

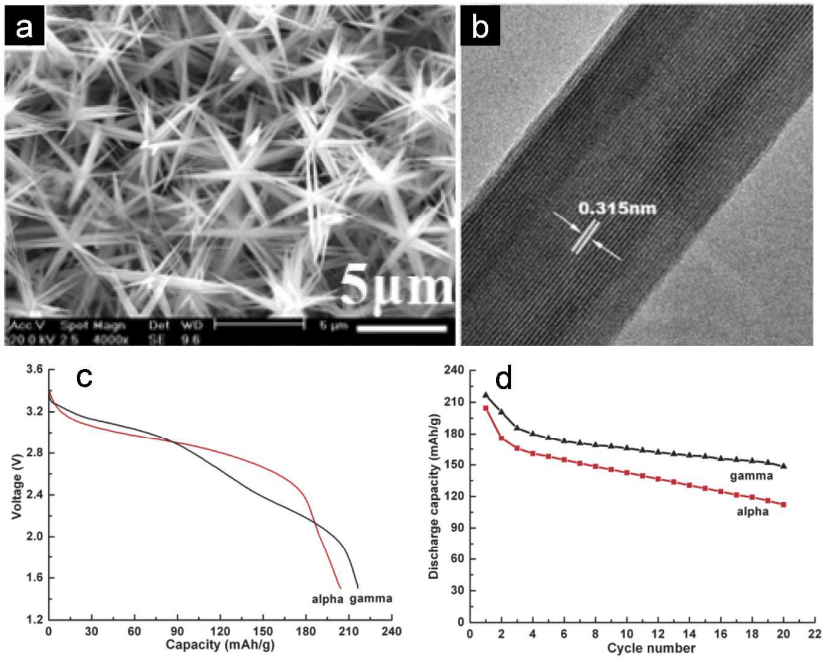

Figure 15 (a, b) SEM and TEM images of MnO_2 nanorods hydrothermal synthesized form $Mn(NO_3)_2$ precursor. (c) Discharge curves and (d) first 20 cycles of α- and γ-MnO_2 phase nanostructures in the laboratory Li -MnO_2 cells. Reproduced with permission from Ref. 272.

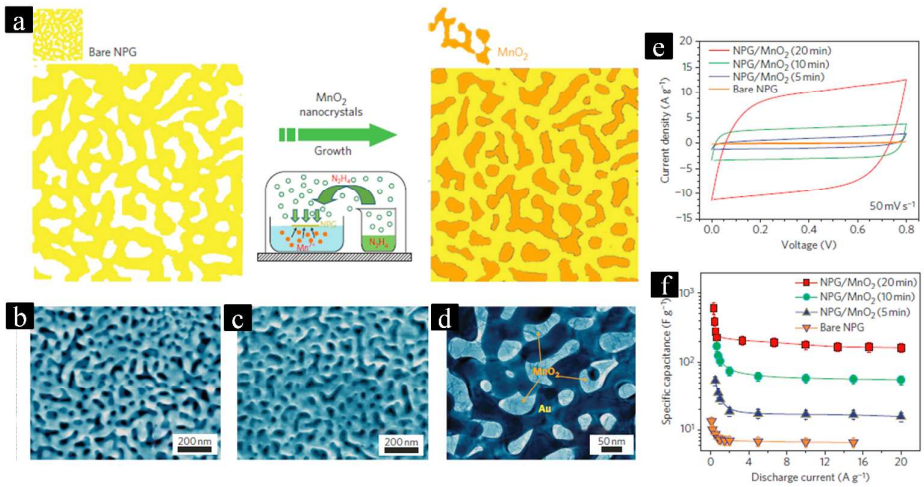

Figure 16 (a) Schematics of the nanoporous Au/MnO_2 hybrid materials by chemical precipitation of MnO_2 on surfaces of porous Au template. (b-d) SEM images, (e) CV curves and (f) rate capability of nanoporous Au/MnO_2 hybrid materials. Reproduced with permission from Ref. 273.

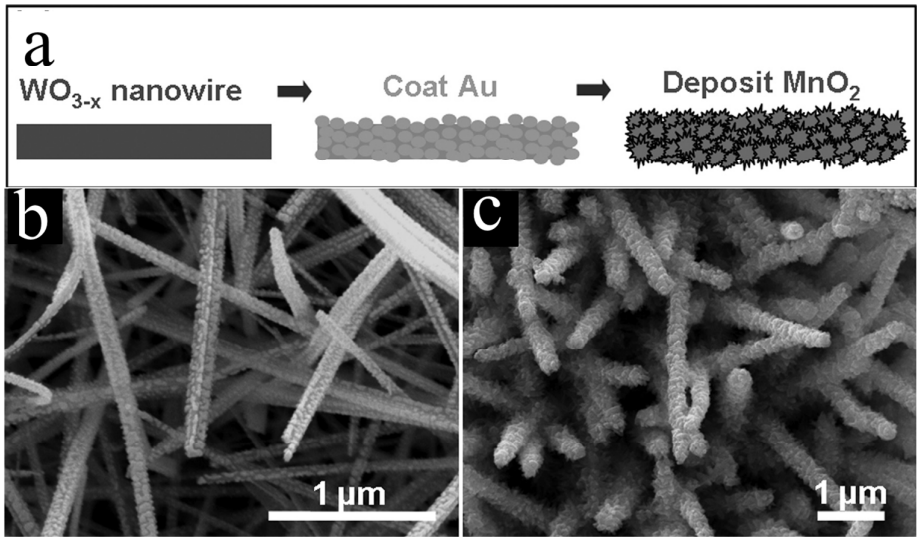

Figure 17 (a) Schematics of the fabrication process for WO_{3-x}@Au@MnO_2 composite nanowires. The MnO_2 outer shell is by electro-deposition. SEM images of (b) WO_{3-x}@Au nanowires, and (c) WO_{3-x}@Au@MnO_2 nanowires on carbon cloth. Reproduced with permission from Ref. 316.

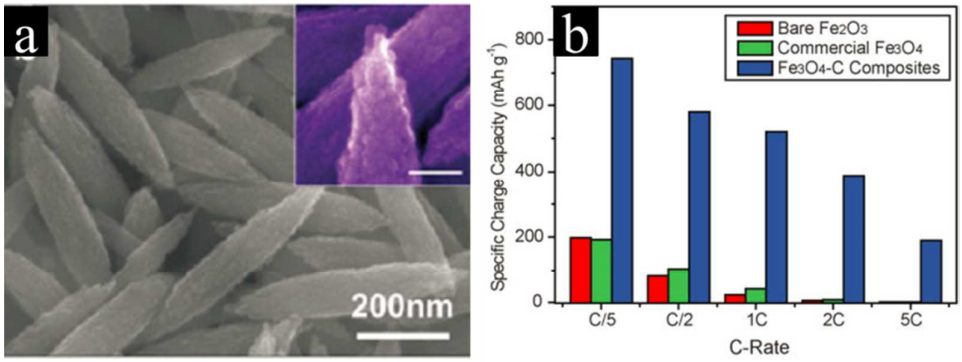

Figure 18 (a) SEM images of hydrothermal synthesized Fe_3O_4 spindles with additional carbon coating. (b) Rate capability of the HT-Fe_3O_4/C spindles electrode compared to bare Fe_2O_3 without carbon, and commercial Fe_3O_4 powders. Reproduced with permission from Ref. 367.

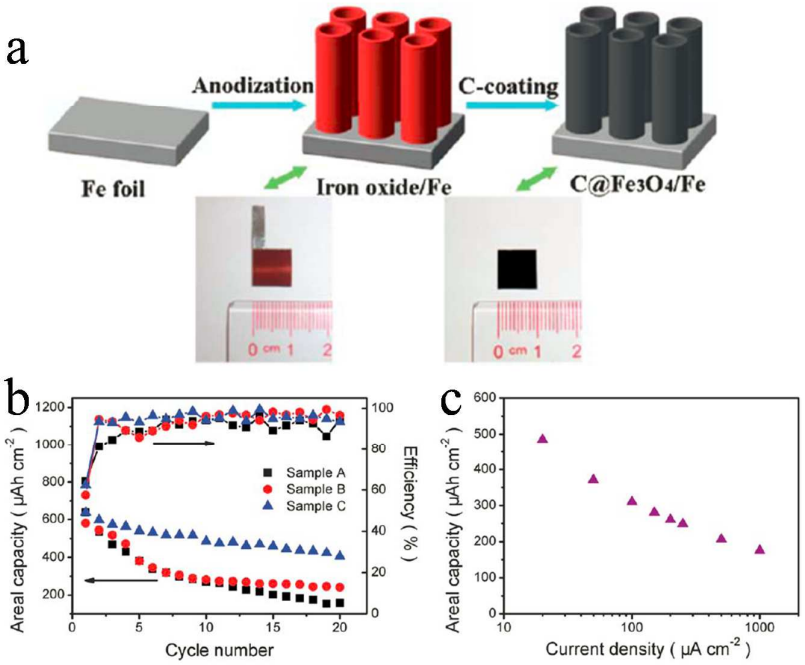

Figure 19 (a) Schematics of the synthesis of the C@Fe_3O_4 composite electrode. (b, c) Li-ion battery cycling life and rate capability of C@Fe_3O_4 composite electrode. Reproduced with permission from Ref.383.

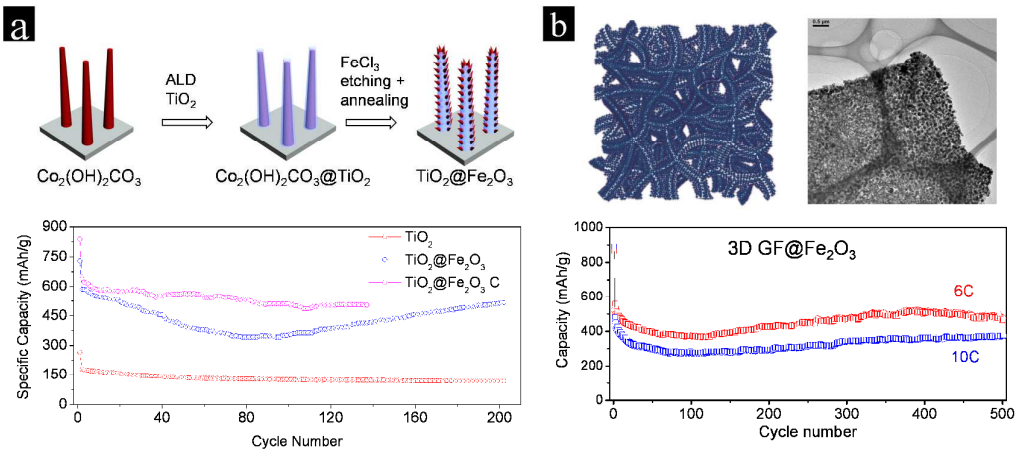

Figure 20 Fe_2O_3 nanostructures obtained by chemical precipitation for the Li-ion battery anode materials. (a) $Co_2(OH)_2CO_3$ nanowires as the sacrificial template and ALD TiO_2 as the support for the final Fe_2O_3 nanoparticles. The battery cycling life is shown below. Reproduced with permission from Ref. 324. (b) 3D graphene foam supported ALD ZnO as the sacrificial template for chemical precipitation reaction. Reproduced with permission from Ref. 385.

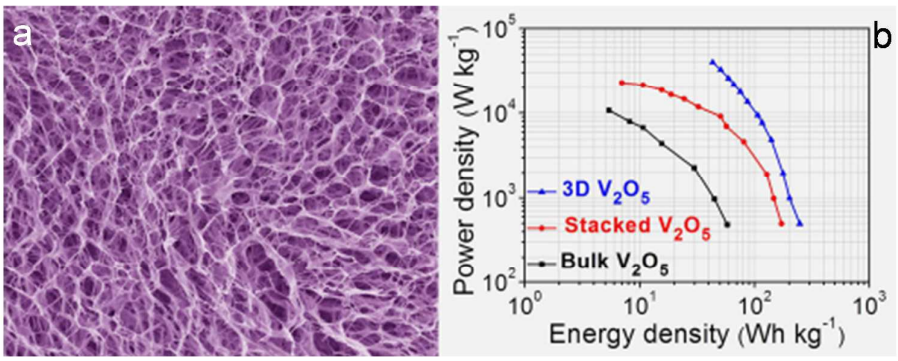

Figure 21 (a) SEM image and (b) Ragone plot of hydrothermal-synthesized V_2O_5 porous film composed of nanosheets. Reproduced with permission from Ref. 395.

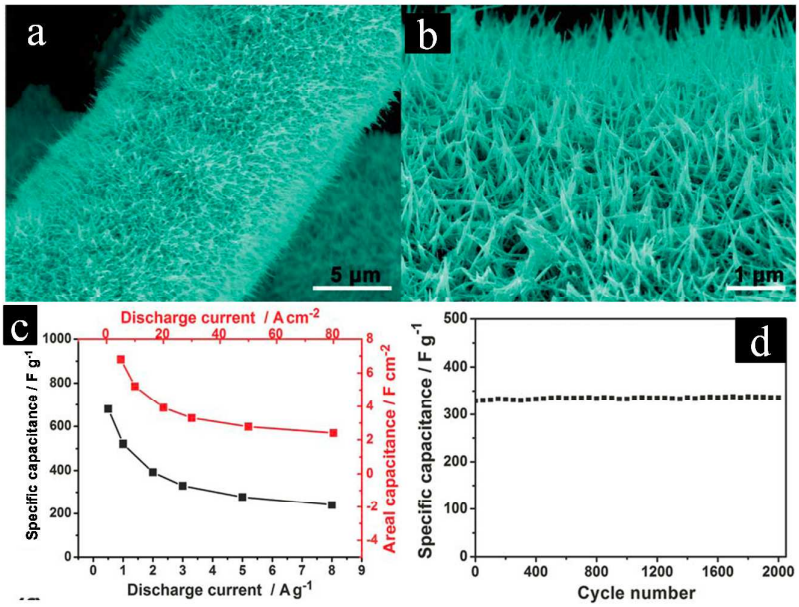

Figure 22 (a, b) SEM images of the hydrothermal synthesized WO_3 nanowire arrays on the carbon cloth. (c) Pseudocapacitive rate capability and (d) cycling life of the WO_3 nanowire array electrode. Reproduced with permission from Ref. 435.

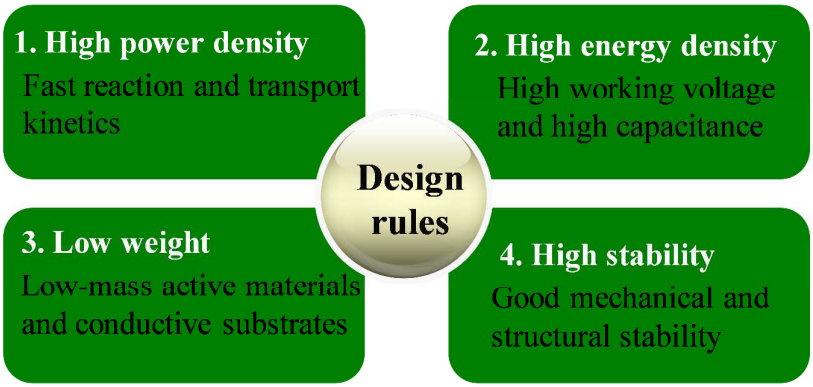

Figure 23 Proposed basic rules for designing high-performance electrodes for supercapacitors.